

Hybrid AC/DC Grid with Parallel LCC-VSC Interlinking Converters

by

Rouzbeh Reza Ahrabi

A thesis submitted in partial fulfillment of the requirements for the degree of

Doctor of Philosophy

in

Energy Systems

Department of Electrical and Computer Engineering

University of Alberta

© Rouzbeh Reza Ahrabi, 2022

Abstract

Hybrid AC/DC grids have been of interest to scholars in recent years. A hybrid AC/DC grid can have higher efficiency and power quality by incorporating renewable base generations and power electronics of any kind into a system. Furthermore, the collection of power electronics in such a system can accommodate several ancillary services within the grid (e.g., unbalanced voltage, power quality, etc.). Line commutated converters (LCC) are a mature technology widely used in the grid due to their high power capacity and are usually known for adversely affecting the power quality. On the other hand, the fully controllable power electronics based on voltage source converters (VSC) are increasingly adopted because of their flexible control and better power quality.

This work proposes the configuration of a parallel LCC-VSC interlinking converter (IC) to be used in hybrid AC/DC grids. The parallel LCC-VSC configuration takes advantage of the low cost of the LCC system as well as the bidirectional power flow capability of VSCs in a multi-terminal DC grid and offers an excellent option for lowering system costs while retaining high performance. Moreover, the LCC's drawbacks, such as low power quality, reactive power consumption, and commutation failure, can be addressed using the parallel LCC-VSC configuration with proper control and coordination. In this work, an example of the parallel LCC-VSC system can be considered as a capacity expansion of the initially unidirectional LCC interlinking converters due to system growth, which may also require reverse power flow functions. A second scenario is that this

parallel LCC-VSC system can be considered when the power flows in two directions are not equal.

The unified control scheme is important for such a system considering various operational modes. Due to the LCC's limitation in control and operation, it is essential to develop a compatible control scheme to achieve the desired function. Having considered the above two application scenarios, two unified control schemes are proposed in this work: 1) a control scheme for the expansion of the available LCC-based installations, and 2) a control scheme for new installations with parallel LCC-VSC interlinking units. As mentioned, the first control scheme is intended for expansion of the existing LCC units with parallel VSCs. The VSCs are controlled by a frequency-based droop equivalent control. In addition, the second control scheme implements an AC frequency-DC voltage-based droop equivalent control for new installations with unequal power flow in two directions. The expansion of the available installations is implemented by saving the LCC's original V-I control graph. However, in new installations, the control scheme will be developed independently of the LCC's conventional V-I graph by a constant supportive response from the VSCs.

Power quality issues have been a serious concern with LCCs. Conventionally, passive components are used for harmonic and reactive power compensation. Therefore, in LCC-based installations with an intension of expansion by VSC-based units such passive components will be preserved. However, in new installations, active harmonics compensation is recommended based on the extended flexibility of the control scheme and the interlinking unit. The proposed

compensation method is designed to operate under the low switching frequency of the interlinking VSCs without interfering in the main control scheme. In order to achieve the desired superior performance, the power system is modeled and stability studies are performed. Unbalanced voltage is an expected issue of the current power grid, which can adversely affect the performance of the system. Temporary or permanent loading conditions can contribute to unbalanced AC voltage leading to instability in the power system and LCC commutation failure. Such phenomena can be damaging for the power system and should be mitigated. In this thesis a compensation scheme is developed to mitigate the issue.

Acknowledgements

First and foremost I want to thank my Ph.D. supervisor, Professor Yunwei (Ryan) Li. It has been an honor to be his Ph.D. student, and his advice on both research as well as on my career have been inevitable. I appreciate all his contributions of ideas and time to make my Ph.D. experience productive. His profound knowledge in the area of power engineering and also his enthusiasm to research was contagious and motivational for me, and I will forever be thankful to him.

I would also like to thank Dr. Farzam Nejabatkhah, and Dr. Li Ding for their help and support during my Ph.D.

I would also like to thank Alberta Innovates Graduate Student Scholarships program for their financial support during my Ph.D.

Table of Contents

ABSTRACT II

ACKNOWLEDGEMENTS V

TABLE OF CONTENTS VI

TABLE OF TABLES IX

TABLE OF FIGURES X

LIST OF ACRONYMS XIV

CHAPTER 1 HYBRID AC/DC GRIDS 1

1.1 INTRODUCTION TO HYBRID AC/DC GRID 2

1.2 ADVANTAGES AND CHALLENGES OF THE HYBRID AC/DC GRID 3

1.3 CONVENTIONAL LCC-BASED GRIDS 4

1.4 CONVENTIONAL VSC-BASED GRIDS 7

1.5 PROPOSED PARALLEL LCC/VSC 9

1.6 THESIS OBJECTIVE AND MOTIVATIONS 11

1.7 THESIS OUTLINE 14

CHAPTER 2 UNIFIED CONTROL SCHEME - EXPANSION OF THE EXISTING LCC-BASED GRID BY PARALLEL LCC/VSCS INTERLINKING CONVERTERS 17

2.1 PROPOSED PARALLEL LCC-VSC - CONTROLLED BY LCC-BASED INSTALLATION'S EXPANSION CONTROL SCHEME 19

2.2 MODELING OF VS-ICS 21

2.3 MODELING OF THE LC-IC 23

2.3.1 Modeling of LC-IC's Proposed Control Scheme 24

2.3.2 Modeling of LC-IC's Droop Equivalent Control for the Proposed LCC-based Installation's Expansion 27

2.3.3 Modeling of LC-IC's VDCOL Control for the Proposed LCC-based Installations Expansion 28

2.4 OPERATION MODES AND STABILITY STUDIES 28

a. Power-sharing Operation 29

b. AC sub-grid Support 32

c. DC sub-grid Support 35

2.5 REAL-TIME SIMULATION RESULTS 39

■ Real-time simulation test for the LCC-based installations expansion control scheme 40

2.6	EXPERIMENTAL RESULTS	46
2.7	CONCLUSION	49
CHAPTER 3 UNIFIED CONTROL SCHEME - PARALLEL LCC-VSC-BASED NEW		
INSTALLATION		51
3.1	THE HYBRID AC/DC GRID WITH PROPOSED PARALLEL LCC-VSC-BASED NEW INSTALLATION'S CONTROL SCHEME.....	52
3.2	MODELING OF VS-ICs AND LC-IC.....	53
	<i>3.2.1 Modeling of LC-IC's Droop Equivalent Control for the Proposed Parallel LCC-VSC-</i> <i>based New Installation's Control Scheme</i>	<i>54</i>
3.3	OPERATION MODES AND STABILITY STUDIES OF PARALLEL LCC-VSC-BASED NEW INSTALLATION'S CONTROL SCHEME.....	55
	<i>3.3.1 Power-sharing Operation</i>	<i>55</i>
	<i>3.3.2 AC Sub-grid Support.....</i>	<i>58</i>
	<i>3.3.3 DC Sub-grid Support</i>	<i>60</i>
3.4	REAL-TIME SIMULATION RESULTS	62
	■ <i>The real-time Simulation Test for the Parallel LCC-VSC-based New Installation's Control</i> <i>Scheme.....</i>	<i>63</i>
3.5	CONCLUSION	69
CHAPTER 4 HARMONICS MITIGATION TECHNIQUE FOR PARALLEL LCC-VSCS		
INTERLINKING CONVERTERS		71
4.1	PROPOSED COMPENSATING SCHEME OF THE VS-ICs	72
	<i>a) The proposed Compensating Technique.....</i>	<i>72</i>
	<i>b) Equivalent Model of the System.....</i>	<i>74</i>
4.2	MODELING AND DESIGN OF THE VIRTUAL IMPEDANCE.....	76
4.3	PEAK POWER CAPACITY OF THE PARALLEL VS-IC	79
4.4	SIMULATION RESULTS.....	85
4.5	EXPERIMENTAL RESULTS.....	91
4.6	CONCLUSION	97
CHAPTER 5 UNBALANCED PCC VOLTAGE COMPENSATION WITH PARALLEL		
LCC/VSC INTERLINKING CONVERTERS.....		98
5.1	LC-IC's CONTROL SCHEME UNDER UNBALANCED CONDITION.....	99
5.2	VSC CONTROL UNDER UNBALANCED CONDITION	103
5.3	SYSTEM MODELLING AND STABILITY ANALYSIS UNDER UNBALANCED CONDITION...	104
5.4	POWER RATING STUDIES.....	108
5.5	REAL-TIME SIMULATION RESULTS.....	111

5.6	CONCLUSION	114
CHAPTER 6 CONCLUSION AND FUTURE PLANS.....		115
6.1	THESIS CONCLUSIONS AND CONTRIBUTIONS.....	115
6.2	SUGGESTIONS FOR FUTURE WORKS	118
REFERENCES		119
APPENDIX		133
6.3	PARAMETERS DESIGN BASED ON A POWER-SHARING OPERATION STATE	133
6.4	PARAMETERS DESIGN BASED ON DC SUB-GRID SUPPORT OPERATION STATE.....	137
6.5	FINALIZING THE CONTROL PARAMETERS	140
6.6	EXCHANGED POWER CAPACITY DESIGN	141

Table of Tables

Table 2.1: Grid Parameters for the LCC-based installations expansion control scheme test	40
Table 2.2: Experiment Circuit Parameters.....	47
Table 3.1: Grid Parameters for the parallel LCC-VSC-based new installation's control scheme test.	64
Table 4.1: The tested grid's parameters.	86
Table 4.2: Control system's controlling parameters for simulation and experiment.....	87
Table 4.3: Virtual impedance and compensation value of the simulation and experiment.....	97
Table 5.1: The VS-IC parameters and control.....	105
Table 5.2: The tested grid's parameters.	111

Table of Figures

Fig. 1.1: Architecture of conventional hybrid AC/DC grid.	2
Fig. 1.2: A point-to-point 12-pulse LCC grid.	5
Fig. 1.3: Conventional V-I graph of the point-to-point LCC-based DC grid.	6
Fig. 1.4: General configuration of a multiterminal DC grid.	7
Fig. 1.5: General schematic of a half-bridge MMC.	9
Fig. 1.6: The proposed parallel LCC-VSCs in a hybrid AC/DC grid.	11
Fig. 2.1: General layout of hybrid AC/DC grid with proposed parallel LCC-VSC interlinking converters.	19
Fig. 2.2: VS-IC's control overview.	21
Fig. 2.3: Line frequency small signal model of the VSC's P - f droop.	22
Fig. 2.4: Point-to-point LCC-based DC system's conventional control method (example: rectifier current-controlled inverter voltage-controlled) and LC-IC's proposed (f - P) droop control system.	23
Fig. 2.5: Line frequency small-signal model of the LC-IC power control.	25
Fig. 2.6: Line frequency small-signal model of the LC-IC constant extinction angle control.	26
Fig. 2.7: LC-IC's control overview for LCC-based installations expansion control scheme.	27
Fig. 2.8: The respond function of VDCOL control scheme.	37
Fig. 2.9: Opal-RT real-time simulator.	39
Fig. 2.10: Power-sharing to AC sub-grid support test by the LCC-based installations expansion control scheme. a) LC-IC active power (p.u.), b) VS-IC active power (p.u.), c) DC voltage (p.u.), and d) Frequency (p.u.).	42
Fig. 2.11: Power-sharing to AC sub-grid support with AC voltage sag test by the LCC-based installations expansion control scheme. a) LC-IC active power (p.u.), b) VS-IC active power (p.u.), c) DC voltage (p.u.), and d) Frequency (p.u.).	43
Fig. 2.12: Power-sharing to DC sub-grid support test by the LCC-based installations expansion control scheme. a) LC-IC active power (p.u.), b) VS-IC active power (p.u.), c) DC voltage (p.u.), and d) Frequency (p.u.).	45
Fig. 2.13: Power-sharing to DC sub-grid support with unstable controlling parameters test by the LCC-based installations expansion control scheme. a) LC-IC active power (p.u.), b) VS-IC active power (p.u.), c) DC voltage (p.u.), and d) Frequency (p.u.).	46
Fig. 2.14: Experimental test circuit layout.	47
Fig. 2.15: Experimental setup.	48
Fig. 2.16: Normal and frequency support operations states experimental results.	49
Fig. 2.17: Normal and DC support operations states experimental results.	49

Fig. 3.1: General layout of hybrid AC/DC grid with the proposed parallel LCC-VSC-based new installation's related environment.	53
Fig. 3.2: The proposed control scheme of the LC-IC for improved unified control.	55
Fig. 3.3: Normal operation condition poles-placement analysis. a) overall poles-placement, b) impact of individual tests.	57
Fig. 3.4: Simplified equivalent circuit of an LCC paralleled with half-bridge MMC during the fault demonstrating circulating current.	60
Fig. 3.5: DC fault operation condition poles-placement analysis. a) overall poles-placement, b) impact of individual tests.	62
Fig. 3.6: The layout of the tested grid.	63
Fig. 3.7: Transmitted power by LC-IC and VS-IC in power-sharing operation test by the parallel LCC-VSC-based new installation's control scheme.	64
Fig. 3.8: AC sub-grid frequency support test by the parallel LCC-VSC-based new installation's control scheme. a) LC-IC and VS-IC transmitted power. b) AC sub-grid frequency.	65
Fig. 3.9: AC sub-grid under fault state with voltage sag test results in improved unified control technique. a) LC-IC and VS-IC transmitted power. b) AC sub-grid frequency. c) Firing angle.	66
Fig. 3.10: DC sub-grid under fault state test results in improved unified control technique. a) LC-IC and VS-IC transmitted power. b) DC sub-grid voltage level.	67
Fig. 3.11: DC sub-grid under fault state with negative transmitted power test results in improved unified control technique. a) LC-IC and VS-IC transmitted power. b) DC sub-grid voltage level.	68
Fig. 3.12: Injected and consumed reactive power by LC-IC and VS-IC in power-sharing operation condition, respectively, in parallel LCC-VSC-based new installation's control scheme.	69
Fig. 4.1: The proposed VS-ICs double loop control with virtual impedance harmonic compensation/rejection feedforward.	73
Fig. 4.2: Equivalent model of the system.	74
Fig. 4.3: Equivalent model of the system in the presence of parallel VS-ICs.	75
Fig. 4.4: Equivalent impedance model of the system in the presence of parallel VS-ICs.	76
Fig. 4.5: Bode plot of system impedance from load point of view, compensation for 11 th , 13 th , 23 rd and, 25 th harmonics.	78
Fig. 4.6: Pole-placements of the control function in several virtual impedance values.	78
Fig. 4.7: Curve of the LCC's alternating current. (a) Ideal, (b) with commutation reactance effect.	81
Fig. 4.8: Conventional passive filter units.	81
Fig. 4.9: The percentage of the 12-pulse LCC harmonics to fundamental and IEEE standard for injected harmonics limits.	82
Fig. 4.10: Reactive power required according to variation of active power [85].	84
Fig. 4.11: Simulation and experimental tests circuit structure.	86

Fig. 4.12: Uncompensated simulation results. (a) Grid current. (b) LCC current. (c) Grid current THD in first interval. (d) Grid current THD in second interval.....	88
Fig. 4.13: Compensated simulation results. (a) Grid current. (b) LCC current. (c) Grid current THD in first interval. (d) Grid current THD in second interval.....	89
Fig. 4.14: Simulation results for grid current with and without compensation. (a) Grid frequency 60 Hz. (b) Grid frequency is dropped 0.1 Hz.	91
Fig. 4.15: The experimental setup.	92
Fig. 4.16: Experimental results for the condition without compensation.	93
Fig. 4.17: Load voltage THD without harmonics compensation. (a) First loading condition. (b) Second loading condition.	94
Fig. 4.18: Load current THD without harmonics compensation. (a) First loading condition. (b) Second loading condition.	94
Fig. 4.19: Experimental results for the condition with harmonics compensation.....	95
Fig. 4.20: Load Voltage THD with harmonics compensation. (a) First loading condition. (b) Second loading condition.....	95
Fig. 4.21: Load current THD with harmonics compensation. (a) First loading condition. (b) Second loading condition.....	96
Fig. 5.1: Reduction of commutation region due to, (a) commutation voltage reduction, (b) commutation voltage backward phase shift, and (c) DC current increase.	100
Fig. 5.2: LCC's inverter unit circuit layout.	101
Fig. 5.3: Thevenin equivalent model of the LCC seen from inverter bus.....	101
Fig. 5.4: VS-IC's control structure.	103
Fig. 5.5: The proposed VS-ICs double loop control.....	103
Fig. 5.6: Block diagram of a typical VUC controller.	104
Fig. 5.7: Bode diagrams of positive-sequence and negative-sequence closed-loop transfer functions.	106
Fig. 5.8: Bode diagrams of positive-sequence and negative-sequence impedance.....	106
Fig. 5.9: The equivalent system circuit for calculation of I_o –.....	107
Fig. 5.10: Poles of G_{CL} for different K_n values.	107
Fig. 5.11: VS-IC's droop-based unified control scheme.	109
Fig. 5.12: Negative sequence model of the VS-IC.	109
Fig. 5.13: Real-time simulation results without VUC control. (a) LCC current. (b) PCC Voltage.	112
Fig. 5.14: Real-time simulation results with VUC control. (a) LCC current. (b) PCC Voltage. ...	113
Fig. 5.15: Real-time simulation results for PCC voltage with and without compensation.	113
Fig. 5.16: Real-time simulation results for unstable controlling condition. (a) LC-IC current. (b) PCC voltage.....	114

Fig. 8.1: Stability study of LC-IC's $G_{1, LCC}$ function, changing K_{LCC} 's and H_{LCC} 's values and their impact on poles placement.	134
Fig. 8.2: Stability study of LC-IC's $G_{2, LCC}$ function, changing K_{LCC} 's and H_{LCC} 's values and their impact on poles placement.	134
Fig. 8.3: Impact of $G_{c_i}(s)$ on $P_{IC}(s)$ poles-placement of the function $G_{3, IC1}(s)$. a) Overall poles placement. b) Impact of individual changes.	136
Fig. 8.4: Impact of $G_{c_i}(s)$ and $G_{DLCC}(s)$ on the poles placement of the $G_{D3}(s)$. a) Overall poles placement. b) Impact of individual changes.	139
Fig. 8.5: ICs overall system level power exchange control.	141

List of Acronyms

$P_{DC_s,pu}$	DC sub-grid's slack power in per-unit
$P_{DC_p,pu}$	DC power terminals in per-unit
$P_{AC_s,pu}$	AC sub-grid's slack power in per-unit
$P_{AC_p,pu}$	AC power terminals in per-unit
$\omega_{AC,pu}$	Grid frequency
$\omega^*_{AC,pu}$	Reference frequency
$u_{DC,pu}$	Actual DC voltage
$U^*_{DC,pu}$	Reference value of DC voltage
$P^*_{AC,pu}$	Aggregated slack terminals AC active power reference value
$P^*_{DC,pu}$	Aggregated slack terminals DC active power reference value
P_{AC_s}	Slack terminals aggregated AC active power
P_{DC_s}	Slack terminals aggregated DC active power
ω_B	Base AC grids' frequency
S_B	Base AC grids' power
U_{DC_B}	Base DC voltage
$P_{IC_i,pu}$	Exchanged power by i -th VS-IC
$P_{IC_LCC,pu}$	Exchanged power by LC-IC
$P_{AC_B,pu}$	Rated power of the AC aggregated slack
$P_{DC_B,pu}$	Rated power of the DC aggregated slack
K	Power-sharing ratio between aggregated slack terminals
ΔP_{s_i}	Power difference between AC and DC sub-grids
$P_{set_i,pu}$	Active power reference value
E_B	AC voltage base value
K_{p_i}	Active power's droop coefficients

K_{q_i}	Reactive power's droop coefficients
H_{p_i}	Active power's inertia coefficients
H_{q_i}	Reactive power's inertia coefficients
$\omega_{ref_i,pu}$	AC sub-grid frequency's reference value
$\omega_{set_i,pu}$	AC sub-grid frequency's setting value
$\Delta\omega_{i,pu}$	AC sub-grid frequency's error signal value
$E_{ref_i,pu}$	AC voltage reference amplitude
$E_{set_i,pu}$	AC voltage setting value
$\Delta E_{i,pu}$	AC voltage error
$P_{set_i,pu}$	i -th IC active power desired value
$Q_{set_i,pu}$	i -th IC reactive power desired value
$P_{IC-i,pu}$	LC-IC's measured active power
$Q_{IC-i,pu}$	LC-IC's reactive power
S_{ep_I}	Exchanged power function from DC sub-grid to AC
$\Delta\delta_i$	Angle difference, i -th VS-IC and AC sub-grid
X_i	Reactance between i -th VS-IC and AC sub-grid
E_i	Phase-to-ground voltage of the i -th VS-IC
U_i	Phase-to-ground voltage AC sub-grid
P_{i0}	Power transferred by i -th VS-IC
ζ_i	Damping factor
ω_{n_i}	Natural angular frequency
t_{s_i}	Settling time
η_i	Proportional gain's value
τ_{l_i}	Desired lead time
τ_{d_i}	Desired delay time
K_{LCC}	LC-IC droop coefficient
H_{LCC}	LC-IC inertia coefficient

$\omega_{set_LCC,pu}$	Desired frequency of the LC-IC
$\omega_{LC_IC,pu}$	Measured frequency of the LC-IC
$P_{ref_LCC,pu}$	LC-IC's power's reference value
$P_{set_LCC,pu}$	LC-IC's power's setting value
$\Delta P_{LCC,pu}$	LC-IC's droop equivalent control's required power
$u_{DC_LCC,pu}$	DC voltage of the LC-IC
$I_{DC_LCC,pu}$	DC current of the LC-IC
$E_{L-L,pu}$	Grid's line-to-line voltage value in per-unit
L_t	Transformer's leakage inductance
γ	Extinction angle
$\Delta u_{DC_LCC,pu}$	Gives voltage lost in per-unit
β	Ignition angle
R_{L_t}	DC line resistance
L_{L_t}	DC line inductance
$E_{L-L0,pu}$	Grid side line-to-line voltage
β_0	Ignition angle setting value
n_B	Number of LCCs parallel on the AC and in series on the DC
γ_0	Extinction angle's setting value
μ	Overlap angle
γ_{ref}	Desired extinction angle
K_d	VDCOL slope coefficient
K_g	VDCOL inertia coefficient
$u_{DC_LCC,pu}$	Locally measured DC voltage LC-IC
$u_{DC_i,pu}$	Locally measured DC voltage VS-IC
$u_{DC,pu}$	DC sub-grids busbar voltage
$V_{inv_i_h}$	Inverter output harmonic voltage
V_{PCC_h}	PCC's harmonic voltage

$Z_{L_i,pu}$	Inverter filter inductance
$Z_{C_i,pu}$	Inverter filter capacitance
Z_V	Equivalent harmonic impedance
$Z_{eq,h,pu}$	Equivalent impedance of all parallel VS-ICs on the desired frequency order
Q	Quality factor
ω_h	Desired harmonic frequency
G_{delay}	Switching and computation delay time
I_{IC_LCC}	Current on the LCC's AC
I_{DC_LCC}	Current on the LCC's DC
I_n	Magnitude of the n th harmonic current
I_1	Magnitude of the fundamental current
μ	Overlap angle
α	Firing angle
i_{ov}	Current magnitude with overlap angle
i	Current magnitude without overlap angle
D_I	Current distortion power
D_V	Voltage distortion power
S_H	Harmonic's apparent power
P_{d_LCC}	LCC's supplied power on the DC side
x_{com}	Commutation reactance
$\cos\gamma$	Extinction angle
Z_F	Fault impedance
Z_u	Upper sides impedances
Z_l	Line impedances

x	Fault location from inverter
$\Delta\alpha$	Angle deduction for a safe commutation
γ_{min}	Minimum extinction angle to avoid commutation failure
E_t	Thevenin equivalent voltage
V_b	Voltage measurements
ϕ_b	Phase angle
α_i	Valves firing angle
Z_t	Thevenin equivalent impedance
u_{rms}	rms value of the rated voltage
$i_{o,\alpha}^-$	Negative sequence component of the output current
$i_{o,\beta}^-$	Negative sequence component of the output current
Q^-	Negative-sequence reactive power
K_n	Negative-sequence voltage droop gain
G_{V_i}	Control system closed-loop transfer function
Z_{V_i}	Output impedance
P_{VS-IC}^+	Positive sequence of the VS-IC's average active power
P_{VS-IC}^-	Negative sequence of the VS-IC's average active power
Q_{VS-IC}^+	Positive sequence of the VS-IC's average reactive power
Q_{VS-IC}^-	Negative sequence of the VS-IC's average reactive power
u_o^+	Positive sequence components of the PCC voltage
u_o^-	Negative sequence components of the PCC voltage
i_o^+	Positive sequence components of the VS-IC's output current
i_o^-	Negative sequence components of the VS-IC's output current
\tilde{p}_{VS-IC}	Oscillatory terms of instantaneous active power

\tilde{q}_{VS-IC}	Oscillatory terms of instantaneous reactive power
Z^+	Positive sequence impedances seen from the PCC
Z^-	Negative sequence impedances seen from the PCC

Chapter 1

Hybrid AC/DC Grids

In recent years, power grids have been increasingly studied for the augmentation of DC renewable generations, energy storage systems (ESS), and modern DC loads. Considering the existing century-long AC power grids and DC grid expansion, a hybrid AC/DC grid is expected to be an attractive solution for emerging power systems. Distributed generation (DG) as an alternative to concentrated generation has gained substantial attention in recent years. The worldwide increase in DGs raises the need for further studies regarding the system's power quality, stability, and contingency plans [1], [2]. ESSs are one of the necessities for such a highly integrated renewable generation grid [3]. Power electronics also play a significant role in establishing the desired performance by constructing the necessary control and energy management for the growing power system.

Higher controllability, higher efficiency, and lower cost are some of the highlights of an ideal conversion unit. These features may not be accessible in a single design but may be scattered among different configurations. Combining the conversion units (i.e., parallel or in a series) is a widely used technique to take advantage of different technologies and improve one in various terms such as transferred power capacity. Hybrid AC/DC grids are the prime example of such a system that aggregates several forms of power generation in a system and provides the opportunity for comprehensive ancillary services. However, the presence of such a variety of generation units, ESSs, and power electronics requires a more in-depth study of the system (i.e., its modeling, design, and control) to address challenges and obstacles.

1.1 Introduction to Hybrid AC/DC Grid

Expansion of power system in both AC and DC pose new challenges to the power grid. Coordinating conversion units and energy storage systems, as well as generation and demand with adequate stability and power quality, need a proper platform.

The hybrid AC/DC grid builds an integrated platform for both the AC and DC system [4], as shown in Fig. 1.1, as a solution of the future power system integrating advantages of both grids [5]. A century-long well-established AC grid is linking to the newly developed DC grid. The DC transmission benefits are higher power transfer capacity, lower losses, facilitating the interconnection of energy sources such as wind and solar, and large modern DC loads to the grid.

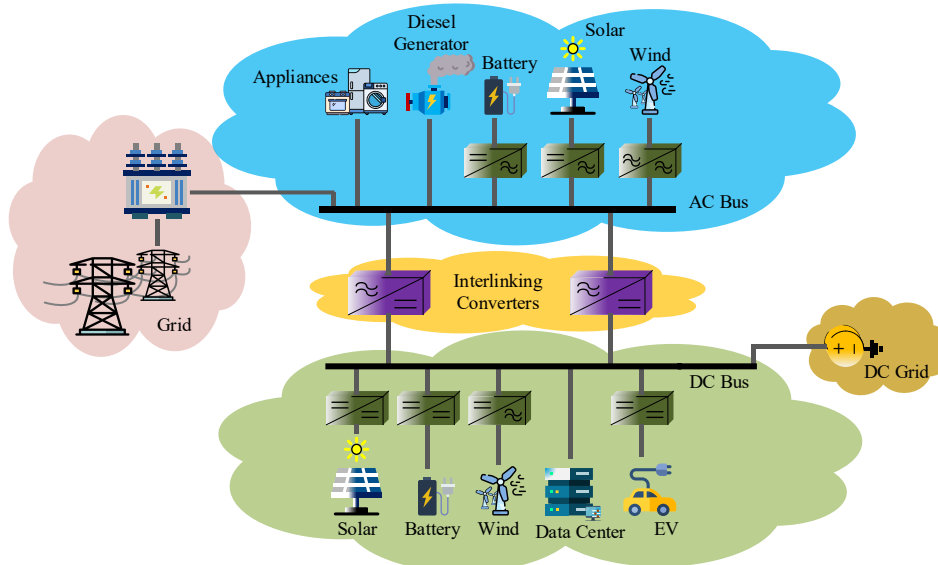


Fig. 1.1: Architecture of conventional hybrid AC/DC grid.

The power system expansion and governmental projections show that the renewable-based DC generation and modern DC loads are envisioned as equally dominant as AC grids centralized production [6], [7].

Local generation and consumption are more economical, reliable, and efficient, especially for electrification of off-grid, remote, or widely distributed communities. However, uncertainty and occasional randomness in renewable power generation can substantially affect the system's robustness in highly renewable energy

penetrated grids. In this regard, energy storage systems can serve as an auxiliary unit by offering an opportunity to determine the grid's stability for a short duration in case of a disturbance in a generation. Also, the hybrid AC/DC grid's added integration can substantially increase power grid security. Such a system establishes a more stable and controlled environment for a distributed and inherently low inertia generation [8], [9].

1.2 Advantages and Challenges of the Hybrid AC/DC Grid

The hybrid AC/DC grids, as discussed previously, contribute several advantages to the power system, such as lower power loss, higher power quality, and wide access to the ESSs. Accessibility to AC and DC power grids helps to remove some unnecessary conversions. As a result, in such a structure, the system's overall efficiency and reliability can be improved [10]. The significant number of power electronics in the hybrid AC/DC grid due to the nature of distributed generation creates an excellent opportunity to deploy various control schemes. Also, accordingly, introduce control system's synergy challenges that need to be taken seriously.

In order to achieve the aforementioned advantages, some of the hybrid AC/DC grid challenges need to be carefully addressed. It is expected that in future hybrid AC/DC grids, power quality can quickly become a series issue due to the increasing penetration of single-phase/unbalance loads, non-linear loads, and single-phase/unbalance distributed generations. In general, the power quality issues in AC sub-grids can be harmonics, voltage oscillation, and unbalances. Similarly, DC sub-grids problems can be harmonics and voltage oscillation. Furthermore, system properties control in a hybrid AC/DC grid can be an additional obstacle that need to be dealt with. This is due to the fact that generation and consumption in such a system can be challenging and need constant observation and control to establish a smooth system properties control.

The available mitigating techniques in AC and DC grids with some modifications

can be employed to deal with power quality issues in the hybrid AC/DC systems. At the same time, in some cases, new studies are required. Power fluctuation smoothening by ESS units has been proposed for several applications such as grids and ships [8], [11], [12], [13]. Similar techniques have been employed to improve the power quality and compensate for short term power generation fluctuation in the hybrid AC/DC grids. Furthermore, the installation of additional compensation units can mitigate the issue of power quality; however, this can increase the investment cost of the grid [6], [14], [15]. Despite the arguments above, power quality in hybrid AC/DC grids can be significantly improved compared to a conventional structure with some extra attention.

VSCs and LCCs are two of the leading technologies that can be found in the power grid. Understanding the feature and controlling aspects of such units can substantially help to prompt the system's performance.

1.3 Conventional LCC-based grids

The LCCs are traditionally used in the DC grids with over 150 point-to-point installations worldwide due to the mature technology, lower cost, and efficient high-power transmission. Such converters are commonly used in submarine power transmission, long-distance power transmission, two AC grids interconnection with different frequencies, two unsynchronized AC grids interconnection, and controllable power exchange between two AC grids [16]. Thyristor-based converters are commonly used in high voltage applications due to their physical characteristics that can withstand excessive voltages. Therefore, high voltage DC (HVDC) and medium voltage DC (MVDC) applications are one of the areas in which LCC is dominantly being used [17], [18], [19], [20], [21]. It is proven that in DC transmission, the initial capital investment is higher than AC transmission due to converter costs. However, the benefits of the DC grid balance the capital investment at a certain distance. The breakeven distance for submarine cables is 40-70 km and 600-800 km for overhead lines. The point-to-point installations are one of the most dominant structures for LCCs, shown in Fig. 1.2.

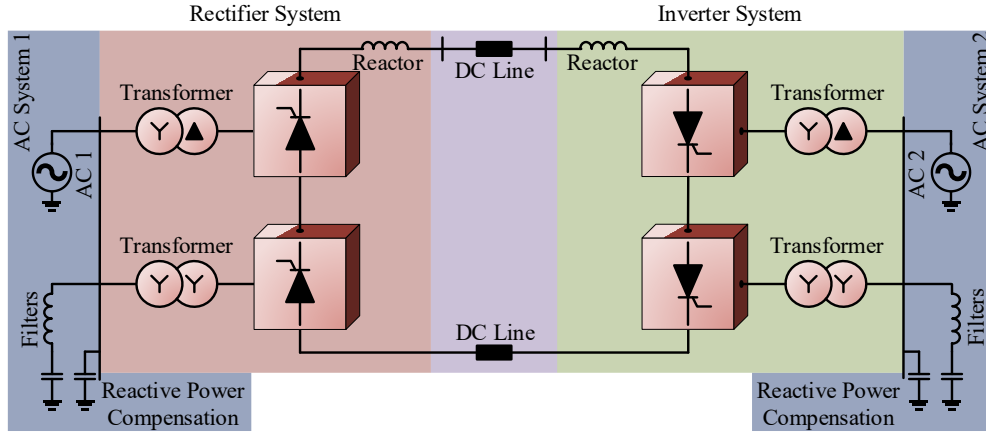


Fig. 1.2: A point-to-point 12-pulse LCC grid.

As can be seen, the point-to-point structure is consisting of rectification and inversion units on each front end. Several configurations for the converters are available. The 6-pulse design that includes a single conversion unit is the simplest form. The higher-order structure, such as 12-pulse and 24-pulse can also be used similarly, providing higher power quality. The LCCs are connected to the grid through tap changing transformers on the AC side. The transformers are designed to operate with high harmonic currents and also withstand the AC and DC voltage stress. The tap changing transformers will help the conversion units to optimize the voltage level and firing angle to minimize the reactive power consumption. On the DC side, the LCCs are connected to the DC line through large reactors. The size of reactors is determined considering DC fault response, commutation, and dynamics. The point of common couplings (PCCs) on both rectification and inversion sides are equipped with capacitance banks and harmonic filters. In addition to that the LCCs typically need reactive power of around 60% of the converter power rating. Due to the limited switching frequency, LCCs are likely to inject low order harmonics into the grid. In the case of a 12-pulse configuration, the harmonic orders 11th, 13th, 23rd, and 25th will appear in the grid. Therefore, passive filters and capacitive banks are located on the AC side to compensate for power quality and supply the required reactive power. A large portion of the reactive power in such configurations is provided with filter banks, and capacitor banks will offer the remaining parts. Typically, the capacitor banks are equipped with mechanical

switches to adjust to the system's needs.

The LCCs have limited controllability due to their restrictions in commutation. Consequently, the control scheme of such conversion units should adapt accordingly. The state of the system determines the LCC's control scheme. The constant voltage and constant current controls are two of the main commonly used operation schemes. In the point-to-point configuration, to avoid any competition, one of the conversion units should be controlled with a constant voltage scheme, and the other unit should adopt the constant current. The conventional V-I control graph of the point to point LCC-based DC grid can be found in Fig. 1.3 [16]. As can be seen, control schemes of the rectifier unit are constant firing angle control, constant current control, and VDCOL. The inversion unit's control scheme includes constant current control, constant voltage control, VDCOL, and constant extinction angle control. The rectifier minimum firing angle is typically selected in a range as $\alpha_{\min} = 2^\circ$ to avoid triggering the valves when they are reverse biased. The rectification unit adopts the VDCOL scheme when the DC voltage has substantially disrupted due to a faulty AC grid. The process will help the system to recover faster and get out of the fault.

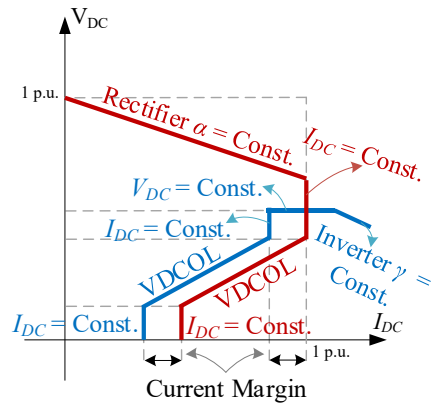


Fig. 1.3: Conventional V-I graph of the point-to-point LCC-based DC grid.

The constant extinction angle (γ) control of the inversion unit should be adopted to avoid commutation failure. The minimum γ required for safe commutation with high-power thyristor-based valves is around 10° – 15° . A similar explanation is applicable for the VDCOL mode of operation of the inversion unit

as rectification. As can be understood from the available control schemes for conversion units on both front ends, several precautionary measures are introduced to avoid commutation failure or help the system to get out of the fault as much as possible.

Unlike the point-to-point configuration, the DC-grid-connected LCCs, such as in the multi-terminal DCs, as shown in Fig. 1.4, are limited to the unidirectional power flow which is inadequate for current power grid. LCC's reactive power consumption and low power quality are other restricting factors for current grid standards.

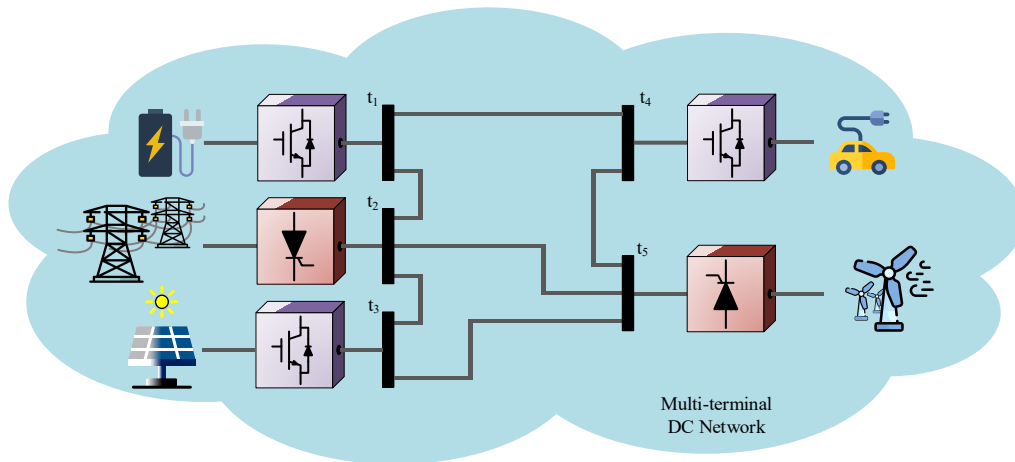


Fig. 1.4: General configuration of a multiterminal DC grid.

1.4 Conventional VSC-based Grids

The VSCs are growing technology in power system due to advancements in power electronics and controls. The VSCs offer higher control flexibility, independent reactive power control, bidirectional current flow, and potentially smaller footprint. Furthermore, the VSCs are immune to commutation problems due to distortion or voltage drop. Lastly, VSCs have considerably higher power quality and also can be controlled for ancillary services such as mitigating grid distortions.

The VSCs have been developed in numerous applications and designs. The

VSCs can be classified in different configurations such as two-level converter, three-level converter, modular multilevel converter (MMC), and hybrid VSC. The two-level converter (6-pulse bridge) consists of IGBT-based valves with inverse parallel diodes [22]. One of the drawbacks of such design would be a high switching loss that is basically due to IGBTs constant on/off process to achieve higher quality waveforms. The three-level converter has significantly higher power quality compared to the two-level structure. The DC capacitors are connected between valves to produce a higher number of voltage levels. In general, the neutral-point-clamped (NPC) topology as one of the most used VSC can offer advantages such as low output harmonic distortion, less switching losses, high-voltage staircase-like waveform capabilities, and the ability to transfer power bidirectionally [23]. The MMC is generally designed based on the 6-pulse bridge configuration, but with submodules in a position of single switch valves as shown in Fig. 1.5. Based on their design, the submodules can accommodate four, for full-bridge, and two, for half-bridge, switches with a capacitor to store the energy. Furthermore, the number of submodules in each leg is a matter of design and power quality preference. Very high power-quality and very low power-loss are some of the advantages of MMCs. It is proven in [26] that IGCT-based MMC units demonstrate a lower amount of power loss compared to their IGBT-based counterparts. In some cases, it is shown that the power loss of the IGCT-based MMCs can be similar to the thyristor-based LCC. Eventually, the hybrid VSCs is one of the most complicated configurations where it combines two-level and MMC converters [28]. This combination's main objectives are to reduce power loss and maintain the MMC's high power quality while providing a compact design that can operate efficiently. However, voltage balancing can be challenging for MMCs based on their complicated structure [24], [25].

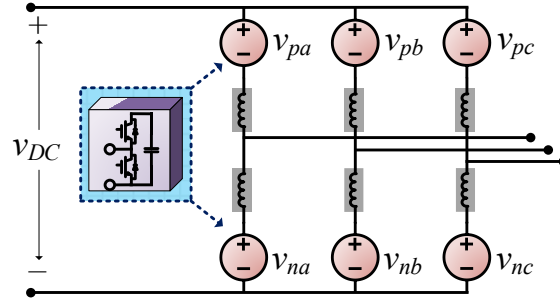


Fig. 1.5: General schematic of a half-bridge MMC.

In general, the VSCs have disadvantages like lower power capacity, higher cost, and higher operation loss than LCCs (the state-of-the-art MMCs can have similar efficiency as LCCs [26]). Based on the inherent limitations of the VSCs in riding through the DC faults and the LCCs in riding through the AC faults, a combined LCC-VSCs topology can unite these two technologies' merits.

1.5 Proposed Parallel LCC/VSC

VSCs and LCCs technologies appear to have several advantages and disadvantages. A combination of LCCs and VSCs in the form of a single unit can establish an opportunity to take advantage of both technologies. Therefore, the parallel LCC/VSCs is proposed to utilize both configurations' advantages and compensate for each other disadvantages with proper control.

In summary, the VSCs' advantages are controllability, higher power quality, and flexibility to operate in distorted and weak grids. LCCs have higher power capacity, efficiency, and lower cost [16], [27]. The combination of LCC-VSC has the potential to bring the best out of each technology and provide a promising solution with lower cost and improved performance for the desired system.

An example of the parallel LCC-VSCs system can be considered as capacity expansion of initially unidirectional LCC interlinking converters, which may also require reverse power flow functions (e.g., adding loads and energy storage close to a wind farm [29], [30], [31]). A second application example of the LCC-VSCs system is for a new interlinking converter station where the power flows in two directions are not the same in design (e.g., remote islands or weak grids with storage

units or distributed generation). Both scenarios (expanding the available LCC-based unit with a parallel VSC, or a new LCC-VSC construction) can be an economically viable solution due to VSC's higher power quality, future proof, and smaller footprint (i.e., lower land cost).

The LCC power quality concerns, as explained, are conventionally compensated by mechanically switched passive components. The need for costly and time-consuming regular maintenance along with slow response time are the drawbacks of such a method. Furthermore, passive filters used to mask the harmonics in LCC based grids are also physically constrained by parasitic components causing loss and inefficiency in performance. The aging effect can impact the filter design's accuracy due to component values fluctuating over the time. It is worth mentioning that these passive filters and the reactive power compensating units can take up to 50 - 60% of the LCCs station. FACTS devices are a well-established alternative method for power quality improvements [32], [33]. However, due to cost constraints, this method is not widely used. The proposed structure lowers the cost by increasing the utilization of existing LCC-based installations for a more extended time while the grid's power quality and system stability are enhanced. In [34], a series-connected VSC and a 12-pulse diode rectifier is proposed with an application in wind farms. It is claimed that the series integration of these two conversion units brings advantages such as cutting the production cost and reducing the power loss to the system while the quality of the exchanged power is kept within standards.

The efficiency of LCCs is reported to be higher than most common VSCs. It has been mentioned in [35] and [38] that LCCs' power losses are around 0.7%-0.8% per converter, resulting in 1.4%-1.6% for a 12-pulse unit. Such a feature can be valuable for high power transmission. The global agreements regarding the establishment of super grids all around the world, such as north and south America, Europe, East Asia, etc. [39], [40], [41], [42], is promising news for such a proposed design. Due to the high power/voltage rating of the LCCs, the improved power quality and dynamic/response of the VSCs while the cost is kept low.

In summary, the parallel LCC-VSCs configuration, as shown in Fig. 1.6, can lower the production cost and system loss, while the transmitted power quality is preserved almost the same as the VSC-based system [34]. This structure can also enable a considerable reduction in the size of passive filters associated with the LCC unit due to the VSC's harmonics and reactive power compensation capability. Supporting LCC during the transients in addition to the bi-directional power flow in the DC grids are other critical features of the proposed configuration.

Several studies in the literature address the operation of LCCs and VSCs in a power grid [17], [36], [37]. However, these studies only include the independent operation of conversion units (i.e., LCCs and VSCs) on each front end of the power system without any direct interaction. Therefore, it is necessary to study the promising features of such parallel LCC/VSCs interlinking converters in great detail. The explained features and opportunities are accessible provided proper control and coordination is applied.

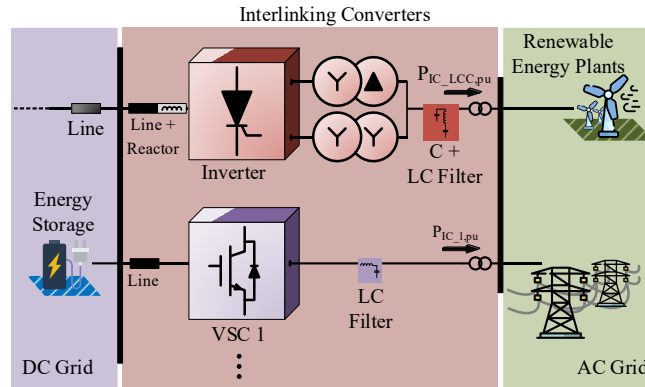


Fig. 1.6: The proposed parallel LCC-VSCs in a hybrid AC/DC grid.

1.6 Thesis Objective and Motivations

The overall objective of this thesis is to propose a practical interlinking converter (IC) configuration for a hybrid AC/DC grid to successfully control the system properties and improve system stability and performance while keeping the

cost low. Given the adverse effect of the system properties' control loss (e.g., AC voltage/frequency and DC voltage), it is critical for ICs to maintain system stability in any condition while keeping the cost low. Therefore, this thesis introduces two scenarios for the configuration of the ICs in a hybrid AC/DC grid. The first scenario is an expansion plan for the available LCC-based installations with the intention of improving the IC's power exchange capacity and the LCC's commutation, adding bidirectional power flow, and supporting the LCC during the transients, especially during sudden changes to the power system. The second scenario introduces new installations with the proposed parallel LCC/VSC ICs in a hybrid AC/DC grid. In this condition, in addition to the objectives of the first scenario, the VS-ICs aim to improve the power exchange quality by removing the unintended harmonics and providing the LC-IC's required reactive power.

For the LCC's expansion projects in the hybrid AC/DC grids, the focus of the study will be on the integration of the VS-IC and LC-IC units. In this regard, the control scheme of the system will be developed to support system properties with both types of interfacing units (IFC). With the available hybrid AC/DC grids researchers have focused on the control scheme of the ICs to maintain and improve power system performance in every operational state. However, based on available studies, the operation and control of VSC-based units has been the center of attention due to their unique features. This is despite the fact that LCCs are also widely used in power systems and accommodate a large portion of the energy conversion units. Therefore, the presence of LCC-based conversion units in the hybrid AC/DC grids is expected. Therefore, the control system should be improved to accommodate such a change to the power system. In the available LCC based installations, due to the nature of the thyristor-based valves, limitations such as slow response time, complex control system, unidirectional power flow in DC grids, and commutation failure are noticeable. The expansion and improvement of the LCC-based power systems to achieve superior performance in a hybrid AC/DC grid has not been addressed previously by researchers. Therefore, in addition to the implementation of the proposed configuration, it is necessary to formulate a control system for the proposed grid, investigate system stability in a variety of power

system states, and design the control parameters.

Furthermore, in a hybrid AC/DC grid in which the power exchange direction is considerably unsymmetrical, the parallel LCC/VSC installations can be utilized to lower the cost and reach a greater power exchange quality. The proposed configuration can be utilized to maximize the performance of the system by implementing the necessary controlling loops. However, due to the lack of research in this area, a thorough study of parallel LCC/VSCs in a hybrid AC/DC grid environment with the proposed control system is necessary. For such a configuration in a given scenario, in addition to the system properties' control of the AC and DC sub-grids, other supplementary control schemes can be implemented to improve system stability, power quality, and control. Moreover, additional practical concerns regarding the implementation and maintenance cost are also critically important and should be addressed in the study.

Designing the parallel VS-IC power capacity for the first and second scenarios is a multi-objective procedure. Such a problem should be addressed considering the equipment cost, cost of installations and maintenance, and the system's exchanged power requirement, such as universal control, harmonics compensation, reactive power compensation, unbalanced control, etc. It will be shown that the exchanged power by the unified control has a direct connection to the amount of support that sub-grids require to control the AC frequency and DC voltage during the fault. Furthermore, as known, the required reactive power to support the operation of the LCC has a high ratio compared to its exchanged active power (about 50-60% of the exchanged active power). The LCC's reactive power compensation can take a considerable portion of the VS-IC power capacity if it is only desired to be provided by VSC. It will be explained that using a combination of active and passive reactive power compensation is a more realistic approach. However, the ratio between active and passive power compensation requires an in-depth calculation of the cost, including installation, land, maintenance, etc. and the desired performance assuming flexibility and control. Furthermore, ancillary services such as harmonics compensation and unbalanced voltage compensation required power are separately

calculated (around 10% and 0.1p.u. respectively). The provided studies will demonstrate that harmonics and unbalanced voltage compensation do not take a considerable amount of the transferred power capacity and can be entirely provided by VS-IC.

Motivated by the above considerations, the following research tasks are carried out in this work:

Task 1 Develop parallel LCC/VSCs configuration in a hybrid AC/DC grid along with an augmented control strategy managing power grid properties in every operation states.

Task 2 Develop a control strategy for parallel LCC/VSCs configuration in new installations with unsymmetrical power delivery to improve performance, increase flexibility, and lower the cost. Develop a design procedure for the proposed power system in order to reach a stable operation and control.

Task 3 Develop supplementary control schemes to improve system stability and power quality.

1.7 Thesis outline

In chapter 2, the parallel LCC/VSCs configuration in a hybrid AC/DC grid is explained. Then voltage source and current source ICs are modelled in detail. The VS-IC's power system model can be used in all power grid's operation states. The LC-IC's model is developed for every operation state of the system including normal and supported conditions. Two types of implementation scenarios are introduced for the proposed configuration, including expansion of available LCC-based installations with VSCs and new installations based on parallel LCC/VSCs configuration in chapter 2 and 3, respectively. The application of both types of systems are explained. In order to take an advantage of the proposed configurations, different controlling systems are developed for each implementation scenarios.

Then a droop like control scheme is developed for the ICs based on the AC and DC sub-grid's aggregated slack terminal's droop functions. Therefore, the conventional (V-I) control graph of the LC-IC is improved to support droop like control in possible operation states. The operation states of the hybrid AC/DC grid are studied and suitable control schemes for both types of conversion technologies are introduced. In order to achieve a superior performance for the system, the power exchange formulations are developed for each state and stability analysis are conducted. The validity of the proposed configuration and respected control scheme is verified by real-time simulation.

In chapter 4, initially, the harmonics profile of the LCC's is introduced. The conventional mitigation procedures are briefly explained. Then, the proposed harmonic compensation technique is presented. The proposed configuration is developed for new installation with an intention of using VS-ICs to mitigate desired harmonic orders. The equivalent model of the proposed power system is developed, and respected stability analysis is conducted. The harmonics compensation intensity and VS-ICs required power exchange capacity is evaluated using available standards and system equivalent model. The proposed technique is validated by simulations and experiments.

The performance of the proposed configuration and respected control system and implementation technique in an unbalanced grid is studied in chapter 5. Initially, the conventional control scheme regarding the operation of the LCC in an unbalanced grid is discussed. Then, a compensating control technique is introduced to by utilizing the VS-IC units. In order to achieve the maximum efficiency in performance the proposed power system is modelled, and stability analysis is conducted. Based on the proposed power system configuration, control scheme, and stability analysis, suitable controlling parameters are chosen, and power rating of the system is calculated. To validate the performance of the proposed system simulation results are provided.

Finally, in chapter 6, the main conclusions and contributions of this thesis are presented. Also, suggestions for future works are provided.

Chapter 2

Unified Control Scheme - Expansion of the Existing LCC-based Grid by Parallel LCC/VSCs Interlinking Converters

A unified control scheme has been recently proposed for hybrid AC/DC grids which considers their variety in operation modes. Extending the unified control scheme to support the proposed parallel LCC/VSC configuration in a hybrid AC/DC grid can benefit the system in several areas, such as improved power quality and enhanced controllability. Moreover, the line commutated interlinking converter's (LC-IC) response and commutation can be improved if properly supported by parallel VSCs.

There are many studies on the control of converters in the hybrid AC/DC grid [43]-[53]. Some focus on the individual control of an AC or DC sub-grid [54]-[57], while others study the control scheme of both AC and DC sides with the operating principles of interlinking converters (ICs) [43]-[46], [50], [52], [53]. The power-controlled method is one of the widely studied methods for the ICs control [43], [44], [46], [50]-[53], [58]. However, it is not a suitable solution for direct AC/DC voltage/frequency support. On the other hand, there are some studies on the combination of power-controlled, AC voltage/frequency-controlled, and DC voltage-controlled schemes with an automated mode changing procedure [47]-[49], [51]. These methods can experience oscillations and even instability during the transition from one control scheme to another. A unified control scheme, proposed recently, offers seamless operation under various operating conditions without the need for operation mode detection [45], [59]. Also, the performance of the ICs is further improved by adopting the virtual impedance concept in the control system, which helps to improve the power-sharing and power quality [60]-[62]. However,

studies in this area have been limited to the VSC-based ICs. For the parallel LCC-VSC ICs, the variety of operation and control requirements presents great coordination and control challenges, which have not yet been studied.

In this section, the proposed unified control scheme of a hybrid AC/DC grid with a parallel LCC-VSC interlinking converter will be studied. This unified control scheme is proposed for the scenario of an expansion project where an LCC was originally used and a VSC unit is added to increase power capacity and implement bidirectional power flow. Therefore, the LC-IC conventional V-I graph's original structure is maintained while necessary improvements are applied to the AC and DC grid support function's control. In this method, a droop equivalent control is inserted to replace a constant current control state, which is made possible by proper control of the parallel voltage source interlinking converters (VS-ICs). The VS-ICs bidirectional power flow also adds to the IC's control flexibility to support the transients and DC sub-grid. In this control scheme, the LC-IC should follow the voltage dependent current order limiter (VDCOL) control for the DC support. The power-sharing and AC support will be conducted through a droop equivalent control. The constant extinction angle control should also be adopted to protect the valves from continuous commutation failure during an AC voltage drop.

■ Control scheme for expansion of the existing LCC-based installations:

- This control scheme is mostly suitable for an expansion project with an original single LCC interface, by adding a parallel VSC unit to enable higher capacity and bi-directional power flow.
- The reactive power compensation and harmonic compensation filters for the LCC are already in place.
- The LC-IC's control is generally consistent with the traditional LCC control such as the VDCOL function in the DC support state, while the LC-IC needs a constant extinction angle control against AC voltage sag.
- The LC-IC is controlled by a frequency-based droop in power-sharing and AC frequency support states.

- The VS-IC is controlled by a frequency-DC voltage droop in all states.
- The parallel LCC-VSC configuration accommodates the original LCC system and control in such an expansion scenario, and therefore this control scheme requires certain operational mode detection (e.g., for LCC commutation control for different states). Also, the droop control is only for AC grid support as the DC voltage control mainly follows the traditional VDCOL function.

2.1 Proposed Parallel LCC-VSC - Controlled by LCC-based Installation's Expansion Control Scheme

A generic hybrid AC/DC system with proposed parallel LCC-VSC ICs is shown in Fig. 2.1. The proposed system consists of an AC sub-grid, a DC sub-grid, and parallel VS- and LC-ICs. The AC and DC sub-grids include an aggregated power terminal and an aggregated slack terminal. The slack terminals offer power balancing for the purpose of adjusting voltage/frequency in the AC sub-grid and voltage in the DC sub-grid under the droop-like characteristics.

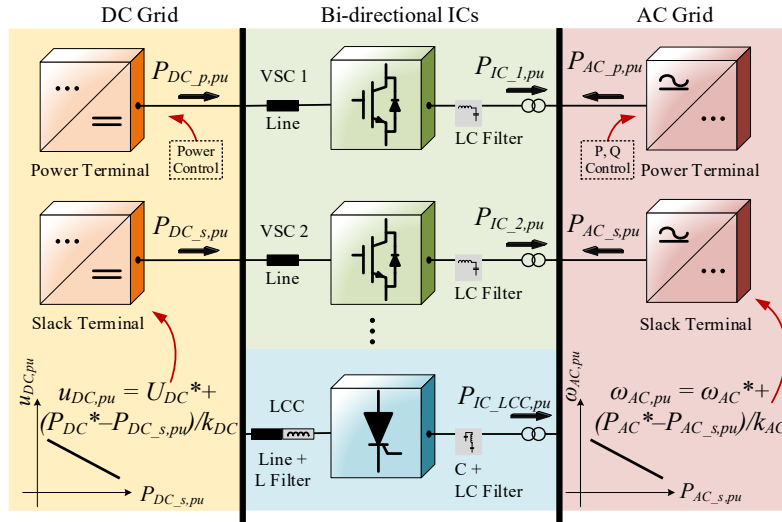


Fig. 2.1: General layout of hybrid AC/DC grid with proposed parallel LCC-VSC interlinking converters.

The aggregated power terminal is including load and generation units targeted for current and power injection/absorption. Renewable energy sources such as

large-scale wind farms can be an example of such a terminal.

The slack terminal is taken as a terminal providing voltage/frequency support (or reference) for the DC and AC sub-grids. The slack terminal is not necessarily an infinite bus, and its stiffness is defined by droop characteristic. The slack terminal's stiffness determines the slope of the droop function (an infinite bus will have zero droop slopes). These features can be found in a more evident way in weak grids. On the other hand, the power terminals are not the voltage/frequency-controlled terminals, and they are only targeted for current and power injection. Clearly, the power units can have different sizes and scales, one as big as a large generation unit such as wind farms.

In this layout, $P_{DC_s,pu}$ and $P_{AC_s,pu}$ represent the per-unit values of AC and DC slack terminal power, respectively, with their positive direction toward IC units. Also, $P_{DC_p,pu}$ and $P_{AC_p,pu}$ are the per-unit values for power terminals in the DC and AC grids, respectively, with their positive direction toward ICs. The per-unit value of the transferred power by the VS-ICs is $P_{IC_i,pu}$ while the per-unit value of the transferred power by the LC-IC is $P_{IC_LCC,pu}$ with their positive direction toward AC sub-grid as shown in Fig. 2.1. For the sake of simplicity, only the AC lines' transformers and the impact of line resistance on the voltage drop across the DC transmission line is taken into consideration.

The proposed unified control scheme consists of a droop equivalent control for the LC-IC and VS-ICs. The operation principles of the proposed unified controls have a direct relationship with the sub-grids state. The AC and DC sub-grids can be controlled off-grid by the droop controls provided in (2.1).

$$\begin{cases} \omega_{AC,pu} = \omega_{AC,pu}^* + (P_{AC,pu}^* - P_{AC_s,pu})/k_{AC} \\ u_{DC,pu} = U_{DC,pu}^* + (P_{DC,pu}^* - P_{DC_s,pu})/k_{DC} \end{cases} \quad (2.1)$$

where $\omega_{AC,pu}$, $\omega_{AC,pu}^*$, $P_{AC,pu}^*$, and $P_{AC_s,pu}$ are the measured grid frequency, the reference frequency, and the reference and measured active powers out of the aggregated slack terminal on the AC grid, respectively. Also, $u_{DC,pu}$, $U_{DC,pu}^*$, $P_{DC,pu}^*$, and $P_{DC_s,pu}$ are the measured DC voltage, the reference DC voltage, and

the reference and measured powers out of the aggregated slack terminal on the DC side. If $P_{AC_B,pu}$ and $P_{DC_B,pu}$ are the rated powers' of the AC and DC sub-grids aggregated slack terminals, respectively, the power ratio between the AC and DC sub-grids can be defined as $P_{AC_B,pu}:P_{DC_B,pu} = K:I$. The power-sharing ratios among parallel IC units directly relate to their power ratings, determined through the droop coefficient factors.

2.2 Modeling of VS-ICs

The exchanged power of the VS-ICs is defined by (2.2), where i represent i -th VS-IC, and this control approach is similar for both proposed unified control schemes. The parallel LCC-VSC-based new installation's control scheme will be introduced in chapter 3.

$$\Delta P_{s_i} = P_{AC_s,pu} - K \times P_{DC_s,pu} \quad (2.2)$$

Substituting (2.1) in (2.2), the difference between AC and DC sub-grids aggregated slack terminals power is defined as (2.3).

$$\Delta P_{s_i} = \left[P_{AC,pu}^* + k_{AC} (\omega_{AC,pu}^* - \omega_{AC,pu}) \right] - K \times \left[P_{DC,pu}^* + k_{DC} (U_{DC,pu}^* - u_{DC,pu}) \right] \quad (2.3)$$

Reflecting the DC line loss's impact in (2.3), the power difference equation changes to (2.4).

$$\Delta P_{s_i} = \left[P_{AC,pu}^* + k_{AC} (\omega_{AC,pu}^* - \omega_{AC,pu}) \right] - K \times \left[P_{DC,pu}^* + k_{DC} (U_{DC,pu}^* - u_{DC,i,pu}) \right] \quad (2.4)$$

The control scheme of the VS-ICs is depicted in Fig. 2.2.

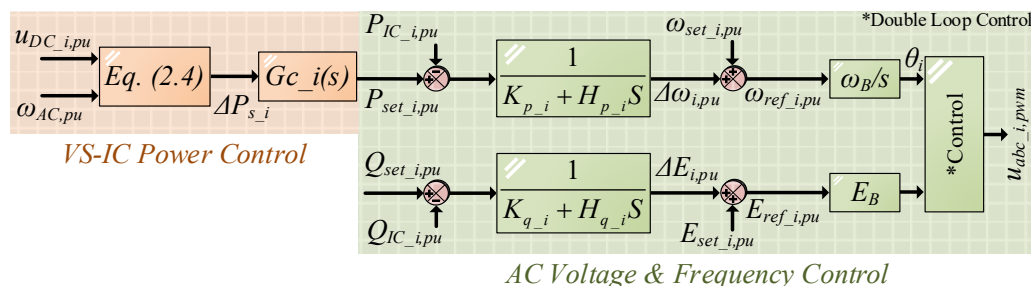


Fig. 2.2: VS-IC's control overview.

Initially, power difference will be calculated as in (2.4) and the active power

reference value is acquired through regulator $G_{c_i}(s)$. The IC's measured active and reactive power will be used in the following for active power–frequency (P - f) and reactive power–voltage (Q - V) droop controls as discussed in [63]-[65]. Finally, determined reference phase-angle and voltage-amplitude values will be tracked, adopting double-loop control [66] for consistent and improved dynamic. The VS-ICs equivalent control signals can be calculated as in (2.5) and (2.6).

$$\begin{cases} H_{p_i} \frac{d\Delta\omega_{i,pu}}{dt} = (P_{set_{i,pu}} - P_{IC_{i,pu}}) - K_{p_i} \Delta\omega_{i,pu} \\ \omega_{ref_{i,pu}} = \omega_{set_{i,pu}} + \Delta\omega_{i,pu} \end{cases} \quad (2.5)$$

$$\begin{cases} H_{q_i} \frac{d\Delta E_{i,pu}}{dt} = (Q_{set_{i,pu}} - Q_{IC_{i,pu}}) - K_{q_i} \Delta E_{i,pu} \\ E_{ref_{i,pu}} = E_{set_{i,pu}} + \Delta E_{i,pu} \end{cases} \quad (2.6)$$

The small-signal model of the (P - f) droop control is given in Fig. 2.3 [64],[67], [68].

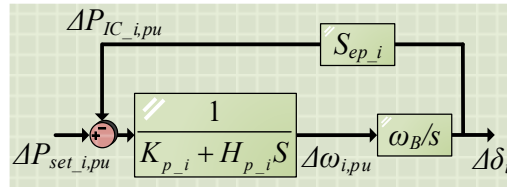


Fig. 2.3: Line frequency small signal model of the VSC's P - f droop.

In Fig. 2.3, S_{ep_i} is given in (2.7).

$$S_{ep_i} = \sqrt{\left(\frac{3E_i U_i}{2X_i} \Delta\delta_i\right)^2 - P_{i0}^2} / S_B \quad (2.7)$$

The closed-loop transfer function of the VS-IC's (P - f) droops control, as given in Fig. 2.3, is provided in (2.8).

$$G_{p_i}(s) = \frac{(\omega_{n_i})^2}{s^2 + 2\zeta_i \omega_{n_i} s + (\omega_{n_i})^2} \quad (2.8)$$

The dynamic of the VS-IC's (P - f) droop can be designed considering ζ_i and t_{s_i} [59] as given in (2.9).

$$\zeta_i = \frac{K_{p_i}}{2\sqrt{S_{ep_i}\omega_B H_{p_i}}}, t_{s_i} = \frac{3.5}{\zeta_i \omega_{n_i}} = \frac{7H_{p_i}}{K_{p_i}} \quad (2.9)$$

Using exchanged power signal (2.4) and the VS-IC's (P - f) droop transfer function (2.8), the exchanged power by i -th VS-IC can be defined as follow:

$$P_{IC_i,pu} = \left(\left[P_{AC,pu}^* + k_{AC}(\omega_{AC,pu}^* - \omega_{AC,pu}) \right] - K \times \left[P_{DC,pu}^* + k_{DC}(U_{DC,pu}^* - u_{DC_i,pu}) \right] \right) G_{c_i}(s) G_{p_i}(s) \quad (2.10)$$

$$G_{c_i}(s) = \eta_i \frac{1 + \tau_{l_i}s}{1 + \tau_{d_i}s} \quad (2.11)$$

where $G_{c_i}(s)$ in (2.11) is defined as a proportional gain and phase compensation transfer function. The proportional gain's value, η_i , is the subject of the rated capacity of the i -th VS-IC.

2.3 Modeling of the LC-IC

The LC-IC control scheme will be developed using a conventional (V - I) graph of the point-to-point thyristor-based DC system, as depicted in Fig. 2.4, to improve the design procedure's simplicity.

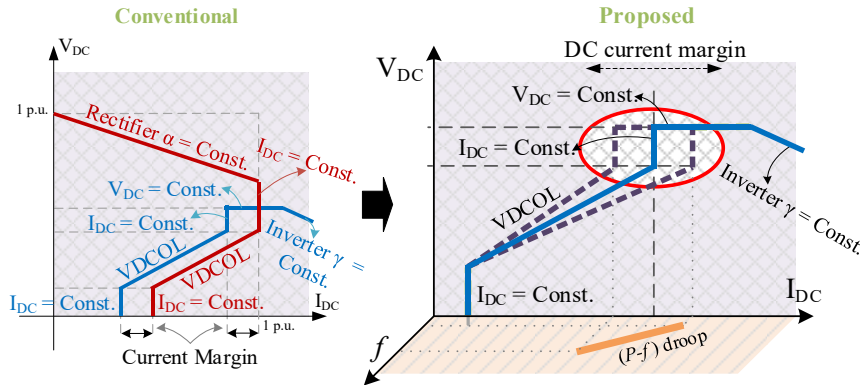


Fig. 2.4: Point-to-point LCC-based DC system's conventional control method (example: rectifier current-controlled inverter voltage-controlled) and LC-IC's proposed (f - P) droop control system.

The conventional inverter side thyristor-based LCC's (V - I) graph usually consists of four operation regions [69]. These operation regions are: constant current control, VDCOL, constant voltage control, and constant extinction angle control. The modeling procedure can be different for each scheme in some states.

Therefore, mutual and distinct modelings for each scheme are discussed separately.

2.3.1 Modeling of LC-IC's Proposed Control Scheme

The small-signal model of LC-IC's power control and constant extinction angle control will be commonly used for both proposed control schemes (control scheme for expansion of the existing LCC-based installations in this chapter and controls scheme for new installations with parallel LCC-VSCs interlinking units in the chapter 3). The power control loop is the LC-IC's small-signal response models in the grid frequency. Also, the constant extinction angle control loop is the small-signal model of LC-IC response to avoid continuous commutation failure in case of AC voltage drops.

■ The small-signal model of the LC-IC power control

By neglecting the losses and assuming balanced performance for the LC-IC, it can be expected that the exchanged active power on the AC and DC side are equal $P_{DC_LCC} = P_{AC_LCC}$. Therefore, the following equations can be defined, given in (2.12) and (2.13).

$$\begin{cases} P_{DC,pu} = u_{DC_LCC,pu} I_{DC_LCC,pu} \\ P_{AC,pu} = 3E_{pu} I_{AC_LCC,pu} \cos(\varphi) \end{cases} \quad (2.12)$$

$$\begin{cases} u_{DC_LCC,pu} = u_{DC0_LCC,pu} \cos(\beta) + \Delta u_{DC_LCC,pu} \\ I_{DC,pu} = \frac{\sqrt{2}E_{L-L,pu}}{2\omega_{AC,pu}L_t} (\cos(\gamma) - \cos(\beta)) \\ u_{DC0_LCC,pu} = \frac{3\sqrt{2}}{\pi} E_{L-L,pu}, \Delta u_{DC_LCC,pu} = \frac{3}{\pi} \omega_{AC,pu} L_t I_{DC_LCC,pu} \end{cases} \quad (2.13)$$

The voltage lost as a result of overlap can be found in [69], [63]. Then a small-signal model of the LC-IC in grid frequency can be derived as depicted in Fig. 2.5 considering (2.13). The small-signal model of the LC-IC's power control is standard for both control schemes.

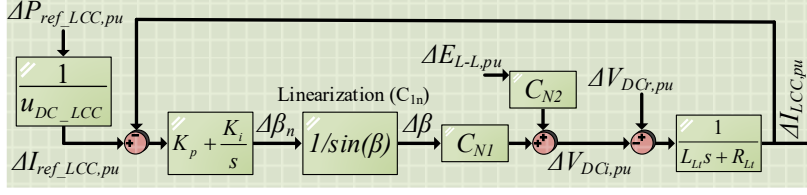


Fig. 2.5: Line frequency small-signal model of the LC-IC power control.

In this model, C_{N1} and C_{N2} are as given in (2.14):

$$\begin{cases} C_{N1} = \frac{3\sqrt{2}}{\pi} n_B E_{L-L0,pu} \sin(\beta_0) \\ C_{N2} = \frac{3\sqrt{2}}{\pi} n_B \cos(\beta_0) \end{cases} \quad (2.14)$$

Based on Fig. 2.5, the small-signal model of the LC-IC's power control can be calculated as given in (2.15).

$$\begin{cases} G_{LCC_D}(s) = \frac{-K_p C_{N1} s - K_i C_{N1}}{G_{LCC_D_Denom}(s)} \\ G_{LCC_D_Denom}(s) = L_L \sin(\beta_0) s^2 + (R_L \sin(\beta_0) - K_p C_{N1}) s - K_i C_{N1} \end{cases} \quad (2.15)$$

■ The small-signal model of the LC-IC constant extinction angle control

The constant extinction angle control is another control scheme adopted by LC-IC during the AC sub-grids voltage sag to prevent commutation failure. The control scheme will help the converter ride through the fault and minimize the possibility of continuous commutation failure. In this regard, the LC-ICs DC link voltage (2.13) should be rewritten as (2.16).

$$\begin{cases} u_{DC_LCC,pu} = u_{DC0_LCC,pu} \cos(\gamma) - \Delta u_{DC,pu} \\ u_{DC0_LCC,pu} = \frac{3\sqrt{2}}{\pi} E_{L-L,pu} \\ \Delta u_{DC,pu} = \frac{3}{\pi} \omega L_t I_{DC_LCC,pu} \end{cases} \quad (2.16)$$

Using (2.16) the LC-IC's small-signal model, operating in constant extinction angle control can be designed, as shown in Fig. 2.6.

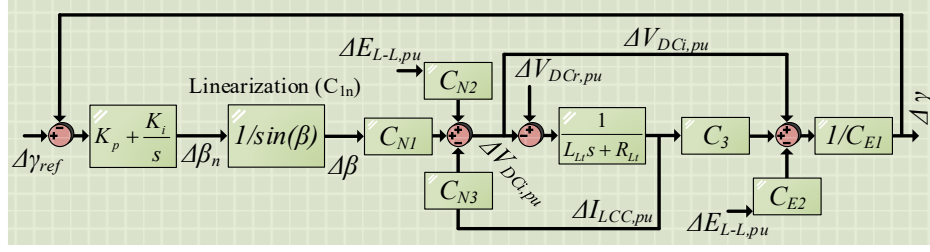


Fig. 2.6: Line frequency small-signal model of the LC-IC constant extinction angle control.

The constants C_{E1} , C_{E2} , and C_3 are defined as (2.17):

$$\begin{cases} C_{E1} = \frac{3\sqrt{2}}{\pi} n_B E_{L-L0,pu} \sin(\gamma_0) \\ C_{E2} = \frac{3\sqrt{2}}{\pi} n_B \cos(\gamma_0) \\ C_3 = \frac{3}{\pi} n_B \omega L_t \end{cases} \quad (2.17)$$

Using Fig. 2.6 and (2.17), the LC-IC's small-signal transfer function, operating in constant extinction angle control mode, is calculated as given in (2.18).

$$\begin{cases} G_{LCC_C}(s) = \frac{G_{LCC_C_Num}(s)}{G_{LCC_C_Denom}(s)} \\ G_{LCC_C_Num}(s) = C_{N1} K_p L_{L_t} s^2 + C_{N1} [(R_{L_t} - 2C_3) K_p + K_i L_{L_t}] s + C_{N1} K_i (R_{L_t} - 2C_3) \\ G_{LCC_C_Denom}(s) = (\sin(\beta_0) C_{E1} L_{L_t} + C_{N1} K_p L_{L_t}) s^2 + \\ \quad \{ [(R_{L_t} - 2C_3) K_p + K_i L_{L_t}] C_{N1} + (R_{L_t} - C_3) C_{E2} \sin(\beta_0) \} s + C_{N1} K_i (R_{L_t} - 2C_3) \end{cases} \quad (2.18)$$

The LC-IC's constant extinction angle-controlled DC current is calculated as follows.

$$I_{DC_LCC,pu} = \frac{\sqrt{2} E_{L-L,pu}}{2 \omega_{AC,pu} L_t} [\cos(\gamma) - \cos(\gamma + \mu)] \quad (2.19)$$

Linearizing (2.19) using the Taylor expansion $\cos(x) = \sum_{n=0}^{\infty} \frac{(-1)^n}{(2n)!} x^{2n}$ and taking $n = 1$ and applying (2.18) to it, (2.20) can be calculated:

$$I_{DC_LCC,pu} = \frac{\sqrt{2}E_{L-L,pu}}{4\omega L_t} (2\mu\gamma_{ref}G_{LCC_c}(s) + \mu^2) \quad (2.20)$$

There are several techniques to measure or predict the value of γ_{ref} [70]-[72], [73]. The details of these procedures are out of the scope of this work to study. The LC-IC's transmitted power for constant extinction angle control is determined in (2.21).

$$P_{IC_LCC,pu} = \frac{\sqrt{2}u_{DC_LCC,pu}E_{L-L,pu}}{4\omega L_t} \times (2\mu\gamma_{ref}G_{LCC_c}(s) + \mu^2) \quad (2.21)$$

2.3.2 Modeling of LC-IC's Droop Equivalent Control for the Proposed LCC-based Installation's Expansion

The constant current control mode repurposed to adopt droop equivalent control for the system's power-sharing and AC frequency support operation states. Provided in Fig. 2.4, the constant current control region of the conventional ($V-I$) graph can be modified to the ($P-f$) droop equivalent control. Then, the following control system, as shown in Fig. 2.7, can be defined.

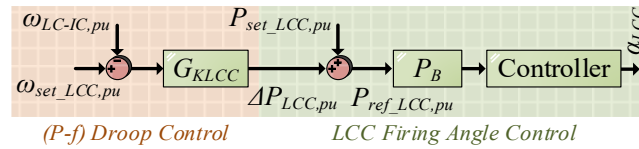


Fig. 2.7: LC-IC's control overview for LCC-based installations expansion control scheme.

The LC-IC's control function is shown in (2.22).

$$\begin{cases} \Delta P_{LCC,pu} = G_{KLCC}(\omega_{set_LCC,pu} - \omega_{LC-IC,pu}) \\ P_{ref_LCC,pu} = P_{set_LCC,pu} + \Delta P_{LCC,pu} \end{cases} \quad (2.22)$$

The G_{KLCC} is defined as $1/(K_{LCC}+H_{LCC}s)$. The inertia function prevents sudden changes in the power value that can affect commutation. Taking proposed droop equivalent control of the LC-IC's for existing installations (2.22) and the small-signal model of the LC-IC's power control (2.15), the exchanged power by LC-IC can be defined, as given in (2.23).

$$P_{IC_LCC,pu} = \left(P_{set_LCC,pu} + [\omega_{AC,pu}^* - \omega_{AC,pu}] G_{KLCC}(s) \right) G_{LCC_D}(s) \quad (2.23)$$

2.3.3 Modeling of LC-IC's VDCOL Control for the Proposed LCC-based Installations Expansion

LC-IC should adopt the VDCOL control scheme in case of a significant voltage drop on the DC sub-grid. Based on the VDCOL control principles, the DC current's value should be adjusted according to the DC voltage level. In this mode, the controller adopts a predetermined VDCOL function based on power system specifications. In this state, the control scheme uses the LC-IC's power control loop to operate. The VDCOL function will be defined as (2.24):

$$P_{IC_LCC,pu} = \left(P_{set_LCC,pu} - [U_{DC,pu}^* - u_{DC_LCC,pu}] \times G_{DLCC}(s) \right) G_{LCC_D}(s) \quad (2.24)$$

where $G_{DLCC}(s)$ is defined to prevent the abrupt changes to the reference value. It is defined as $G_{DLCC}(s) = 1/(K_d + K_g s)$. The details around the VDCOL function and its design procedure can be found in [73] and [74]-[76].

2.4 Operation Modes and Stability Studies

The power system's operation is divided into three main states: power-sharing, DC support, and AC support.

The exchanged power by ICs in every operation state with both control schemes (LCC-based installations expansion control scheme in this chapter and new LCC-based installations in chapter 3) can be defined as (2.25).

$$P_{IC,pu} = P_{IC_LCC,pu} + \sum_{i=1}^N P_{IC_i,pu} \quad (2.25)$$

Locally measured DC voltage $u_{DC_LCC,pu}$ and $u_{DC_i,pu}$ for both LC- and VS-ICs will be substituted with DC sub-grids busbar voltage $u_{DC,pu}$. Therefore, the DC transmission line voltage drop should be replaced in calculations as given (2.26).

$$u_{DC,pu} = \begin{cases} R_{i,pu} P_{IC_i,pu} + u_{DC_i,pu} \\ \text{And} \\ R_{t,pu} P_{IC_LCC,pu} + u_{DC_LCC,pu} \end{cases} \quad (2.26)$$

The DC voltage in VS-ICs and LC-IC exchanged power based on the control schemes 1, (2.10) and (2.24), are altered in the form of (2.27) and (2.28), to represent DC voltage loss, respectively.

$$\begin{cases} P_{IC_i,pu} = \left(\left[P_{AC,pu}^* + k_{AC} (\omega_{AC,pu}^* - \omega_{AC,pu}) \right] - \right. \\ \quad \left. K \times \left[P_{DC,pu}^* + k_{DC} (U_{DC,pu}^* - u_{DC,pu}) \right] \right) G_{IC_i}(s) \\ G_{IC_i}(s) = \frac{G_{c_i}(s) G_{p_i}(s)}{(1 + K k_{DC} R_{i,pu} G_{c_i}(s) G_{p_i}(s))} \end{cases} \quad (2.27)$$

$$\begin{cases} P_{IC_LCC,pu} = \left(P_{set_LCC,pu} - \left[U_{DC,pu}^* - u_{DC,pu} \right] \times G_{DLCC}(s) \right) G_{LCC_D}(s) \\ G_{LCC_DN}(s) = \frac{G_{LCC_D}(s)}{1 - R_t G_{DLCC}(s) G_{LCC_D}(s)} \end{cases} \quad (2.28)$$

As discussed previously, the VS-IC control scheme uses droop control with inertia on its inner loop and phase compensation with a proportional gain for the outer loop [59]. The inner-loop droop function improves the system's dynamics and stability while giving droop equivalent features to the control scheme. The phase compensation function, $G_{c_i}(s)$, specifies its respected VS-IC's rated capacity and improves the system's stability and dynamics. An inertia function is designed for the LC-IC control schemes to establish a droop equivalent control as well as improve the stability and dynamics of the system. The inertia of the LC-IC's droop equivalent control is one of the parameters that should be designed carefully for better stability and dynamics.

a. Power-sharing Operation

In the power-sharing operation state, AC sub-grids voltage/frequency and DC sub-grids voltage are controlled by aggregated slack terminals on AC and DC sub-grids while ICs share power based on proposed control schemes.

The LC-IC and VS-ICs follow the control schemes provided in the previous

section in all operating states. The operation state of the system in the power-sharing condition can be defined as follow:

$$\begin{cases} P_{AC_s,pu} + P_{AC_p,pu} + P_{IC,pu} = 0 \\ P_{DC_s,pu} + P_{DC_p,pu} - P_{IC,pu} = 0 \\ \omega_{AC,pu} = \omega_{AC,pu}^* + (P_{AC,pu}^* + P_{AC_p,pu} + P_{IC,pu})/k_{AC} \\ u_{DC,pu} = U_{DC,pu}^* + (P_{DC,pu}^* + P_{DC_p,pu} - P_{IC,pu})/k_{DC} \end{cases} \quad (2.29)$$

The system's operation state is independent of the ICs control scheme and defined based on the power grid and aggregated slack terminals control. The exchanged power in the power-sharing state can be different for both proposed schemes. Therefore, each control scheme will be studied separately.

■ IC's exchanged power based on the LCC-based installations expansion control scheme in a power-sharing state

The steady-state representation of transferred power for each group of the ICs following the LCC-based installations expansion control scheme is calculated in (2.30).

$$\left\{ \begin{aligned}
P_{IC_i,pu} &= \frac{-(1+K) \sum_{i=1}^N G_{IC_i}(0)}{G_{IC_i_Denom,pu}(s)} \times \left[P_{set_LCC,pu} G_{LCC_D}(0) - P_{AC,pu}^* \frac{G_{iLCC}(0)}{k_{AC}} \right] + \\
&\quad \frac{KG_{IC_i}(0) \left(1 + \frac{G_{iLCC}(0)}{k_{AC}} \right) P_{DC_P,pu} - G_{IC_i}(0) \left(1 - \frac{G_{iLCC}(0)}{k_{AC}} \right) P_{AC_P,pu}}{G_{IC_i_Denom,pu}(s)} \\
P_{IC_LCC,pu} &= \frac{1+(1+K) \sum_{i=1}^N G_{IC_i}(0)}{G_{IC_i_Denom,pu}(s)} \times \left[P_{set_LCC,pu} G_{LCC_D}(0) - P_{AC,pu}^* \frac{G_{iLCC}(0)}{k_{AC}} \right] - \\
&\quad \frac{\frac{G_{iLCC}(0)}{k_{AC}} K \sum_{i=1}^N G_{IC_i}(0) P_{DC_P,pu} - \frac{G_{iLCC}(0)}{k_{AC}} \left(1 + K \sum_{i=1}^N G_{IC_i}(0) \right) P_{AC_P,pu}}{G_{IC_i_Denom,pu}(s)} \\
G_{IC_i_Denom,pu}(s) &= 1 + (1+K) \sum_{i=1}^N G_{IC_i}(0) + \frac{G_{iLCC}(0)}{k_{AC}} \\
P_{IC,pu} &= P_{IC_LCC,pu} + \sum_{i=1}^N P_{IC_i,pu}, \quad G_{IC_i}(0) = \eta_i / (1 + Kk_{DC}R_{i,pu}\eta_i) \\
G_{iLCC}(0) &= 1 / K_{LCC}, \quad G_{LCC_D}(0) = 1
\end{aligned} \right. \quad (2.30)$$

■ IC's exchanged power based on the LCC-based installation expansion control scheme in the power-sharing state

The representation of the exchanged power by ICs assuming the parallel LCC-VSC-based new installation's control scheme will be as (2.31)

$$\left\{ \begin{aligned}
\Delta P_{IC,pu} &= \frac{G_{IC}(s)}{1+(1+K)G_{IC}(s)} \times (K\Delta P_{DC_P,pu} - \Delta P_{AC_P,pu}) \\
G_{IC}(s) &= G_{NLCC}(s) + \sum_{i=1}^N G_{IC_i}(s)
\end{aligned} \right. \quad (2.31)$$

The steady-state representation of the IC's exchanged-power based on the parallel LCC-VSC-based new installation's control scheme can be found in (2.32).

$$\begin{cases} P_{IC_i,pu} = \frac{\eta_i / (1 + Kk_{DC}R_{i,pu}\eta_i)}{1 + (1 + K)G_{IC}(0)} \times (KP_{DC_P,pu} - P_{AC_P,pu}) \\ P_{IC_LC,pu} = \frac{1/K_{p_l}}{1 + (1 + K)G_{IC}(0)} \times (KP_{DC_P,pu} - P_{AC_P,pu}) \\ G_{IC}(0) = 1/K_{p_l} + \sum_{i=1}^N \eta_i / (1 + Kk_{DC}R_{i,pu}\eta_i) \end{cases} \quad (2.32)$$

b. AC sub-grid Support

The aggregated slack terminal on the AC sub-grid has lost control over the AC sub-grids' voltage and frequency. However, the DC sub-grid operation is intact. In this condition and under the proposed unified control principles, the ICs should maintain the voltage level and frequency of the AC sub-grid within the desired range.

In this condition, the operation state can be defined as given in (2.33). The operation state is valid for both proposed control schemes (LCC-based installations expansion control scheme in this chapter and new parallel LCC-VSCs-based installations control scheme in chapter 3).

$$\begin{cases} P_{AC_p,pu} + P_{IC,pu} = 0 \\ P_{DC_s,pu} + P_{DC_p,pu} + P_{AC_p,pu} = 0 \\ u_{DC,pu} = U_{DC,pu}^* + (P_{DC,pu}^* + P_{DC_p,pu} - P_{IC,pu}) / k_{DC} \end{cases} \quad (2.33)$$

■ IC's AC sub-grid frequency support based on the LCC-based installations expansion control scheme

The proposed LCC-based installations expansion control scheme is designed to regulate the AC sub-grid frequency and voltage level. In this state, the transition from power-sharing operation to AC support will be without mode detection. The frequency's reference value can be defined as a function of proposed frequency-based droop equivalent control, given in (2.34):

$$\omega_{ref,pu} = \omega_{set_i,pu} + \frac{\left[\left[P_{AC,pu}^* + \frac{k_{AC}}{G_{KLCC}(s)} \left(\frac{P_{IC_LCC,pu}}{G_{LCC_D}(s)} - P_{set_LCC,pu} \right) \right] \right]}{K_{p_i} + H_{p_i}s} - \frac{K \left[P_{DC,pu}^* + k_{DC} (U_{DC,pu}^* - u_{DC_i,pu}) \right] G_{c_i}(s) - P_{IC_i,pu}}{K_{p_i} + H_{p_i}s} \quad (2.34)$$

By applying the operation state of the system in this condition (2.33) to the IC's exchanged power function, the following equations can be computed:

$$\begin{cases} P_{IC_i,pu} = \left\{ \left[P_{AC,pu}^* + k_{AC} (\omega_{AC,pu}^* - \omega_{AC,pu}) \right] + K \left[P_{DC_p,pu} + P_{AC_p,pu} \right] \right\} G_{IC_i}(s) \\ P_{IC_LCC,pu} = \left\{ P_{set_LCC,pu} + (\omega_{AC,pu}^* - \omega_{AC,pu}) G_{KLCC}(s) \right\} G_{LCC_D}(s) \\ P_{IC,pu} = P_{IC_LCC,pu} + \frac{P_{IC_i,pu}}{G_{IC_i}(s)} \sum_{i=1}^N G_{IC_i}(s) \end{cases} \quad (2.35)$$

The stability of the system in this condition is subject to the stability of $G_{IC_i}(s)$, $G_{LCC_D}(s)$, and $G_{ILCC}(s)$. Considering that the stability of these functions is guaranteed, then the stability of the (2.35) can be confirmed. The steady-state value of frequency and exchanged power by LC-IC and VS-ICs can be calculated as given in (2.36).

$$\begin{cases} \omega_{AC,pu} = \omega_{AC,pu}^* + \frac{P_{AC_p,pu} + P_{set_LCC,pu} + P_{AC,pu}^* \sum_{i=1}^N G_{IC_i}(0) + K (P_{DC_p,pu} + P_{AC_p,pu}) \sum_{i=1}^N G_{IC_i}(0)}{\frac{1}{K_{LCC}} + k_{AC} \sum_{i=1}^N G_{IC_i}(0)} \\ P_{IC_i,pu} = \left\{ \left[P_{AC,pu}^* + k_{AC} (\omega_{AC,pu}^* - \omega_{AC,pu}) \right] + K \left[P_{DC_p,pu} + P_{AC_p,pu} \right] \right\} G_{IC_i}(0) \\ P_{IC_LCC,pu} = P_{set_LCC,pu} - \frac{1}{k_{AC} K_{LCC}} (\omega_{AC,pu}^* - \omega_{AC,pu}) \\ G_{IC_i}(0) = \eta_i / (1 + K k_{DC} R_{i,pu} \eta_i) \end{cases} \quad (2.36)$$

■ IC's AC sub-grid voltage support

In the case of voltage sag in the AC sub-grid, as explained previously, continuous commutation failure is likely for the LC-IC. To avoid such an outcome,

the supporting role of the VS-ICs and the LC-IC's constant extinction angle control scheme should be under effect. The LC-IC's commutation failure can be seen as a DC short circuit on the LCCs' DC end. Although such an incident is predictable for the LCCs, and circuit components are designed to withstand such conditions, the impact of continuous commutation failure can affect the DC sub-grid voltage, and also it can be damaging for a particular type of parallel VS-ICs technologies. The conventional multilevel inverters and MMC VSCs are commonly used in the current power grid that can undertake some devastating impacts due to short circuit. Therefore, it is important to limit such incidents in the power system. The system's operation state is also intact and is similar to the AC sub-grid support as given in (2.33). Also, VS-IC's control system maintains its scheme as before, which will also help the system get out the fault faster.

The control system will take constant extinction angle control for LC-IC in both proposed schemes in such a condition to limit or stop commutation failure. In this method, the LCC valves' firing angles are determined to impose the safest extinction angles while limiting the reactive power consumption to the lowest possible amount. The reference frequency signal in this circumstance will change to (2.37) due to a change in LC-IC's control system.

$$\omega_{ref,pu} = \omega_{set_i,pu} + \frac{\left\{ \left[P_{AC,pu}^* + k_{AC} (\omega_{AC,pu}^* - \omega_{AC,pu}) \right] - K \left[P_{DC,pu}^* + k_{DC} (U_{DC,pu}^* - u_{DC_i,pu}) \right] \right\} G_{c_i}(s) - P_{IC_i,pu}}{K_{p_i} + H_{p_i}s} \quad (2.37)$$

Using the LC-IC's constant extinction angle controlled exchanged power function (2.21), the overall transferred power by the ICs are recalculated as given in (2.38).

$$\begin{cases} P_{IC_i,pu} = \left\{ \left[P_{AC,pu}^* + k_{AC} (\omega^* - \omega) \right] + K \left[P_{DC_p,pu} + P_{AC_p,pu} \right] \right\} G_{IC_i}(s) \\ P_{IC_LCC,pu} = \frac{\sqrt{2}u_{DC-LCC,pu}V_{L-L,pu}}{4\omega L_t} (2\mu\gamma_{ref} G_{LCC_C}(s) + \mu^2) \\ P_{IC,pu} = P_{IC_LCC,pu} + \frac{P_{IC_i,pu}}{G_{IC_i}(s)} \sum_{i=1}^N G_{IC_i}(s) \end{cases} \quad (2.38)$$

The ICs will continue to work in this mode of operation until the AC voltage on the AC sub-grid recovers to its standard range. The output power of the LC-IC, as stated, in this condition is controlled by a constant extinction angle control loop. Thus, its impact on frequency is subject to the AC system voltage level than its frequency. The stability of the system in this mode is a subject of the stability of G_{LCC_C} in $P_{IC_LCC,pu}$, and G_{IC_i} in $P_{IC,pu}$. The stability of these two transfer functions is guaranteed. Then, it can be concluded that the stability of the (2.38) is also guaranteed.

Steady-state representation of the system in this condition is provided in (2.39).

$$\begin{cases} \omega_{AC,pu} = \omega_{AC,pu}^* + \frac{P_{AC_p,pu} + \frac{\sqrt{2}u_{DC-LCC,pu}V_{L-L,pu}}{4\omega L_t} (2\mu\gamma_{ref} + \mu^2)}{k_{AC} \sum_{i=1}^N \eta_i / (1 + Kk_{DC}R_{i,pu}\eta_i)} + \frac{\left[P_{AC,pu}^* + K(P_{DC_p,pu} + P_{AC_p,pu}) \right]}{k_{AC}} \\ P_{IC_i,pu} = \left\{ \left[P_{AC,pu}^* + k_{AC} (\omega^* - \omega) \right] + K \left[P_{DC_p,pu} + P_{AC_p,pu} \right] \right\} G_{IC_i}(0) \\ P_{IC_LCC,pu} = \frac{\sqrt{2}u_{DC-LCC,pu}V_{L-L,pu}}{4\omega L_t} (2\mu\gamma_{ref} + \mu^2) \end{cases} \quad (2.39)$$

c. DC sub-grid Support

In this mode, the DC sub-grid loses its control over DC voltage. ICs can support the DC voltage by injecting the required power from the AC sub-grid to the DC sub-grid or decreasing the value of the exchanged power from the DC sub-grid to the AC sub-grid. In this condition, the system's operation state can be discussed as:

$$\begin{cases} P_{AC_s,pu} + P_{AC_p,pu} + P_{DC_p,pu} = 0 \\ \omega_{AC,pu} = \omega_{AC,pu}^* + (P_{AC,pu}^* + P_{AC_p,pu} + P_{IC,pu}) / k_{AC} \\ \dot{u}_{DC,pu} CU_{dcB} / S_B = P_{DC_p,pu} - P_{IC,pu} \end{cases} \quad (2.40)$$

In (2.40) C represents the equivalent capacitance of the DC sub-grid. The LC-IC's control in this state will be different for each proposed scheme. The LCC-based installations expansion control scheme, as explained previously, will use the VDCOL function to support the grid against DC voltage control loss.

■ IC's DC sub-grid voltage support based on the LCC-based installations expansion control scheme

By detecting the DC voltage drop on the DC sub-grid, the LC-IC will adopt the VDCOL control. The VS-ICs will either decrease transferred power from DC to AC sub-grid or reverse the exchanged power from AC to DC sub-grid all by changing $P_{set_i,pu}$.

The ICs exchanged power in this operation mode is calculated as in (2.41). As can be seen in (2.41), $P_{IC_LCC,pu}$, is a function of the VDCOL graph, in which the exchanged power by LC-IC alters by a change in DC voltage.

$$\begin{cases} P_{IC_i,pu} = -\left([P_{AC_p,pu} + P_{IC,pu}] + K \times [P_{DC,pu}^* + k_{DC} (U_{DC,pu}^* - u_{DC,pu})] \right) G_{IC_i}(s) \\ P_{IC_LCC,pu} = \left(P_{set_LCC,pu} - [U_{DC,pu}^* - u_{DC,pu}] G_{DLCC}(s) \right) G_{LCC_D}(s) \\ G_{LLCC}(s) = G_{DLCC}(s) G_{LCC_D}(s) \\ P_{IC,pu} = P_{IC_LCC,pu} + \sum_{i=1}^N P_{IC_i,pu} \end{cases} \quad (2.41)$$

The steady-state value of the DC voltage on the DC sub-grid terminal and exchanged power by LC- and VS-ICs are given in (2.42) using (2.41).

$$\begin{cases}
u_{DC,pu} = U_{DC,pu}^* + \frac{P_{DC_P,pu} - P_{set_LCC,pu} + (P_{AC_P,pu} + P_{DC_P,pu} + KP_{DC,pu}^*) \sum_{i=1}^N G_{IC_i}(0)}{\frac{1}{k_g} + Kk_{DC} \sum_{i=1}^N G_{IC_i}(0)} \\
P_{IC_i,pu} = - \left(\frac{P_{AC_P,pu} + KP_{DC,pu}^*}{1 + Kk_{DC}k_g \sum_{i=1}^N G_{IC_i}(0)} \right) G_{IC_i}(0) - \\
\quad \left(\frac{Kk_{DC}k_g P_{set_LCC,pu} + P_{DC_P,pu} (1 - Kk_{DC}k_g)}{1 + Kk_{DC}k_g \sum_{i=1}^N G_{IC_i}(0)} \right) G_{IC_i}(0) \\
P_{IC_LCC,pu} = \frac{(Kk_{DC}k_g P_{set_LCC,pu}) \sum_{i=1}^N G_{IC_i}(0)}{1 + Kk_{DC}k_g \sum_{i=1}^N G_{IC_i}(0)} + \\
\quad \frac{(P_{AC_P,pu} + KP_{DC,pu}^* + P_{DC_P,pu}) \sum_{i=1}^N G_{IC_i}(0)}{1 + Kk_{DC}k_g \sum_{i=1}^N G_{IC_i}(0)} \\
\quad + \frac{P_{DC_P,pu}}{1 + Kk_{DC}k_g \sum_{i=1}^N G_{IC_i}(0)} \\
G_{IC_i}(0) = \eta_i / (1 + Kk_{DC}R_{i,pu}\eta_i)
\end{cases} \quad (2.42)$$

In the proposed unified control scheme, the VDCOL function can be designed to follow specific pattern based on the LCCs' grid's features as depicted in Fig. 2.8. The details around the design of the VDCOL function can be found in [86].

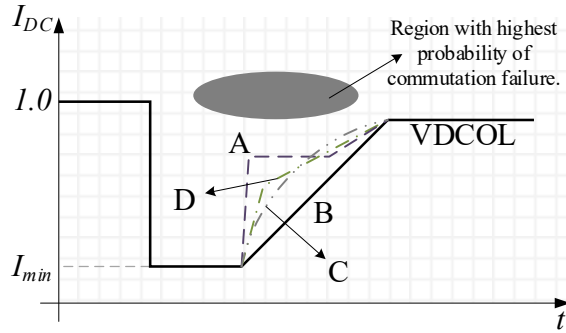


Fig. 2.8: The respond function of VDCOL control scheme.

■ IC's DC sub-grid voltage support based on the parallel LCC-VSC-based new installation's control scheme

In the proposed parallel LCC-VSC-based new installation's control scheme,

the ICs will be more integrated to support the DC sub-grid voltage. Considering the system's operation state as given in (43) and the control scheme of the ICs, the exchanged power will be computed as given in (2.43).

$$\begin{cases} P_{IC_i,pu} = -\left\{ \left[P_{AC_P,pu} + P_{IC,pu} \right] + K \times \left[P_{DC,pu}^* + k_{DC} \left(U_{DC,pu}^* - u_{DC,pu} \right) \right] \right\} G_{IC_i}(s) \\ P_{IC_LCC,pu} = -\left\{ \left[P_{AC_P,pu} + P_{IC,pu} \right] + K \times \left[P_{DC,pu}^* + k_{DC} \left(U_{DC,pu}^* - u_{DC,pu} \right) \right] \right\} G_{NLCC}(s) \\ P_{IC,pu} = P_{IC_LCC,pu} + \sum_{i=1}^N P_{IC_i,pu} \end{cases} \quad (2.43)$$

Using (2.43), the DC voltage dynamic can be calculated as (2.44).

$$\begin{cases} \Delta u_{DC,pu} = \Delta P_{DC_P,pu} G_{D0}(s) + \left[\Delta P_{AC_P,pu} + K \left(\Delta P_{DC,pu}^* + k_{DC} \Delta U_{DC,pu}^* \right) \right] G_{D1}(s) \\ G_{D0}(s) = \frac{1 + G_{NLCC}(s) + \sum_{i=1}^N G_{IC_i}(s)}{G_{D_Denom}(s)} \\ G_{D1}(s) = \frac{G_{NLCC}(s) + \sum_{i=1}^N G_{IC_i}(s)}{G_{D_Denom}(s)} \\ G_{D_Denom}(s) = s \frac{CU_{dcB}^2}{S_B} \left(1 + G_{NLCC}(s) + \sum_{i=1}^N G_{IC_i}(s) \right) + \\ Kk_{DC} \left(G_{NLCC}(s) + \sum_{i=1}^N G_{IC_i}(s) \right) \end{cases} \quad (2.44)$$

Using (2.43) and (2.44), the steady-state value of the DC sub-grid voltage and ICs transmitted power are calculated as (2.45).

The provided equation shows that both the LC-IC and VS-ICs contribute to the regulation of voltage, which can be affected by controlling factors, as explained previously.

$$\begin{cases}
\Delta u_{DC,pu} = \Delta P_{DC_P,pu} G_{D0}(s) + \left[\Delta P_{AC_P,pu} + K(\Delta P_{DC,pu}^* + k_{DC} \Delta U_{DC,pu}^*) \right] \frac{1}{Kk_{DC}} \\
G_{D0}(s) = \frac{1}{Kk_{DC} \left(\frac{1}{K_{p_l}} + \sum_{i=1}^N \eta_i / (1 + Kk_{DC} R_{i,pu} \eta_i) \right)} + \frac{1}{Kk_{DC}} \\
P_{IC_i,pu} = P_{DC_P,pu} \times \frac{\eta_i / (1 + Kk_{DC} R_{i,pu} \eta_i)}{\frac{1}{K_{p_l}} + \sum_{i=1}^N \eta_i / (1 + Kk_{DC} R_{i,pu} \eta_i)} \\
P_{IC_LCC,pu} = P_{DC_P,pu} \times \frac{\frac{1}{K_{p_l}}}{\frac{1}{K_{p_l}} + \sum_{i=1}^N \eta_i / (1 + Kk_{DC} R_{i,pu} \eta_i)}
\end{cases} \quad (2.45)$$

2.5 Real-time Simulation Results

Real-time simulation is performed by Opal-RT (OP5600) as provided in Fig. 2.9 with 25 μ s sampling frequency to verify the proposed LCC-based installations expansion control scheme. In this test, the hybrid AC/DC grid is used, as depicted in Fig. 2.1. The provided grid is modeled into five zones, engaging 5 CPU cores. The grid parameters are selected as provided in Table 2.1 for the LCC-based installations expansion control scheme. The test examines the accuracy of controlling parameters design and proposed procedure. Also, it includes examining the system response and control schemes by forcing the system's state from power-sharing to AC or DC sub-grid support in both techniques.



Fig. 2.9: Opal-RT real-time simulator.

■ Real-time simulation test for the LCC-based installations expansion control scheme

The real-time simulation for the LCC-based installations expansion control scheme starts with AC sub-grid support test. The AC and DC power terminals' values are -1 MW (-1 *p.u.*) and 0.4 MW (0.4 *p.u.*) while the system is in a power-sharing state. The transmitted power by ICs in this state is 0.25 (*p.u.*) and 0.198 (*pu*) for LC-IC and VS-IC, respectively, as shown in Fig. 2.10. The DC voltage and AC frequency also will adapt to the condition by changing to 1.01 (*p.u.*) and 0.998 (*p.u.*), respectively. At 20s, the AC slack terminal loses control over AC sub-grid frequency. The ICs take control of the AC sub-grids frequency by adjusting it to 0.993 (*p.u.*). In the meantime, the DC sub-grids voltage changes to 1.005 (*p.u.*).

TABLE 2.1: GRID PARAMETERS FOR THE LCC-BASED INSTALLATIONS EXPANSION CONTROL SCHEME TEST

System	Parameter	Value	
DC Sub-grid	Rated DC voltage	14 kV	
	DC filter capacitance	10 mH, 0.25 Ω	
	Switching frequency	5 kHz	
	kDC	71.4286	
AC Sub-grid	Rated AC voltage	4.7 kV (peak)	
	Switching frequency	5 kHz	
	Slack terminal filter (LC)	1.9 mH/100 μ F	
	Power terminal filter (L)	10 mH	
	kAC	119.0476	
IC	VS-IC	Switching frequency	5 kHz
		Filter (LC)	0.4 mH/100 μ F
	LC-IC	Filter DC (L)	25 mH
		Filter AC (C)	100 kVAR
		Transformer (n1/n2)	1/1

The control system implemented these values by transmitting 0.55 (*p.u.*) and

0.44 (p.u.) through LC-IC and VS-IC units. The aggregated power terminals in AC and DC sub-grids adopt -1.5 (p.u.) and -0.25 (p.u.) as injected/absorbed power at the 30s of the simulation. The control system reacts to the changes by adjusting the transmitted power by LC-IC and VS-IC units to 0.98 (p.u.) and 0.51 (p.u.), respectively. At $t = 40$ s, the aggregated AC slack terminal takes control of the AC sub-grid, and therefore, the transmitted power by LC-IC and VS-IC change to 0.47 (p.u.) and 0.1 (p.u.), respectively. The DC sub-grid voltage and AC sub-grid frequency are shown in Fig. 2.10(c), (d).

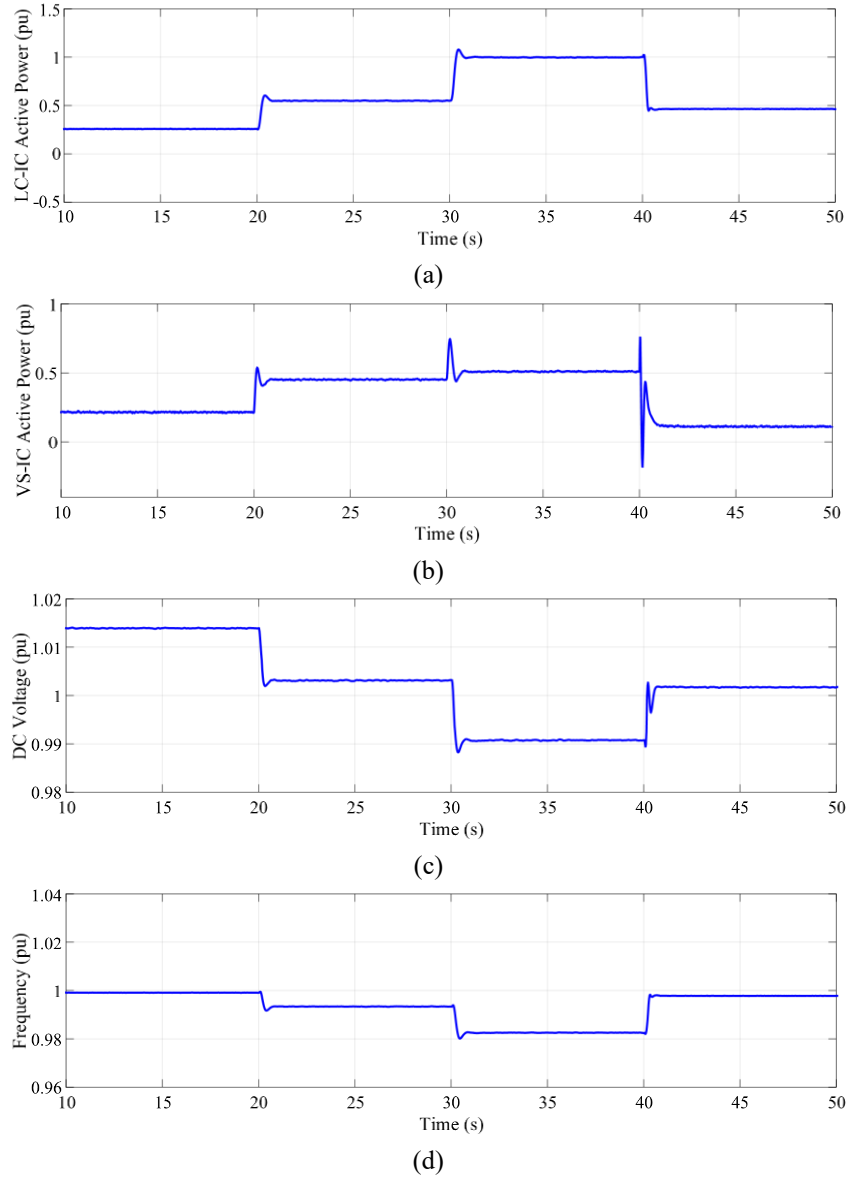


Fig. 2.10: Power-sharing to AC sub-grid support test by the LCC-based installations expansion control scheme. a) LC-IC active power (p.u.), b) VS-IC active power (p.u.), c) DC voltage (p.u.), and d) Frequency (p.u.).

The effectiveness of the AC sub-grid protection against voltage sag is shown in Fig. 2.11. In this test, the AC voltage sag happens at 25s and 35s of the simulation. As can be seen in Fig. 2.11(e), the control system of the LC-IC reacts to the voltage changes by adopting constant extinction angle control to protect the LC-IC unit from continuous commutation failure. Other than this particular measure, the control system works identical to the last test and successfully rides through the fault.

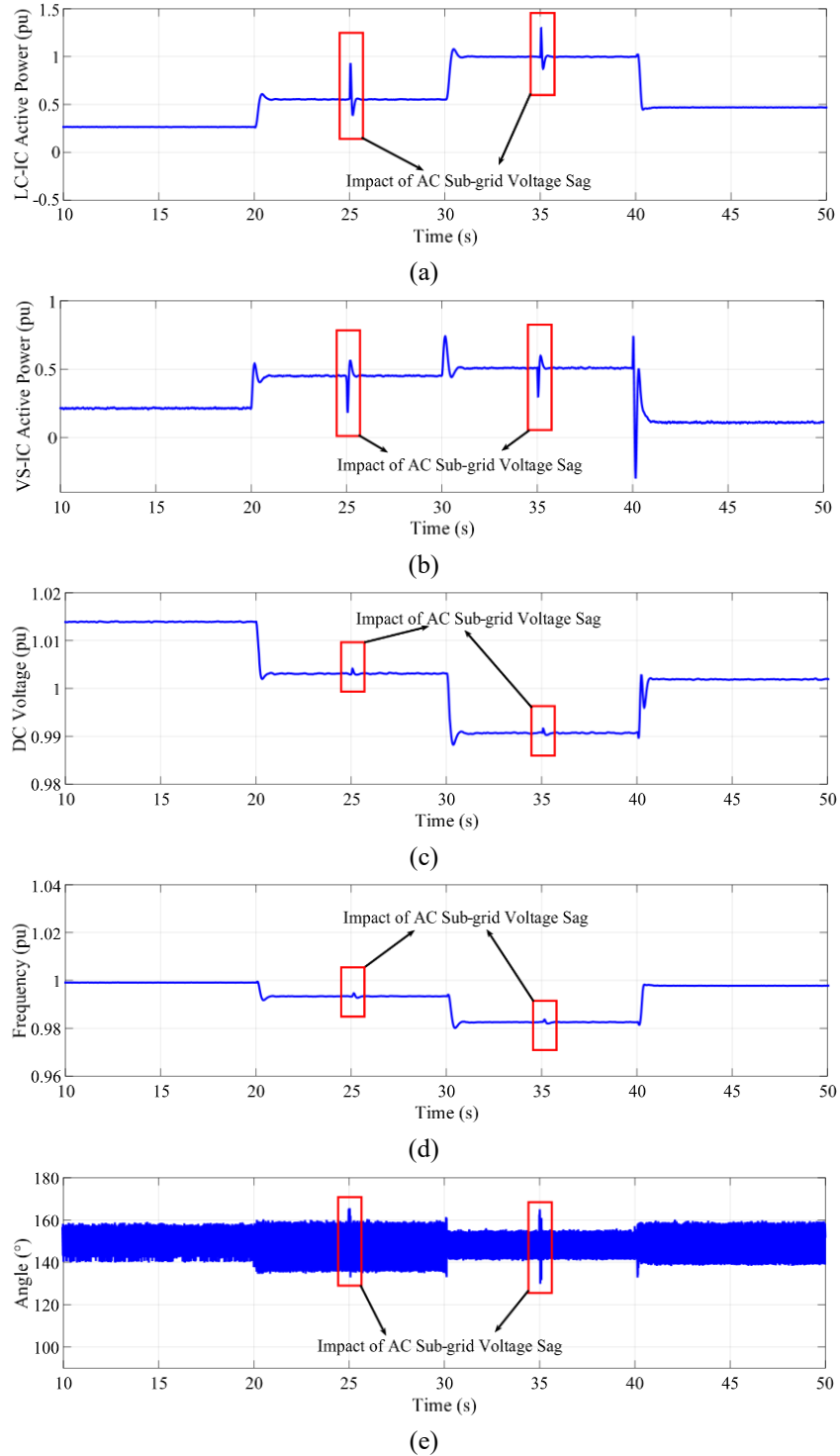


Fig. 2.11: Power-sharing to AC sub-grid support with AC voltage sag test by the LCC-based installations expansion control scheme. a) LC-IC active power (p.u.), b) VS-IC active power (p.u.), c) DC voltage (p.u.), and d) Frequency (p.u.).

The effectiveness of the DC sub-grid support is tested too. The system starts with -1 (pu) and 0.4 (pu) for aggregated power terminals on the AC and DC sub-

grids in power-sharing operation. In this condition, the LC-IC and VS-IC exchanged power are 0.25 (p.u.) and 0.198 (p.u.), respectively, as shown in Fig. 2.12. The DC aggregated slack terminal loses control of the DC sub-grids voltage at the 20s. As expected, the LC-IC will adopt VDCOL control while the VS-IC uses the same control scheme as before to support the DC sub-grids voltage. Therefore, LC-IC and VS-IC alters' transmitted power to 0.39 (p.u.) and 0.0005 (p.u.), respectively. At the 30s of the simulation, the aggregated power terminals on the AC and DC sub-grids change injected/absorbed power to -1.5 (p.u.) and -0.25 (p.u.), respectively. The ICs adapt to the changes by taking minimum acceptable exchanged power for LC-IC and a compensating value for VS-IC. The aggregated DC slack terminal takes control of the DC voltage on the DC sub-grid at 40s. As a result, the ICs have exchanged powers as 0.47 (p.u.) and 0.1 (p.u.) for LC-IC and VS-IC, respectively. The AC sub-grids frequency and DC sub-grids voltage can be seen in Fig. 2.12. The DC voltage and AC frequency are also shown in Fig. 2.12(c), (d), respectively.

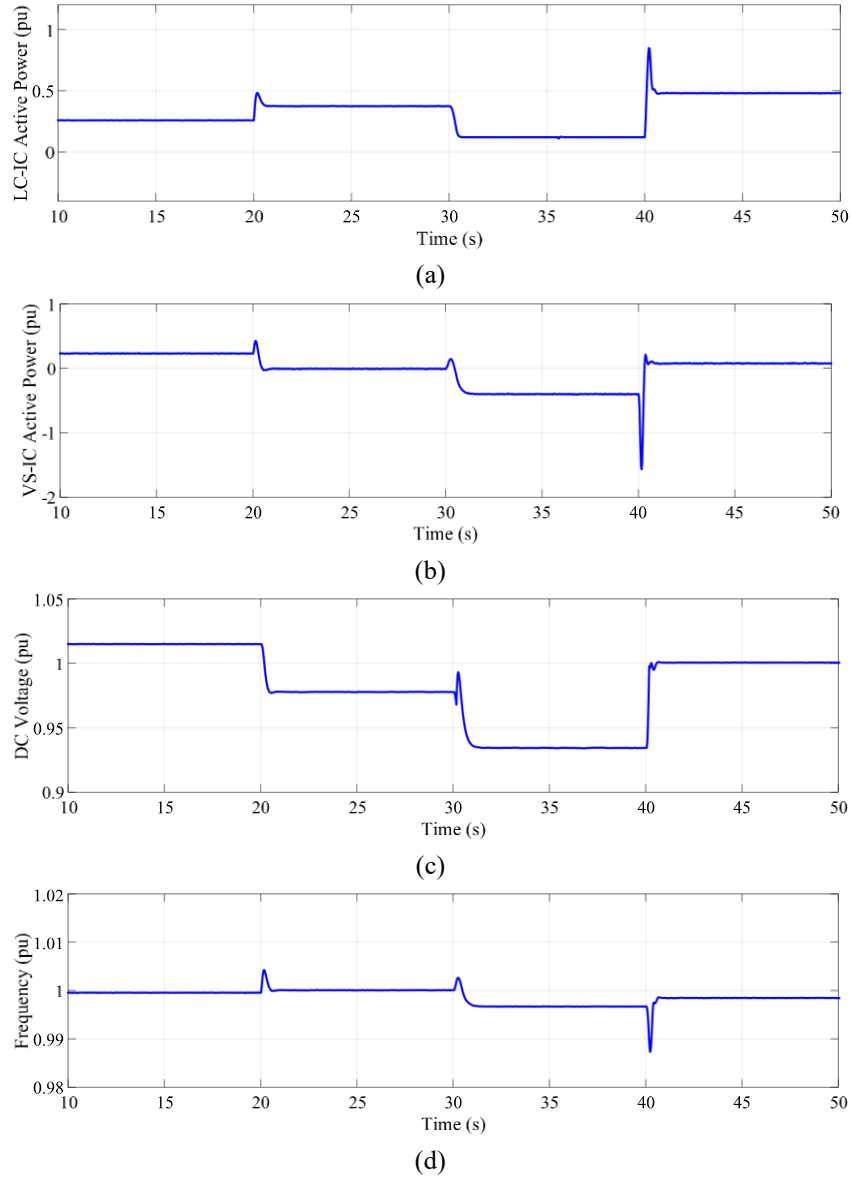


Fig. 2.12: Power-sharing to DC sub-grid support test by the LCC-based installations expansion control scheme. a) LC-IC active power (p.u.), b) VS-IC active power (p.u.), c) DC voltage (p.u.), and d) Frequency (p.u.).

Changing the controlling parameters to push the control system into an unstable region is also tested. The test proceeds with power-sharing to DC sub-grid support operation, shown in Fig. 2.13. The controlling parameters in (0.5) are selected following Fig. 0.4 unstable regions. The aggregated AC and DC power terminals follow similar values as given in the previous tests. At 20s, the aggregated slack terminal on the DC sub-grid loses control over DC voltage. In this condition, as expected, the ICs should take control of the system. As anticipated, the system

becomes unstable, moving from power-sharing condition to DC sub-grid support. Therefore it is expected for the system to lose its control over the DC voltage.

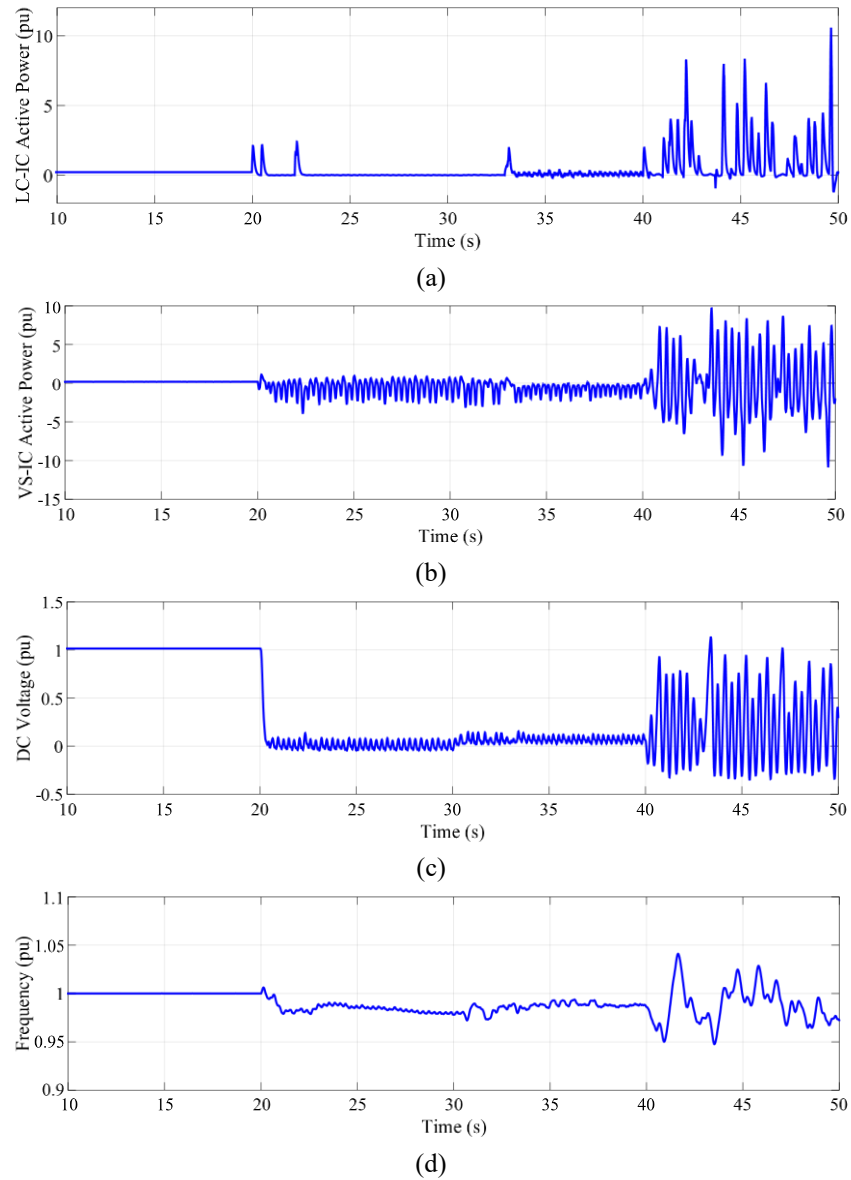


Fig. 2.13: Power-sharing to DC sub-grid support with unstable controlling parameters test by the LCC-based installations expansion control scheme. a) LC-IC active power (p.u.), b) VS-IC active power (p.u.), c) DC voltage (p.u.), and d) Frequency (p.u.).

2.6 Experimental Results

In order to further examine and verify the performance of the proposed system,

a scale-down experimental test is conducted. The hybrid AC/DC grid is simplified to the structure as depicted in Fig. 2.14. The circuit parameters are selected as it is given in Table 2.2.

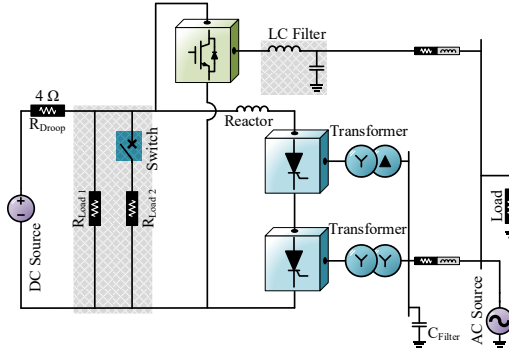


Fig. 2.14: Experimental test circuit layout.

A DC source with a series resistance R_{Droop} is used to mimic droop characteristics for the DC grid. $R_{Load 1}$ and $R_{Load 2}$ are also representing the DC loads. $R_{Load 2}$ is switchable to practice load changing and its impact on the system. A programmable AC source is used to represent the AC grid. A 4.2Ω resistance is positioned in parallel with AC source as a load. A VSC and two current source converters (CSCs) are used as VS-IC and a 12-pulse LC-IC. The CSCs are connected to the AC grid through delta/wye/delta transformers and controlled to mimic a 12-pulse LCC in operation.

TABLE 2.2: EXPERIMENT CIRCUIT PARAMETERS.

DC source voltage level	120 V
AC source voltage level	30 V(rms)
Voltage source switching frequency	5 kHz
AC Load	4.2Ω
Voltage source converter filters	5 mH/80 μ F
Current source converter filters	140 μ F/ 1.2 Ω
AC line parameters	500 μ H/0.2 Ω
$R_{Load 1}/R_{Load 2}$	145 Ω /44 Ω
Transformer	delta/wye/delta, 1:1:1

In this test, the AC grid frequency and DC voltages base are set on 60 Hz and 120 V, and any changes in the measurements of these value's during the tests should be added/subtracted to their origin. The experimental setup is shown in Fig. 2.15.

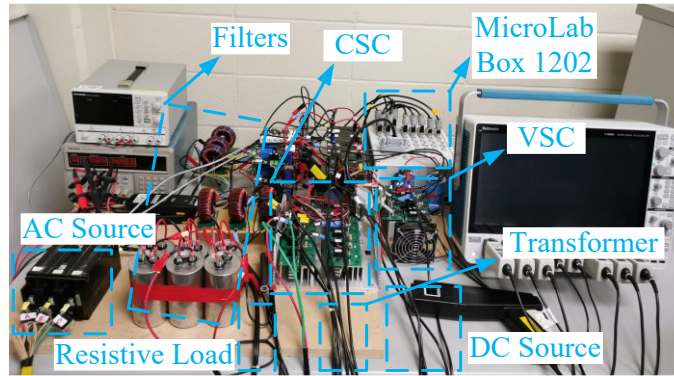


Fig. 2.15: Experimental setup.

The performance of the system is tested in two conditions. The first is testing the system performance in normal and AC frequency support operation states. The system starts with a normal operation state while all of the circuit elements are within the desired range. Then, as shown in Fig. 2.16, the AC grid faces an AC frequency drop from 60 Hz to 59.9 Hz. Eventually, the AC frequency increases back to 60 Hz. The SCR's exchanged power changed from around 100 W to 135 W and back to 100 W due to changes in AC frequency level. Similarly, the VSC's exchanged power changes from 40 W to around 60W and back to 40 W. The DC voltage level will be impacted due to increased exchanged power value, dropping from 111 V to 107 V and back to 111 V.

The second experiment tests system performance in normal and DC support states. The system starts with a normal operation state while all of the circuit elements are within the desired range. To test the system's DC support state, the DC load is changed from 145 Ω to 33.7 Ω and then back to 145 Ω resulting in a shift DC voltage level, as shown in Fig. 2.17. In this process, the DC voltage is changed from around 111 V to 104 V and then back to 111 V resulting in VSC's exchanged power to be equal to 45 W, -32 W, and then back to 45 W, respectively. VSC supports the DC grid during the DC voltage drop by exchanging power from AC to DC grid. As it can be seen, the AC grid frequency is equal to 60 Hz in all test conditions. Similarly, as expected, the SCR's exchanged power doesn't deviate due to the structure of the control scheme.

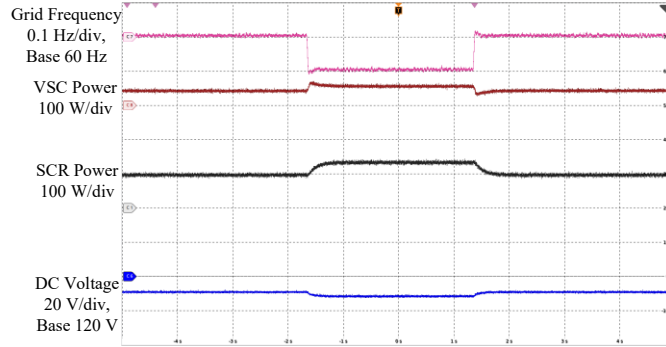


Fig. 2.16: Normal and frequency support operations states experimental results.

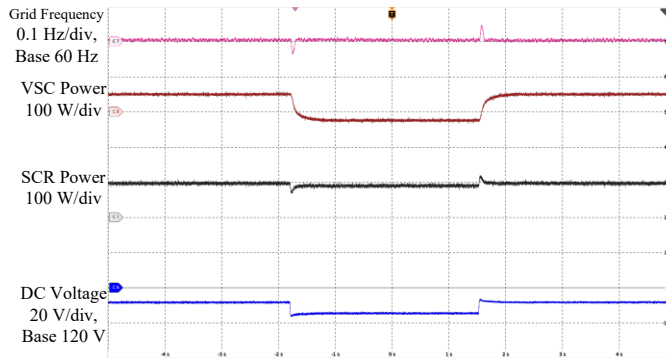


Fig. 2.17: Normal and DC support operations states experimental results.

2.7 Conclusion

This chapter reviewed the proposed unified control scheme for parallel LCC-VSC interlinking converters in a hybrid AC/DC grid. In the proposed control strategy, the VSCs merge the droop functions of the DC and the AC sub-grids into the united control scheme. Also, the LCC uses droop equivalent control, derived from its V-I graph, which enables it to operate with the VSC's droop control. In this thesis, the performance of the proposed control scheme was studied under different operational modes (normal, AC sub-grid support, and DC sub-grid support) by detailed mathematical modeling and real-time simulations. The study verified that the proposed control scheme accurately shares power between the AC and DC sub-grids during normal operation and supports the AC sub-grid's voltage/frequency and the DC sub-grid's voltage in the AC and DC sub-grids' support control modes, respectively. Moreover, the proposed control system provides the required reactive

power, improves the transmitted power quality, and prevents the continuous commutation failure of the LC-IC. Also, the mathematical and simulation studies verified that the bidirectional power flow, an essential requirement for hybrid AC/DC grids, was realized with the parallel LCC-VSC interlinking converter.

Chapter 3

Unified Control Scheme - Parallel LCC-VSC-based New Installation

In Chapter 2, the author proposed that parallel LCC-VSC interlinking converters (ICs) operated as a single terminal in a hybrid AC/DC grid and aimed for expansion of the already available LCC-based installations. Therefore, the conventional structure of the LCC installations, such as passive filters, VDCOL control, and mode detection in some of the operation states are maintained. In this chapter, the general features of such a system based on unified control and basic operational states have been developed. An attempt has been made to make the LCC unit fit to the droop control of the parallel VSCs. The equivalent droop control of the LCC, in Chapter 2, has been designed based on the frequency of the AC sub-grid versus injected active power, while the droop control of the VSC accommodates the DC voltage and AC frequency versus injected/absorbed active power. As is shown, the implementation of the AC frequency into the conventional control scheme of the LCC showed good compatibility. However, in the LCC-based installations expansion control scheme, as was shown in Chapter 2, the operation mode detection is required.

This work studies a parallel integration of LCC-VSC ICs in hybrid AC/DC grids with an enhanced control scheme. Unlike the studies provided in Chapter 2, this work is intended for a system considering both LCC and VSC in the design stage. The control system of the ICs includes AC voltage/frequency control, DC voltage regulations, smooth operation modes' transients, and stability in normal and fault conditions. For this purpose, the conventional (V-I) graph-based control scheme of the LCC is altered to fully support the droop equivalent control, so it is very compatible with parallel droop-controlled VSCs. The constant extinction angle control is essential to protect the unit against the AC voltage drop and, consequently, commutation failure. In order to limit the need for mode detection

and to improve the accuracy of the power-sharing, the propositions of both the AC and DC sub-grids are considered in the LCC's control scheme design. The proposed control for the LCC can improve the system's response and remove unnecessary transients. More importantly, the system's performance under the AC and DC sides' faults is studied, and a proper control scheme is designed to improve the stability and power quality of the grid. The designed control system of the ICs can support the AC voltage/frequency and the DC voltage level in different operational conditions within the desired range, independent of the state of the system.

3.1 The Hybrid AC/DC Grid with Proposed Parallel LCC-VSC-based New Installation's Control Scheme

The generic hybrid AC/DC system with proposed parallel LCC-VSC ICs will be also used for the parallel LCC-VSC-based new installation's control scheme, as shown in Fig. 2.1. Similar description regarding the aggregated slack and power terminals on both AC and DC sub-grids can be used for the parallel LCC-VSC-based new installation's control scheme. Also, the general structure of the power grid for the proposed parallel LCC-VSC-based new installation's control scheme is similar to the LCC-based installations expansion control scheme, the application and operation scenario is vastly different.

As it is stated before, the conventional LCCs has commutation failure issue and limited controllability. Linking the LCC-based inverter with parallel VSC units in a new installation is a promising approach. The proposed configuration improves the commutation by helping the system during the transients and providing extensive controllability for circuit properties in all conditions while keeping the cost low. The LCC's advantages, such as being a mature technology, lower equipment cost, and efficient high-power transmission [16], [27] establishes a low-cost interlinking unit while the power quality is kept high. The variety of operation states for such hybrid AC/DC grids require a unified control scheme that can address system needs in all possible conditions while avoiding or mitigating fault impacts in both AC and DC sides. Also, the proposed configuration will increase

power exchange capacity and add a power reversal capability to the conversion unit while the cost is kept low. The power reversal is needed for ES units in the DC sub-grid of the hybrid AC/DC grid. Furthermore, this parallel LCC-VSC system can also be an effective choice when the power flow levels in two directions are not the same in design. Therefore, a great application of the LCC-VSCs system is for a new interlinking converter station where the power flows in two directions are not the same in design (e.g., remote islands or weak grids with storage units or local distributed generation). The combination of LCC-VSC has the potential to bring the best out of each technology and provide a promising solution with good power quality, efficiency, and lower cost for such a system.

Similar to the power grid in the LCC-based installation expansion control scheme, the aggregated slack terminals on the AC and DC sub-grids are droop controlled. The control functions are defined as provided in (2.1). The power ratio between the AC and DC sub-grids can be defined as $P_{AC_B,pu} \cdot P_{DC_B,pu} = K:1$. Fig. 3.1 is a proper representation of the proposed configuration in a intended operation environment.

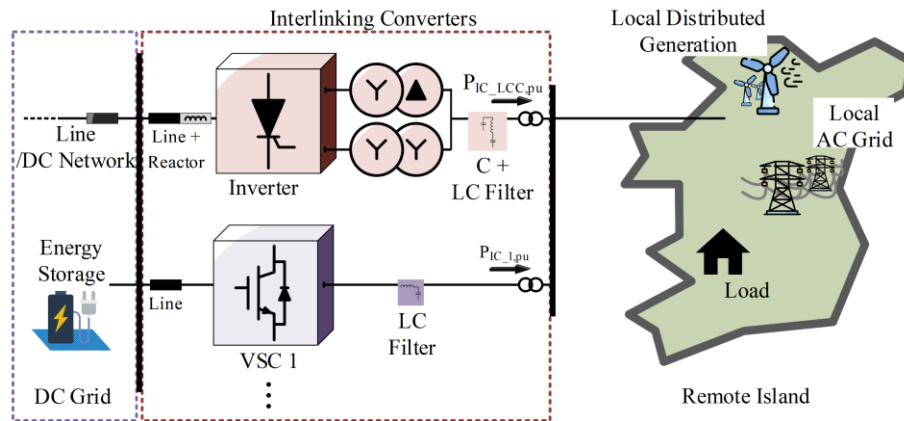


Fig. 3.1: General layout of hybrid AC/DC grid with the proposed parallel LCC-VSC-based new installation's related environment.

3.2 Modeling of VS-ICs and LC-IC

In the parallel LCC-VSC-based new installation's control scheme as well as LCC-based installations expansion control scheme, the exchanged power by the VS-IC will be defined by (2.2). Also, taking into account the AC and DC sub-grid's

droop controls, the power difference equation will be defined as given in (2.4). Therefore using (2.4), the VS-IC's control scheme as shown in Fig. 2.2, and small-signal model of the (P - f) droop control as given in Fig. 2.3 the exchange power by i -th VS-ICs can be defined as (2.10) and (2.11).

Unlike the VS-ICs, the operation states of the LC-IC can be different between LCC-based installations expansion control scheme and parallel LCC-VSC-based new installation's control scheme in some cases. Also, some of operating states are similar for the LC-IC in parallel LCC-VSC-based new installation's control scheme as LCC-based installations expansion control scheme. The power control and constant extinction angle control are the same for both control schemes.

Based on the LC-IC's small signal model as shown in Fig. 2.5, its power control can be defined as it is given in (2.15). Similarly, based on the small-signal model of the LC-IC's constant extinction angle control, Fig. 2.6, the LC-IC's transmitted power in this control scheme will be as it is determined in (2.18). Using (2.18), the exchanged power equation during the constant extinction angle control can also be found as given in (2.21).

3.2.1 Modeling of LC-IC's Droop Equivalent Control for the Proposed Parallel LCC-VSC-based New Installation's Control Scheme

The LC-IC in the parallel LCC-VSC-based new installation's control scheme uses a droop equivalent control based on AC frequency and DC voltage, the same as the VS-ICs control scheme shown in (3.1).

$$\Delta P_{LCC} = \left[P_{AC,pu}^* + k_{AC} (\omega_{AC,pu}^* - \omega_{AC,pu}) \right] - K \times \left[P_{DC,pu}^* + k_{DC} (U_{DC,pu}^* - u_{DC,i,pu}) \right] \quad (3.1)$$

The LC-IC's exchanged active power can be defined as it is given in (3.2), using Fig. 3.2 and a small-signal model of the LC-IC power control (2.15).

$$P_{IC_LC,pu} = \left(\left[P_{AC,pu}^* + k_{AC} (\omega_{AC,pu}^* - \omega_{AC,pu}) \right] - K \times \left[P_{DC,pu}^* + k_{DC} (U_{DC,pu}^* - u_{DC,pu}) \right] \right) G_{LC_K}(s) G_{LC_D}(s) \quad (3.2)$$

In (3.2), the LCC's inertia transfer function, $G_{LC_K}(s)$, is assumed to be equal

to $G_{LC,K} = 1/K_{p,l} + H_{p,l}S$. The $G_{LC,D}(s)$ represents a small-signal model of the LC-IC's power control as given in (2.15). As it is shown in (3.2), the terminals' DC voltage of the LC-IC is already included in the parallel LCC-VSC-based new installation's control scheme's exchanged power following the same procedure introduced for the LCC-based installations expansion control scheme in (2.26).

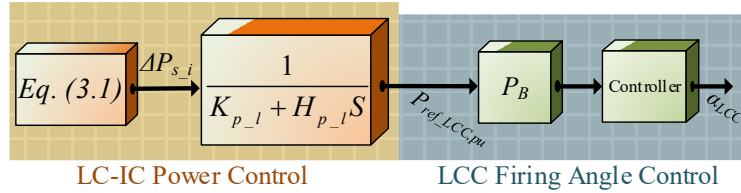


Fig. 3.2: The proposed control scheme of the LC-IC for improved unified control.

3.3 Operation Modes and Stability Studies of Parallel LCC-VSC-based New Installation's Control Scheme

The operation of the power system under parallel LCC-VSC-based new installation's control scheme is divided into three main states: power-sharing, DC support, and AC support.

The exchanged power by ICs in every operation state with both control schemes can be defined as (2.25), similar to the LCC-based installations expansion control scheme. The aggregated exchanged power includes the combination of both LC- and VS-ICs exchanged power equations representing the IC's system as a whole. The VS-IC's inertia and phase compensation functions operate the same for the parallel LCC-VSC-based new installation's control scheme as LCC-based installations expansion control scheme and similar explanations as it is given in section 2.4 is valid for parallel LCC-VSC-based new installation's control scheme. Similarly, the inertia function for LC-IC in the parallel LCC-VSC-based new installation's control scheme is valid just like LCC-based installations expansion control scheme as explained in section 2.4.

3.3.1 Power-sharing Operation

In the power-sharing operation state, AC sub-grids voltage/frequency and DC

sub-grids voltage are controlled by aggregated slack terminals on AC and DC sub-grids while ICs share power based on proposed control schemes 2.

The LC-IC and VS-ICs follow the control schemes provided in the previous section in all operating states. The operation state of the system in the power-sharing condition can be defined as given in (2.29).

As stated before, the system's operation state is independent of the ICs control scheme and defined based on the power grid and aggregated slack terminals control. The exchanged power in the power-sharing state can be defined for parallel LCC-VSC-based new installation's control scheme as it is provided in the following.

$$\begin{cases} \Delta P_{IC,pu} = \frac{G_{IC}(s)}{1+(1+K)G_{IC}(s)} \times (K\Delta P_{DC_P,pu} - \Delta P_{AC_P,pu}) \\ G_{IC}(s) = G_{NLCC}(s) + \sum_{i=1}^N G_{IC_i}(s) \end{cases} \quad (3.3)$$

The steady-state representation of the IC's exchanged-power based on the parallel LCC-VSC-based new installation's control scheme can be found in (3.4).

$$\begin{cases} P_{IC_i,pu} = \frac{\eta_i / (1 + Kk_{DC}R_{i,pu}\eta_i)}{1 + (1 + K)G_{IC}(0)} \times (KP_{DC_P,pu} - P_{AC_P,pu}) \\ P_{IC_LC,pu} = \frac{1/K_{p_l}}{1 + (1 + K)G_{IC}(0)} \times (KP_{DC_P,pu} - P_{AC_P,pu}) \\ G_{IC}(0) = 1/K_{p_l} + \sum_{i=1}^N \eta_i / (1 + Kk_{DC}R_{i,pu}\eta_i) \end{cases} \quad (3.4)$$

Considering the steady-state representation of the exchanged power by ICs in a normal operation state (3.4), the ratio of the exchanged power can be calculated. Therefore, based on the given calculations, the power sharing between ICs in normal operation mode can be defined below (3.5).

$$\frac{P_{IC_i,pu}}{P_{IC_LC,pu}} = \frac{\eta_i / (1 + Kk_{DC}R_{i,pu}\eta_i)}{1/K_{p_l}} \quad (3.5)$$

The stability study of the system in this operating condition can be performed considering (3.3). The pole placements of the transfer function considering a variety of controlling parameters are performed. It can be learned from Fig. 3.3, when τ_{l_i} and τ_{d_i} are equal to 0 and 0.01, respectively, pole-placements have the highest shift

by changing the variables compared to other options. Also, it is expected that the system shows a faster but oscillatory response by increasing the value of η_i from 0.1 to 4. This is based on the presence of a pair of conjugate poles getting closer to the imaginary axis and the pole on the real axis distancing from the imaginary axis, as shown in Fig. 3.3. Comparing the two other testing conditions, $\tau_{l_i} = 0, \tau_{d_i} = 0.5$ and $\tau_{l_i} = 0.1, \tau_{d_i} = 0.5$, the choice with higher τ_{l_i} shows better performance. This is due to the pair of conjugate poles located farther from the real axis than the other option. According to the results, it is expected that the $\tau_{l_i} = 0.1$ and $\tau_{d_i} = 0.5$ performing better for normal operation state (i.e., better settling time, lower overshoot, and oscillations). Based on the system's overall response in this state, it can be concluded that the higher values for η_i result in a better response. However, the value of the η_i cannot be exceedingly high without proper compensation.

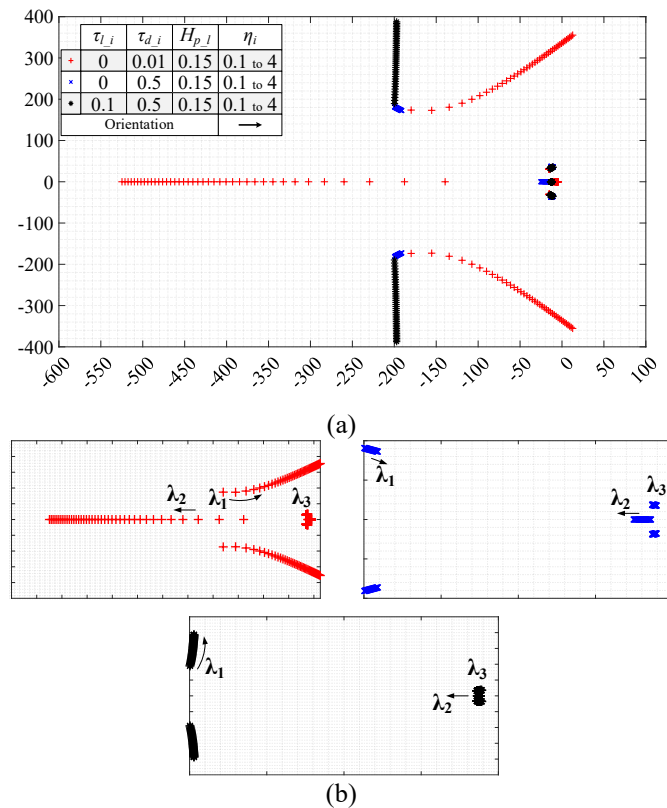


Fig. 3.3: Normal operation condition poles-placement analysis. a) overall poles-placement, b)

3.3.2 AC Sub-grid Support

The aggregated slack terminal on the AC sub-grid has lost control over the AC sub-grids' voltage and frequency. However, the DC sub-grid operation is intact. In this condition and under the proposed unified control principles, the ICs should maintain the voltage level and frequency of the AC sub-grid within the desired range. In this condition, the operation state can be defined as given in (2.33).

The exchanged power by ICs under the parallel LCC-VSC-based new installation's control scheme can be defined by applying the current condition's operation state (2.33) to the LC-IC's and VS-IC's exchanged power functions (3.2) and (2.27), respectively. The small-signal model of the IC's exchanged power can be defined as provided in (3.6).

$$\begin{cases} P_{IC_i,pu} = \left(\left[P_{AC,pu}^* + k_{AC} (\omega_{AC,pu}^* - \omega_{AC,pu}) \right] + K \times [P_{DC_p,pu} + P_{AC_p,pu}] \right) G_{IC_i}(s) \\ P_{IC_LC,pu} = \left(\left[P_{AC,pu}^* + k_{AC} (\omega_{AC,pu}^* - \omega_{AC,pu}) \right] + K \times [P_{DC_p,pu} + P_{AC_p,pu}] \right) G_{NLCC}(s) \\ P_{IC,pu} = P_{IC_LCC,pu} + \frac{P_{IC_i,pu}}{G_{IC_i}(s)} \sum_{i=1}^N G_{IC_i}(s) \end{cases} \quad (3.6)$$

Based on (3.7), the steady-state value of transferred power by ICs and the AC sub-grid frequency can be calculated.

$$\begin{cases} \omega_{AC,pu} = \omega_{AC,pu}^* + \frac{P_{AC,pu}^* + K(P_{DC_p,pu} + P_{AC_p,pu})}{k_{AC}} + \frac{P_{AC_p,pu} / \left(1/K_{p_l} + \sum_{i=1}^N \eta_i / (1 + Kk_{DC}R_{i,pu}\eta_i) \right)}{k_{AC}} \\ P_{IC_i,pu} = \frac{-P_{AC_p,pu} \times \eta_i / (1 + Kk_{DC}R_{i,pu}\eta_i)}{1/K_{p_l} + \sum_{i=1}^N \eta_i / (1 + Kk_{DC}R_{i,pu}\eta_i)} \\ P_{IC_LC,pu} = \frac{-P_{AC_p,pu} \times 1/K_{p_l}}{1/K_{p_l} + \sum_{i=1}^N \eta_i / (1 + Kk_{DC}R_{i,pu}\eta_i)} \end{cases} \quad (3.7)$$

In case of an excessive voltage sag on AC sub-grid, continuous commutation failure is highly possible for the system. In this condition as explained previously, in order for the LC-IC to avoid continuous commutation failure, the constant extinction angle control should be adapted. The VS-ICs also should play a

supporting role by providing the system with required reactive power and trying to stabilize the AC voltage. In this method, the LCC valves' firing angles are determined to impose the safest extinction angles while limiting the reactive power consumption to the lowest possible amount. The reference signal of the LC-IC will change to (2.37) as provided before. Using the LC-IC's constant extinction angle controlled exchanged power function (2.21), the overall transferred power by the ICs are recalculated as given in (2.38). The ICs will continue to work in this mode of operation until the AC voltage on the AC sub-grid recovers to its standard range. The output power of the LC-IC, as stated, in this condition is controlled by a constant extinction angle control loop. Thus, its impact on frequency is subject to the AC system voltage level than its frequency. The stability of the system in this mode is a subject of the stability of G_{LCC_C} in $P_{IC_LCC,pu}$, and G_{IC_i} in $P_{IC,pu}$. The stability of these two transfer functions is guaranteed. Then, it can be concluded that the stability of the (2.38) is also guaranteed. Steady-state representation of the system in this condition is provided in (2.39).

The VS-ICs based on their topology can be affected differently. As studied in [87], the conventional half-bridge MMC and 2- or 3-level VSCs can face severe consequences in case of commutation failure, shown in Fig. 3.4. As depicted in Fig. 3.4, the DC short circuit, resulting from continuous commutation failure, can lead to current circulation, damaging the semiconductors in some cases or disturbing the voltage balance in others with severe outcomes. The MMC units with mixed submodules (half-bridge and full-bridge) and compensating control plans are proposed in [87], [88] to mitigate these issues while the cost of the unit is kept lower. The complication of control due to the AC voltage disturbance confirms that the primary task is to ensure the LC-IC recovers from commutation failure or avoid it.

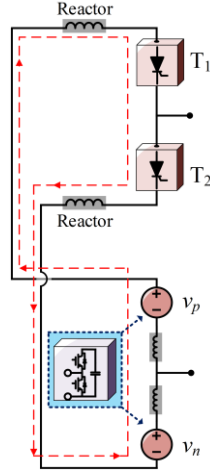


Fig. 3.4: Simplified equivalent circuit of an LCC paralleled with half-bridge MMC during the fault

3.3.3 DC Sub-grid Support

In this mode, the DC sub-grid loses its control over DC voltage. ICs can support the DC voltage by injecting the required power from the AC sub-grid to the DC sub-grid or decreasing the value of the exchanged power from the DC sub-grid to the AC sub-grid. In this condition, the system's operation state can be discussed as given in (2.40).

In the proposed parallel LCC-VSC-based new installation's control scheme, the ICs control will be more integrated to support the DC sub-grid voltage. Considering the system's operation state as given in (2.40) and the control scheme of the ICs, the exchanged power will be computed as given in (3.8).

$$\begin{cases}
 P_{IC_i,pu} = -\left\{ \left[P_{AC_P,pu} + P_{IC,pu} \right] + K \times \left[P_{DC,pu}^* + k_{DC} \left(U_{DC,pu}^* - u_{DC,pu} \right) \right] \right\} G_{IC_i}(s) \\
 P_{IC_LCC,pu} = -\left\{ \left[P_{AC_P,pu} + P_{IC,pu} \right] + K \times \left[P_{DC,pu}^* + k_{DC} \left(U_{DC,pu}^* - u_{DC,pu} \right) \right] \right\} G_{NLCC}(s) \\
 P_{IC,pu} = P_{IC_LCC,pu} + \sum_{i=1}^N P_{IC_i,pu}
 \end{cases} \quad (3.8)$$

Using (3.8), the DC voltage dynamic can be calculated as (3.9).

$$\begin{cases}
\Delta U_{DC,pu} = \Delta P_{DC_P,pu} G_{D0}(s) + \left[\Delta P_{AC_P,pu} + K(\Delta P_{DC,pu}^* + k_{DC} \Delta U_{DC,pu}^*) \right] G_{D1}(s) \\
G_{D0}(s) = \frac{1 + G_{NLCC}(s) + \sum_{i=1}^N G_{IC_i}(s)}{G_{D_Denom}(s)} \\
G_{D1}(s) = \frac{G_{NLCC}(s) + \sum_{i=1}^N G_{IC_i}(s)}{G_{D_Denom}(s)} \\
G_{D_Denom}(s) = s \frac{CU_{dcB}^2}{S_B} \left(1 + G_{NLCC}(s) + \sum_{i=1}^N G_{IC_i}(s) \right) + \\
\qquad \qquad \qquad Kk_{DC} \left(G_{NLCC}(s) + \sum_{i=1}^N G_{IC_i}(s) \right)
\end{cases} \quad (3.9)$$

Using (3.8) and (3.9), the steady-state value of the DC sub-grid voltage and ICs transmitted power are calculated as (3.10).

The provided equation shows that both the LC-IC and VS-ICs contribute to the regulation of voltage, which can be affected by controlling factors, as explained previously.

$$\begin{cases}
\Delta U_{DC,pu} = \Delta P_{DC_P,pu} G_{D0}(s) + \left[\Delta P_{AC_P,pu} + K(\Delta P_{DC,pu}^* + k_{DC} \Delta U_{DC,pu}^*) \right] \frac{1}{Kk_{DC}} \\
G_{D0}(s) = \frac{1}{Kk_{DC} \left(1/K_{p_l} + \sum_{i=1}^N \eta_i / (1 + Kk_{DC} R_{i,pu} \eta_i) \right)} + \frac{1}{Kk_{DC}} \\
P_{IC_i,pu} = P_{DC_P,pu} \times \frac{\eta_i / (1 + Kk_{DC} R_{i,pu} \eta_i)}{1/K_{p_l} + \sum_{i=1}^N \eta_i / (1 + Kk_{DC} R_{i,pu} \eta_i)} \\
P_{IC_LCC,pu} = P_{DC_P,pu} \times \frac{1/K_{p_l}}{1/K_{p_l} + \sum_{i=1}^N \eta_i / (1 + Kk_{DC} R_{i,pu} \eta_i)}
\end{cases} \quad (3.10)$$

The power-sharing in this condition can also be calculated using (3.10). The power-sharing will be as it is provided in (3.5). The capacity of the parallel VS-ICs can be calculated by understanding the required negative exchanged power based on the system needs.

The stability of the system under the DC sub-grid fault condition is subject to the stability of the $G_{D0}(s)$ and $G_{D1}(s)$. Therefore, $G_{D1}(s)$ will be tested to evaluate system stability based on the changes in the controlling parameters as shown in Fig. 3.5. Taking the τ_{l_i} and τ_{d_i} equal to 0 and 0.01, respectively, results in a slower but

less oscillatory response. Changing the values of the τ_{l_i} and τ_{d_i} to 0 and 0.5 and increasing the η_i results in oscillatory and, on some occasions, unstable responses. Eventually, τ_{l_i} and τ_{d_i} to 0.1 and 0.5, overall, can produce desired reasonable, especially in lower values of η_i . The impact of the LCC's transfer function dynamic on the pole positioning is also provided considering τ_{l_i} , τ_{d_i} , and η_i equal to 0.1, 0.2, and 2, respectively, and changing the H_{p_l} from 0.001 to 0.5. The impact of the H_{p_l} on pole positioning shows stable response in all conditions. However, the selecting a proper value for H_{p_l} system response and LCC's limited dynamic should be considered.

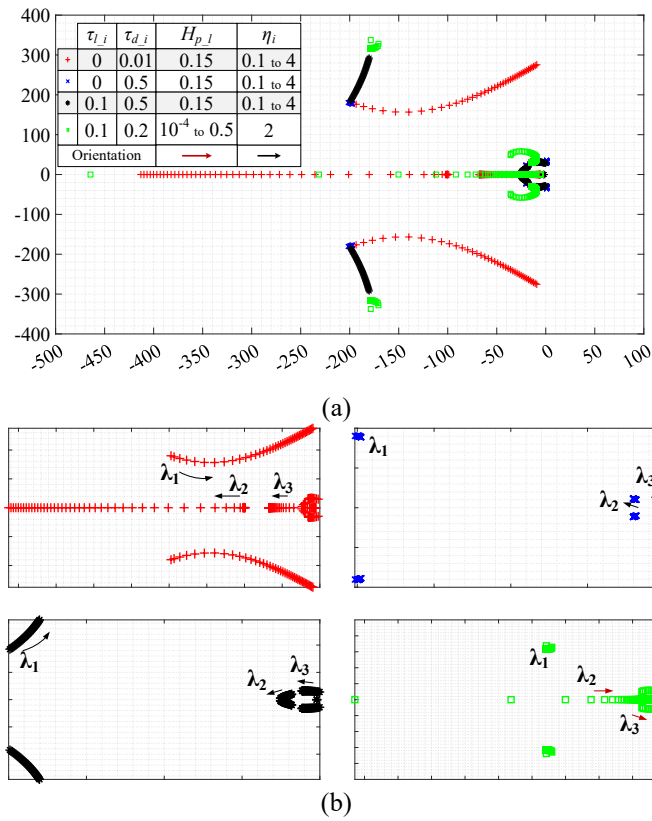


Fig. 3.5: DC fault operation condition poles-placement analysis. a) overall poles-placement, b)

3.4 Real-time Simulation Results

The performance of the proposed control system for the parallel LCC-VSCs ICs in a hybrid AC/DC grid will be evaluated in this section. Different operation

conditions are tested to verify the effectiveness of the proposed circuit structure and the control scheme. The proposed system will be tested for both normal and under fault states using a realtime simulator using the power system as shown in Fig. 3.6. The model of the realtime simulator used in this study is OP5600, and the grid is modelled in 5 zones. The value of K for the tests is assumed to be 1. The system parameters and controlling parameters in accordance with stability studies can be found in Table 3.1.

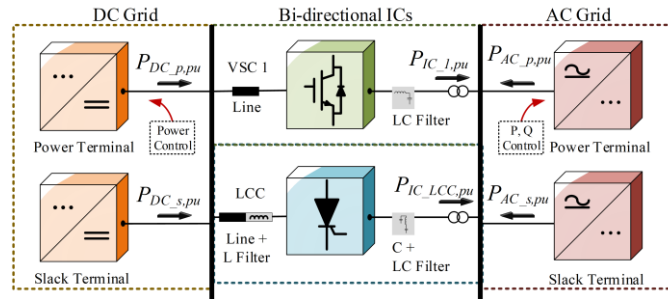


Fig. 3.6: The layout of the tested grid.

■ The real-time Simulation Test for the Parallel LCC-VSC-based New Installation's Control Scheme

A similar approach like the LCC-based installations expansion control scheme will be taken for the parallel LCC-VSC-based new installation's control scheme to verify the performance of the proposed controls parallel LCC-VSC-based new installation's control scheme. In this test, the system parameters are selected as given in Table 3.1.

For the power-sharing state the simulation starts by taking the $P_{AC_p,pu} = -1.5$ MW ($-1.5 p.u.$) and $P_{DC_p,pu} = 2.5$ MW ($2.5 p.u.$). The exchanged power values by LC-IC and VS-IC will be approximately equal to $1.36 p.u.$ and $0.29 p.u.$, respectively, as shown in Fig. 3.7. At the $t = 20s$, the aggregated power terminals' value in AC and DC sub-grids change to $-1 p.u.$ and $2 p.u.$, respectively.

TABLE 3.1: GRID PARAMETERS FOR THE PARALLEL LCC-VSC-BASED NEW INSTALLATION'S CONTROL SCHEME TEST.

System		Parameter	Value
DC Sub-grid		Rated DC voltage	14kV
		DC filter capacitance	12mH, 0.25Ω
		Switching frequency	5kHz
AC Sub-grid		Rated AC voltage	4.7kV (peak)
		Switching frequency	5kHz
		Slack terminal filter (LC)	3mH/100μF
		Power terminal filter (L)	5mH
IC	VS-IC	Switching frequency	5kHz
		Filter (LC)	5mH/100μF
	LC-IC	Filter DC (L)	25mH
		Filter AC (C)	100kVAR
		Transformer (n1/n2)	1/1

The control system responds to the changes by altering the transmitted power values to $1.02 p.u.$ and $0.22 p.u.$ for LC-IC and VS-IC, respectively.

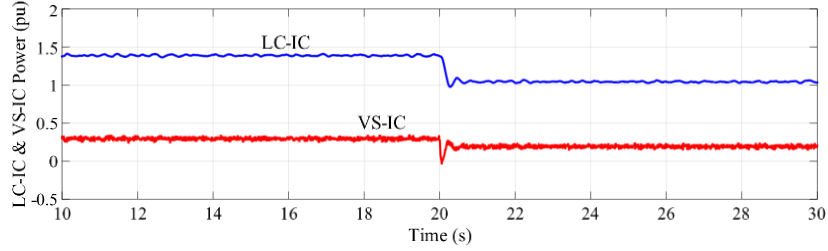


Fig. 3.7: Transmitted power by LC-IC and VS-IC in power-sharing operation test by the parallel LCC-VSC-based new installation's control scheme.

In the following, the system's operation under the AC sub-grid voltage and frequency control lost will be performed. The AC sub-grid supported test is performed with similar values for aggregated power terminals in two variants. In the first test effectiveness of the proposed structure on frequency control will be examined, as shown in Fig. 3.8. For the second test, in addition to control loss over frequency, the AC sub-grid will face voltage sag on the specific points of simulation, as shown in Fig. 3.9. In the frequency support state, the transmitted power by LC-IC and VS-IC will be equal to $1.2 p.u.$ and $0.27 p.u.$ for the first interval and $0.82 p.u.$ and $0.18 p.u.$ for the second interval, as shown in Fig. 3.8(a). The ICs regulate the AC sub-grid frequency within the desired range, as shown in

Fig. 3.8(b). The frequency is adjusted to 1.015 p.u. for the first interval and 1.018 p.u. for the second interval.

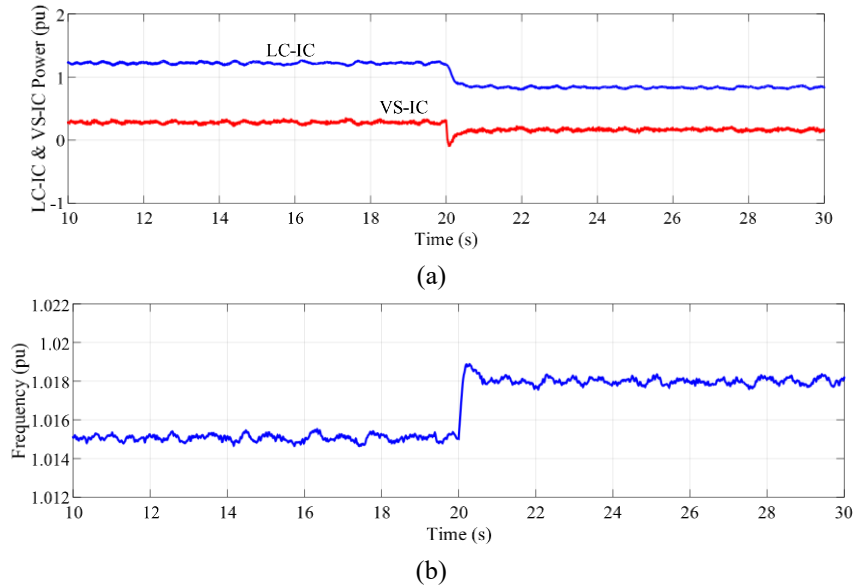


Fig. 3.8: AC sub-grid frequency support test by the parallel LCC-VSC-based new installation's control scheme. a) LC-IC and VS-IC transmitted power. b) AC sub-grid frequency.

The exchanged power by ICs and AC sub-grid frequency is shown in Fig. 3.9(a), (b). As can be seen, the exchanged power by ICs and frequency has the same values as the condition without voltage sag. However, as can be seen in Fig. 3.9(c), the LC-IC's firing angle is changed to constant extinction angle control in the 15s and 25s of the simulation during the AC sub-grid voltage sag. The impact of this control measure is also clear in IC's exchanged power and AC sub-grid frequency.

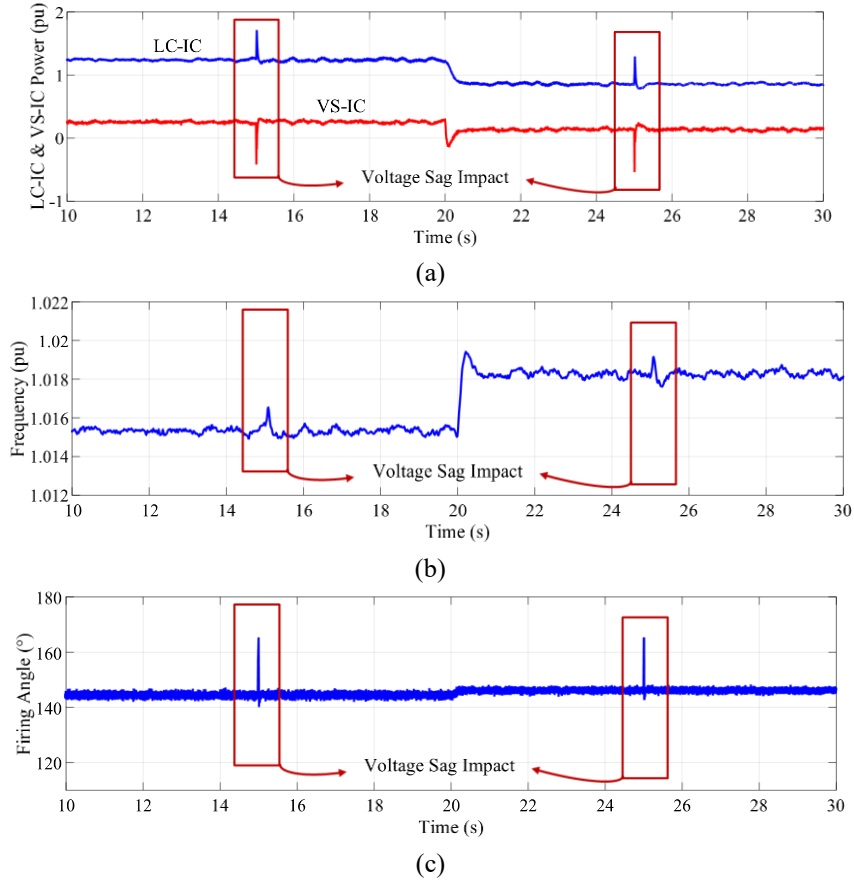


Fig. 3.9: AC sub-grid under fault state with voltage sag test results in improved unified control technique. a) LC-IC and VS-IC transmitted power. b) AC sub-grid frequency. c) Firing angle.

Taking this measure prevents continuous commutation failure. That helped the system to recover to its original point of operation quickly.

The DC sub-grid supported control is aimed to adjust the DC voltage level to the desired level in the absence of the aggregated slack terminal using ICs. The aggregated power terminals on both AC and DC sub-grids take the same values as previous tests. In the first interval, LC-IC and VS-IC's exchanged power is equal to $2.05 p.u.$ and $0.45 p.u.$, respectively, as shown in Fig. 3.10(a). For the second interval, LC-IC and VS-IC change the exchanged power to $1.64 p.u.$ and $0.36 p.u.$, respectively. The value of the DC voltage on the DC sub-grid equals $1.06 p.u.$ for the first and $1.05 p.u.$ for the second interval, as shown in Fig. 3.10(b).

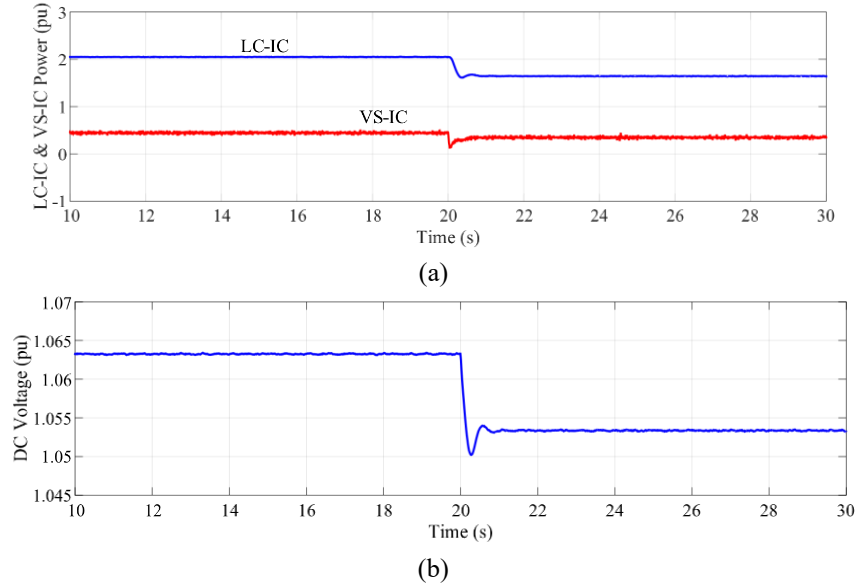


Fig. 3.10: DC sub-grid under fault state test results in improved unified control technique. a) LC-IC and VS-IC transmitted power. b) DC sub-grid voltage level.

The effectiveness of the proposed structure in exchanging a negative power is shown in Fig. 3.11. In the first interval, the aggregated power terminals values on the DC and AC sub-grids are as $2.5 p.u.$ and $-1.5 p.u.$ Consequently, the LC-IC and VS-IC adopt $2.05 p.u.$ and $0.45 p.u.$ as transmitted power, respectively. Also, similar to the previous test for the first interval, the value of the DC voltage on the DC sub-grid will be equal to $1.06 p.u.$ However, in the second interval, the aggregated power terminals' value changes to $-1 p.u.$ and $0.5 p.u.$ for the DC and AC sub-grids, respectively. Therefore, the ICs respond to the applied changes by adopting $0.13 p.u.$ for LC-IC and $-1.13 p.u.$ for the VS-IC, as shown in Fig. 3.11(a).

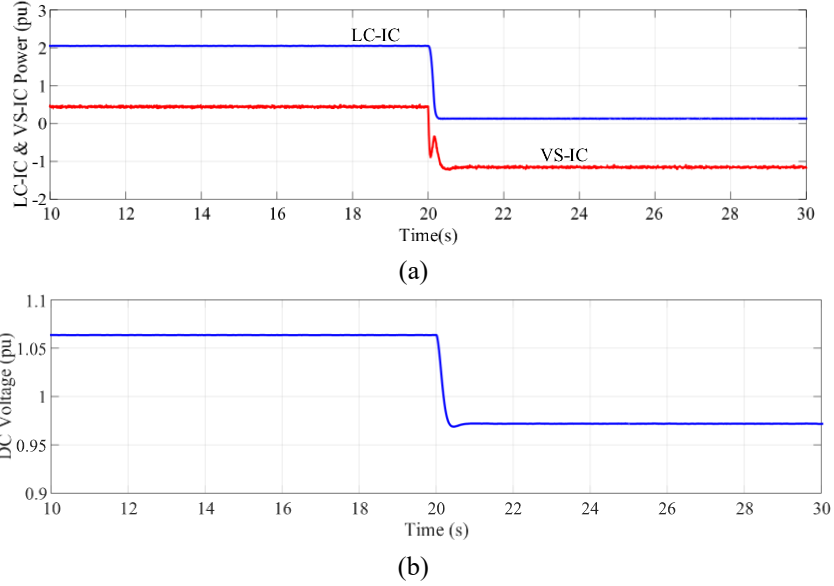


Fig. 3.11: DC sub-grid under fault state with negative transmitted power test results in improved unified control technique. a) LC-IC and VS-IC transmitted power. b) DC sub-grid voltage level.

In this condition, due to the physical limitation of the LC-IC in transmitting a negative power, its corresponding value should drop to a minimum possible amount. The volume of the DC voltage on the DC sub-grid in the second interval also can be found in Fig. 3.11(b), which is equal to $0.97 p.u.$

The reactive power consumption/injection of the ICs are tested, as shown in Fig. 3.12. The aggregated power terminals are tuned as $P_{AC,p,pu} = -1.5 p.u.$ and $P_{DC,p,pu} = 2.5 p.u.$ The grid is assumed to be operating in the power-sharing operation state. The exchanged active power is expected to be equal to the values as is shown in Fig. 3.7. The LC-IC is expected to consume reactive power while the VS-IC should provide the required reactive power following the parallel LCC-VSC-based new installation's control scheme. The LC-IC's consumed reactive power and injected reactive power of the VS-IC can be found in Fig. 3.12. As it can be seen, the LC-IC's required reactive power is mostly provided by VS-IC. A passive reactance is designed to deliver 0.136 Mvar along with parallel VS-IC. In the first interval, $t = 10 - 20s$, the LC-IC consumes 0.6 Mvar, and VS-IC provides 0.47Mvar to keep PCC voltage within the desired range. The LC-IC's reactive power consumption changes to 0.45 Mvar due to a lower amount of injected active power in the second interval $t = 20 - 30s$. Therefore, expectedly, the VS-IC's

injected reactive power will change to 0.3 Mvar to keep up with the system changes.

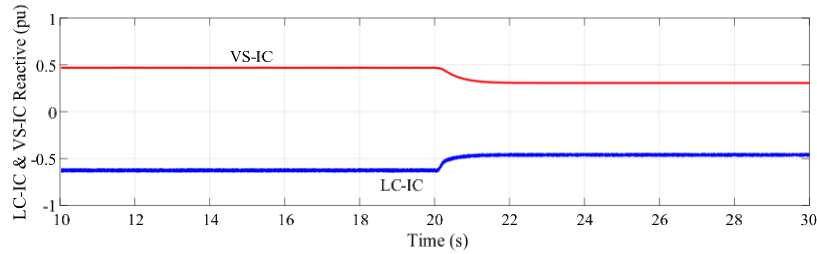


Fig. 3.12: Injected and consumed reactive power by LC-IC and VS-IC in power-sharing operation condition, respectively, in parallel LCC-VSC-based new installation's control scheme.

As can be seen, the VS-IC was able to actively support the LC-IC with required reactive power in all the operations states and avoid the commutation failure despite the changes in the exchanged active power.

3.5 Conclusion

This chapter reviewed the proposed unified control scheme for the paralleled VSC and LCC configuration in a hybrid AC/DC grid in a form of new installation. The proposed structure and control scheme provides the opportunity for the system to operate under various operational conditions (normal and under fault) with stable and smooth transients. The performance of the proposed control scheme for the parallel LCC-VSC configuration has been verified by several tests under different operational conditions. The proposed structure and control scheme have been designed to maintain the DC voltage of the DC sub-grid and the AC voltage/frequency of the AC sub-grid within the desired ranges. The adoption of the proposed droop equivalent control for the LCCs not only improved their performance significantly but saved costs by allowing the system to adopt the parallel LCC-VSC configuration. The normal operational test result shows an effective response to the aggregated power terminal changes based on the adjustments to the exchanged power. The AC sub-grid fault operation condition with and without AC voltage sag showed that, despite the changes to the aggregated power terminal, the AC frequency is kept within the 1 pu range by proper control

of the ICs. Similarly, the DC voltage is controlled by ICs and kept within the 1 *pu* range in the DC sub-grid fault conditions despite changes in aggregated power terminals. The parallel LCC-VSC configuration has removed LCC's control limitations to a great extent and improved its fault response as provided in the AC sub-grid fault test with AC voltage sag. This is achieved by minimizing the continuous commutation failure as a primary limiting factor of the LCC's operation. It can be concluded that the real-time simulation results for the proposed system satisfy the system's desires with minimal or non-commutation failure.

Chapter 4

Harmonics Mitigation Technique for Parallel LCC-VSCs Interlinking Converters

The power quality of LCCs is a well-known burden on power system. The proposed control scheme will guarantee a superior performance for the system and refrain from interrupting harmonics mitigation. The proposed configuration, as explained previously, grants the power system several advantages if properly controlled. The VSCs in the proposed structure can be actively used to address some of the LCC's drawbacks, namely, reactive power consumption, limited dynamic response, and low power quality. The reactive power consumption and limited dynamic response are successfully addressed in previous sections. However, the issue of the LCC's low power quality still needs to be addressed. Conventionally passive components are used to mitigate power distortions in such units. Therefore, according to previous discussions about existing LCC-based installations, the use of an expansion control scheme is recommended. However, the active harmonic compensation can be crucial for the parallel LCC-VSC-based new installation's control scheme, since the active compensation is essential for new installations with limited passive compensation units.

The ancillary services of the VSC-based power grids are widely available. There are several works addressing harmonics compensation and power quality improvement techniques in VSC-based hybrid AC/DC grids [77],[79],[80]. The virtual impedance control technique is one of the effective methods available for harmonic compensation in VSC-based systems [78],[81],[82], [83]. In this method, the VSCs are controlled to make a low impedance path for the harmonics on the desired frequency. The intensity of the compensation can be adjusted based on the power capacity of the units. As mentioned previously, the parallel LCC-VSC

configuration is designed to be used in a hybrid AC/DC grid to establish a stage to benefit both technologies' advantages. The power quality and stability improvement techniques of the parallel LCC/VSC is one of the proposed configuration advantages which has not been investigated in the literature.

Therefore, it is essential to study the proposed IC configuration for such services in more detail in the hybrid AC/DC grids. As explained, the interaction between ICs is more accessible in the proposed parallel LCC-VSC-based new installation's control scheme. This simply makes it more feasible for VS-ICs to adapt several supplementary control services without affecting the system's properties control. Thus, such techniques make it easier for the proposed parallel LCC-VSC-based new installation's control scheme to be used in new installations with minimum passive compensating units. In this regard, the design aspects of the harmonic compensation for the parallel LCC-VSC-based new installation's control scheme need to be studied (e.g., the extent of the harmonics compensation and system stability).

In this chapter, a compensating technique is developed for VS-ICs to mitigate the LC-ICs harmonics issue based on the virtual impedance control scheme. In order to improve the performance of such a compensating scheme, low switching frequency features of the VS-ICs in a medium to high power hybrid AC/DC grid is taken into consideration, and appropriate solutions are offered.

4.1 Proposed Compensating Scheme of the VS-ICs

a) The proposed Compensating Technique

The proposed parallel LCC-VSCs configuration can facilitate system performance in several areas. In addition to active power and bidirectional power transfer in DC grids, the reactive power and harmonics compensation are some of the features to be named. The reactive power compensation can be achieved based on the proposed unified control scheme and its controlling properties. However, the harmonic compensation technique is applicable as a complementary control

scheme. The proposed compensating technique can be applied to the system independent of the main control loop.

The VS-ICs can impact the PCC's voltage quality by deploying a virtual impedance control scheme. In this regard, the proposed technique can determine the rejection or damping of the PCC harmonics with a correct feedforward function design. The harmonic rejection technique improves the VS-ICs' output voltage quality. However, the damping technique intends to compensate for the voltage harmonics at the PCC to enhance grid performance. The compensation function is applied to the PCC voltage feedforward by extracting the desired harmonics order [62]. The control scheme of the VS-ICs is shown in Fig. 4.1.

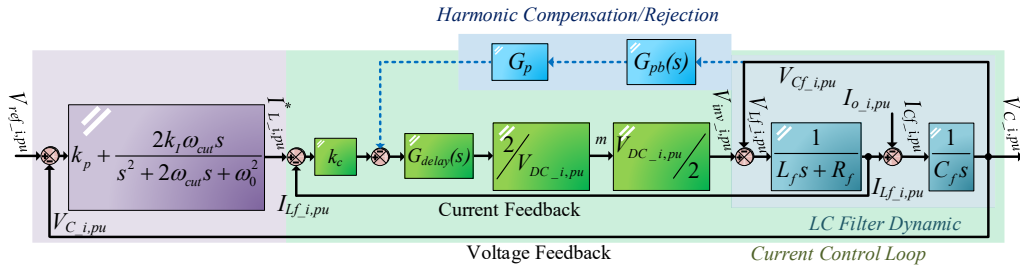


Fig. 4.1: The proposed VS-ICs double loop control with virtual impedance harmonic compensation/rejection feedforward.

In the proposed technique, as described in [62], the voltage harmonics are feedforwarded directly to the modulation references with a sufficient design of the G_p (compensation gain). The power grid as shown in Fig. 1.3, can be represented with an equivalent model as depicted in Fig. 4.2. In this design, the LC-IC is assumed to appear as a load for VS-ICs. Therefore, the LC-IC and nonlinear load are modeled as a harmonic current source parallel with an impedance that accounts for load in fundamental frequency. The grid also can be modeled as a voltage source and an impedance in series.

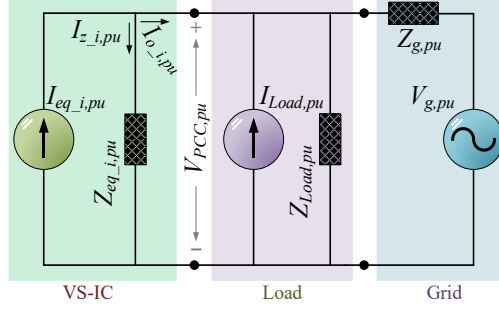


Fig. 4.2: Equivalent model of the system.

b) Equivalent Model of the System

Using the system's equivalent model as shown in Fig. 4.2 and the proposed compensation/rejection technique, the VS-IC's output terminal harmonic voltage can be represented as in (4.1), assuming an averaged linear model for the inverter.

$$V_{inv_i_h}(s) = -G_p \cdot V_{PCC_h}(s) \quad (4.1)$$

where $V_{inv_i_h}$, G_p , and V_{PCC_h} are inverter output harmonic voltage, feedforward gain, and PCC's harmonic voltage.

Based on the Norton equivalent circuit theory, the equivalent impedance and current of the VS-ICs can be found as given in (4.2) and (4.3).

$$Z_{eq_i,pu}(s) = \frac{Z_{L_i,pu}(s)Z_{C_i,pu}(s)}{Z_{L_i,pu}(s) + Z_{C_i,pu}(s)} \quad (4.2)$$

$$I_{eq_i,pu}(s) = \frac{Z_{C_i,pu}(s)}{Z_{L_i,pu}(s)Z_{C_i,pu}(s)} V_{inv_i,pu}(s) \quad (4.3)$$

$Z_{L_i,pu}(s)$ and $Z_{C_i,pu}(s)$ are inverter filter inductance and inverter filter capacitance.

Considering (4.4) in accordance with Fig. 4.2, the equivalent harmonic impedance Z_V of the VS-IC (4.5) can be obtained, substituting (4.2) and (4.3) in (4.4).

$$I_{eq_i_h,pu}(s) = \frac{V_{PCC_h,pu}(s)}{Z_{eq_i,pu}(s)} + I_{o_i_h,pu}(s) \quad (4.4)$$

$$Z_{V,pu}(s) = -\frac{V_{PCC_h,pu}}{I_{o_i_h,pu}} = \frac{Z_{L_i,pu}(s)Z_{C_i,pu}(s)}{Z_{L_i,pu}(s) + Z_{C_i,pu}(s)[1 + G_p]} \quad (4.5)$$

As can be understood from (4.5), the value of the G_p can change $Z_{V,pu}(s)$ to compensate or reject the desired harmonic order on the PCC.

In the complete model, the Norton equivalent model of the system can be represented, as it is shown in Fig. 4.3. In this layout, VS-ICs are denoted as parallel compensation units. The required compensation signal can be shared between VS-ICs to reach the desired impedance with more stability.

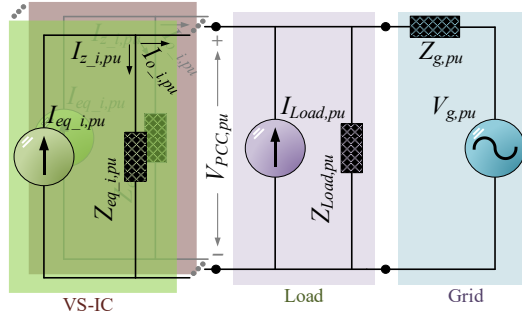


Fig. 4.3: Equivalent model of the system in the presence of parallel VS-ICs.

As explained previously in the proposed structure, the power-sharing capacity of the VS-ICs is limited to their rated capacity $\eta_1 : \dots : \eta_i = S_{VS-IC_1} : \dots : S_{VS-IC_i}$. Where S_{VS-IC_i} shows the rated capacity of the i -th VS-IC. A similar approach can be taken to design a proper virtual impedance control. Based on this design, VS-ICs with higher power transferring capacity can provide a lower impedance path for the desired harmonic order. Therefore, the impedance model of the targeted harmonic order can be depicted as Fig. 4.4.

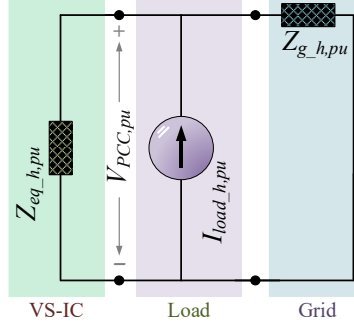


Fig. 4.4: Equivalent impedance model of the system in the presence of parallel VS-ICs.

In this model $Z_{eq_h,pu}$ represents the equivalent impedance of all parallel VS-ICs on the desired frequency order as it is obtained in (4.6).

$$Z_{eq_h,pu} = Z_{eq_i_h,pu} | \dots | Z_{eq_j_h,pu} \quad (4.6)$$

4.2 Modeling and Design of the Virtual Impedance

In order to achieve a stable and effective performance for harmonic compensation/rejection, the proposed virtual impedance control scheme should be modeled in detail.

The control system of the VS-IC uses double-loop control, as depicted in Fig. 4.1. To extract the desired harmonic orders, the function $G_{pb}(s)$ is used.

$$G_{bp}(s) = \frac{(\omega_h / Q)s}{s^2 + (\omega_h / Q)s + \omega_h^2} \quad (4.7)$$

Where Q represents as quality factor and ω_h is the desired harmonic frequency. Also, the proportional resonance controller is selected as (4.8) [66].

$$G_{PR}(s) = k_p + \frac{2k_i \omega_{cut} s}{s^2 + 2\omega_{cut} s + \omega_0^2} \quad (4.8)$$

The value of the compensation gain, G_p , should be carefully selected since, in addition to the harmonic compensation strength of the VS-ICs, the system's stability can also be affected. In this work, the G_p will be chosen to create a low impedance path on the desired harmonic order to compensate for the PCC voltage. The PCC harmonic rejection also can be achieved by proper design of the G_p value, which is not an objective of this work.

VS-ICs output voltage with respect to a reference voltage in the presence of the harmonic compensation/rejection feedforward is given in (4.9).

$$\begin{cases} G_V(s) = \frac{V_{C_i,pu}}{V_{ref_i,pu}} = \frac{G_{PR_i}(s)G_{delay}(s)k_c}{G_{V_Den}(s)} \\ G_{V_Den_i}(s) = G_{pb_i}(s)G_{p_i}(s)G_{delay}(s) + G_{PR_i}(s)G_{delay}(s)k_{c_i} + \\ \quad G_{delay}(s)Z_{C_i,pu}^{-1}k_{c_i} + Z_{L_i,pu}Z_{C_i,pu}^{-1} + 1 \end{cases} \quad (4.9)$$

Here $G_{delay}(s)$ represent switching and computation delay time. The details of the delay function can be found in [62].

As can be understood from (4.9), the control system's stability can be affected by harmonic compensation feedforward. Therefore, a system stability study should be performed along with the proper design of the compensation gain.

The equivalent impedance seen on the PCC of each VS-IC is also calculated. The transfer function between $V_{C_i,pu}$, and $I_{o_i,pu}$ will be defined as Z_V . As can be learned from (4.10), several controlling parameters can affect the equivalent impedance of the VS-ICs. However, computing the Z_V , the objective is to reach the desired impedance for the target harmonics order by designing the $G_p(s)$.

$$\begin{cases} -\frac{V_{C_i,pu}}{I_{o_i,pu}} = \frac{k_c G_{delay}(s) + Z_{L_i,pu}}{G_{ZV_Den}} = Z_V \\ G_{ZV_Den} = G_{pb_i}(s)G_{p_i}(s)G_{delay}(s) + G_{PR_i}(s)G_{delay}(s)k_{c_i} + \\ \quad G_{delay}(s)Z_{C_i,pu}^{-1}k_{c_i} + Z_{L_i,pu}Z_{C_i,pu}^{-1} + 1 \end{cases} \quad (4.10)$$

The frequency response of a VS-IC's equivalent impedance can be obtained using (4.10), taking $V_{C_i,pu}$ as the input and I_{o_i} as an output. The bode graph of the system impedance seen by the load is depicted in Fig. 4.5, representing several harmonic orders in different impedance magnitudes.

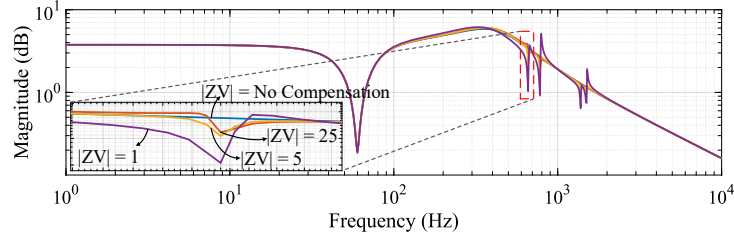


Fig. 4.5: Bode plot of system impedance from load point of view, compensation for 11th, 13th, 23rd and, 25th harmonics.

The frequency response pictures the harmonic compensations for a typical 12-pulse LCCs harmonic orders such as 11th, 13th, 23rd, and 25th. The bode graph shows that by sufficient selection of feedforward gain for the desired harmonic order, the compensation/rejection can be achieved.

In order to examine the stability of the system in the presence of the harmonic compensation/rejection feedforward, (4.9) is taken into consideration. In this regard, the virtual impedance feedforward is set to compensate/reject the 13th harmonic order. Furthermore, the effect of the virtual impedance gain in different quantities is also incorporated into the test procedure.

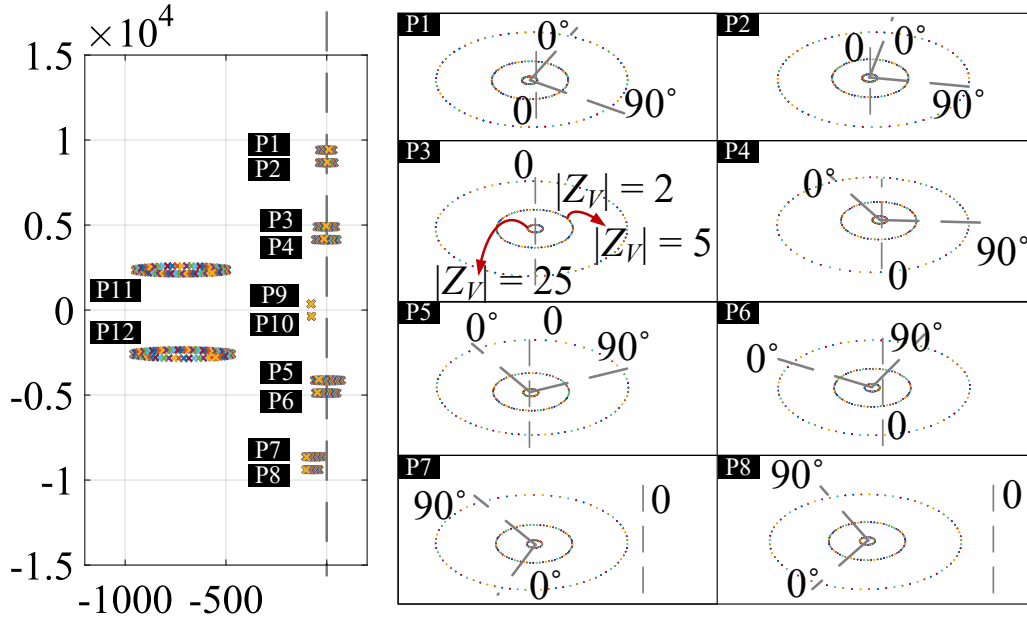


Fig. 4.6: Pole-placements of the control function in several virtual impedance values.

The pole positioning is tested by considering the virtual impedance norm as 1, 5, and 25 and the angle as 0 to 2π , as shown in Fig. 4.6. As shown in Fig. 26, the norm and angle can significantly impact the system's stability proposition.

Increasing the norm's value results in a smaller radius for circular scatter of poles by changing the angle of Z_V from 0 to 2π . The lower values for the norm that equally represent the higher harmonic compensation quality of the proposed control system show that a set of right half plane poles can be detected in several settings based on the compensation angle. However, as it can be seen by changing the virtual impedance angle to certain values, it is possible to achieve stability. Therefore, similar to the norm, this component proves to play an essential role in designing feedforward gain. The norms with higher magnitude show greater stability in a broader range of angles. However, higher norm values may not satisfy the desired compensation effect due to less attenuation factor.

Assuming the norm as small as $|Z_V| = 2$, the poles scatter in the bigger circle as the angle changes from 0 to 2π . In this condition, the P_1 and P_4 sets of poles are the ones with the most appearance in the unstable region. P_2 and P_3 also appear in the unstable region but within a smaller range. The pole sets P_5 , P_6 , and P_7 all appear on the stable side independent of the feedforward gain and its angular limit. The pole positioning shows that for the norm equal to 2, the system displays stable performance when the virtual impedance angle is between $10\pi/9$ to 2π . As depicted in Fig. 4.6, the changes to the norm value from 2 to 5 and 25 puts all poles in the left-hand plane independent of their angle. However, as it is stated previously, the higher norms cutback the compensation quality of the control system. Based on the provided explanation, it can be concluded that a slight increase in the virtual impedance norm can considerably boost the stability margin of the system while providing reasonable compensation.

4.3 Peak Power Capacity of the Parallel VS-IC

The current quality of LCCs can be found significantly inferior by the available standards [84]. The produced harmonics can significantly impact grid voltage quality resulting in loss and instability in the system. In this matter, VS-IC can substantially rectify the grid's voltage quality considering a proper compensation technique and availability of the power capacity.

In the proposed control schemes, the AC and DC sub-grid's properties determine the power reference in such a hybrid AC/DC grid as it is given in Fig. 2.1. The proposed harmonic compensation and reactive-power support can add to the expected power capacity of the VS-ICs. Therefore, to determine a stable and consistent performance the power rating of the VSCs should be well determined [81]. In this regard, in addition to the VS-IC's main control's expected active and reactive power limits, their harmonic compensation capacity should also be considered.

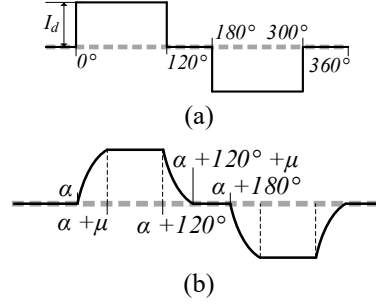
At full power, the AC current for a 12-pulse LCC, as shown in Fig. 1.2 connected through a wye-delta and wye-wye to the AC grid, can be expressed as follow:

$$I_{IC_LCC} = \frac{2\sqrt{3}}{\pi} 2I_{DC_LCC} \left[\sin \omega t - \frac{1}{11} \sin 11\omega t + \frac{1}{13} \sin 13\omega t - \dots \right] \quad (4.11)$$

where I_{IC_LCC} and I_{DC_LCC} represent the current on the LCC's AC and DC sides. It can be learned from (4.11) that the harmonic order's magnitude can be reported based on the fundamental harmonic as given in (4.12).

$$I_n = \frac{I_1}{n} \quad (4.12)$$

I_n is the magnitude of the n th harmonic current, and I_1 is the magnitude of the fundamental current, which is also proportional to the DC power. The first harmonic magnitude based on the DC current for a 12-pulse converter can be defined $I_1 = 2\sqrt{6}/\pi I_{DC_LCC}$. The curve for LCC current in an ideal situation is depicted in Fig. 4.7(a). In the non-ideal circumstance, the impact of the commutation reactance results in an overlap angle that will round off the square edges of the current waves resulting in a reduction of the magnitude of harmonic components Fig. 4.7(b).



Therefore, the ratio between the ideal current and the current with commutation reactance impact is provided in (4.13).

$$\frac{i_{ov}}{i} = \frac{\sqrt{H^2 + K^2 - 2HK \cos(2\alpha + \mu)}}{\cos\alpha - \cos(\alpha + \mu)} \quad (4.13)$$

$$H = \frac{\sin(n+1)\mu/2}{(n+1)}$$

$$K = \frac{\sin(n-1)\mu/2}{(n-1)}$$

where μ , α , n , i_{ov} , and i are overlap angle, firing angle, current magnitude with overlap angle, and current magnitude without overlap angle.

Traditionally, as depicted in Fig. 2.1, passive filters are used to remove harmonics. In the 12-pulse structure, the passive filter harmonics are expected to be formed, as shown in the following Fig. 4.8 [16]. As it can be seen in Fig. 4.8, the 11th and 13th harmonic orders are directly targeted, and higher harmonic orders are mitigated using a high pass filter.

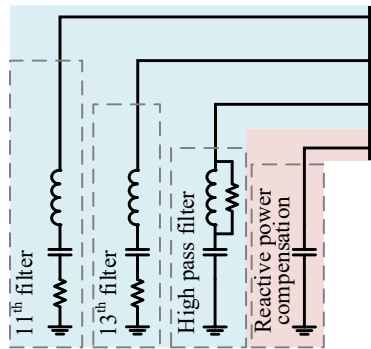


Fig. 4.8: Conventional passive filter units.

Due to the structure and characteristics of the LCCs, it is possible for the grid to deal with non-characteristic harmonic orders. In such an environment, the source of non-characteristic harmonics on the AC side is:

- 1) Unbalanced AC system fundamental voltage.

- 2) Commutation reactance unbalance between 6-pulse bridges in a 12-pulse or higher configuration.
- 3) Commutation reactance unbalance between phases within a 6-pulse bridge.
- 4) Firing angle jitter within a 12-pulse group.

These kinds of harmonics are possible to be present in the system, but their randomness and the fact that they are project dependent can postpone their studies to the lunch stage.

As mentioned in the IEEE Std 519-2014 standard [84] the harmonics orders 11th, 13th, 23rd, and 25th current ratio compared to the rated current should not exceed 2%, 2%, 0.6%, and 0.6%, as shown in Fig. 4.9. Therefore, the virtual impedance limitations for each harmonics order based on the [84] can be defined as it is given in (4.14). The produced harmonics can significantly impact grid voltage quality resulting in loss and instability in the system. In this matter, VS-IC can significantly rectify the grid's voltage quality considering a proper compensation technique and availability of the power capacity.

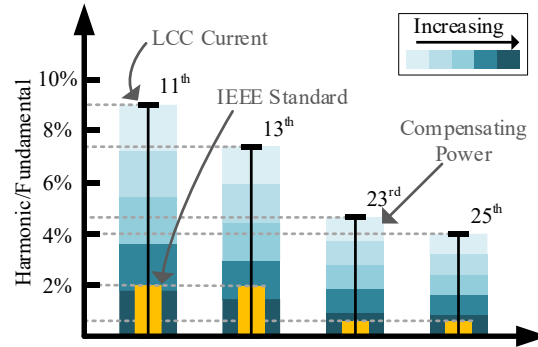


Fig. 4.9: The percentage of the 12-pulse LCC harmonics to fundamental and IEEE standard for

Therefore, it can be concluded that compensation of LCC's harmonics is necessary for all orders.

$$\begin{aligned}
 Z_{Z_T_11} &\leq 0.28Z_{g_11} \\
 Z_{Z_T_13} &\leq 0.35Z_{g_13} \\
 Z_{Z_T_23} &\leq 0.16Z_{g_23} \\
 Z_{Z_T_25} &\leq 0.17Z_{g_25}
 \end{aligned} \tag{4.14}$$

Using (4.10), (4.11), and (4.14) and assuming that VS-ICs are compensating

for all LC-IC's harmonic orders, the apparent compensating power of the VS-IC's can be defined as follow based on [89]:

$$S_N^2 = D_I^2 + D_V^2 + S_H^2 \quad (4.15)$$

D_I , D_V , and S_H are current distortion power, voltage distortion power, and harmonic's apparent power. As depicted in Fig. 4.5 and according to (4.15), lower virtual impedance for compensating the LCC harmonics will require a higher amount of compensating power.

Furthermore, the VS-ICs reactive power compensation based-on the unified control scheme also needs to be considered designing the VS-ICs. In general, the reactive power consumption in LC-IC can take up to 50 to 60% of the supplied active power at the rated load [85]. The approximated consumed reactive power based on LCC's DC exchanged power can be defined as shown in (4.16).

$$Q_{LCC} = P_{d_LCC} \sqrt{\left[\frac{1 + 0.5x_{com}P_{d_LCC}}{\cos\gamma} \right]^2 - 1} \quad (4.16)$$

P_{d_LCC} , x_{com} , and $\cos\gamma$ are LCC's supplied power on the DC side, commutation reactance, and extinction angle. The required reactive power based on the exchanged active power is shown in Fig. 4.10. As it can be seen, the LCC unit consumes 0.58 pu reactive power while exchanging 1 pu active power.

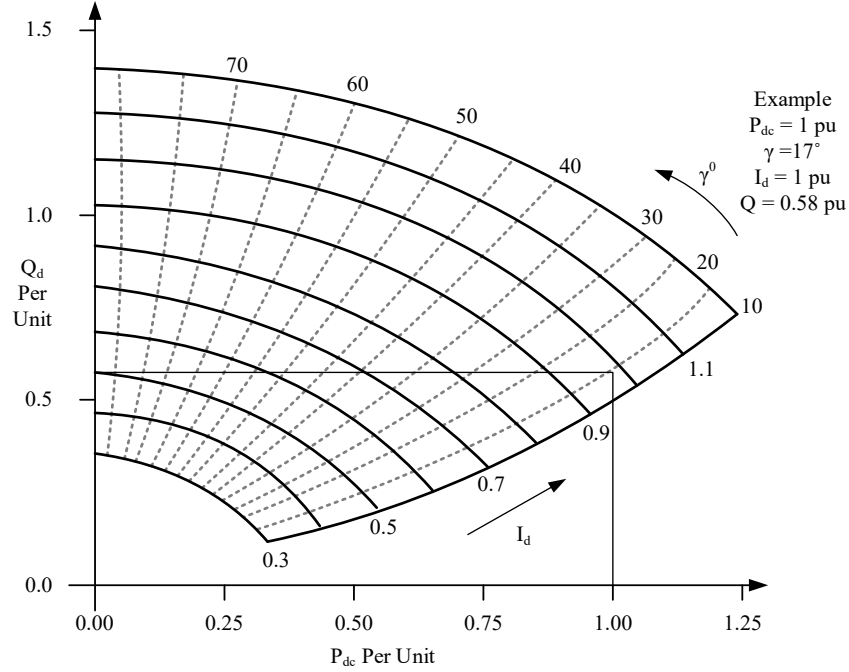


Fig. 4.10: Reactive power required according to variation of active power [85].

Assuming an active compensation for a 12-pulse LCC unit, the required power can be defined as it is given in (4.17).

$$\begin{aligned}
 S_{Comp}^2 &= S_{11th}^2 + S_{13th}^2 + S_{23rd}^2 + S_{25th}^2 + \dots \\
 S_{11th} &= 3I_{11th}^2 Z_{V11th} \\
 S_{13th} &= 3I_{13th}^2 Z_{V13th} \\
 &\vdots
 \end{aligned} \tag{4.17}$$

Therefore, considering (4.16), (4.17), and the proposed unified control exchanged active power, the rating of the VS-IC units can be defined as follow:

$$\begin{cases}
 S_{Total}^2 = S_{Comp}^2 + S_{IC}^2 \\
 S_{IC}^2 = Q_{LCC}^2 + P_{IC_i}^2
 \end{cases} \tag{4.18}$$

In order to facilitate the understanding of rated power capacity for VS-ICs an example is given. This example assumes that the VS-IC unit conducts harmonic and reactive power compensation. Taking a 1pu power exchange for the LCC unit, the required reactive power will be around 0.58pu. Also, it is assumed that the exchanged power rating of the VS-IC based on the unified control is half of the LC-IC unit, $P_{IC_1} = 0.5pu$.

The line impedance is taken as given in the Simulink model ($R = 0.01273 \Omega/\text{km}$ and $L = 0.93337\text{e-}3 \text{ H/km}$). The line impedance for each harmonic order in a 20km line can be calculated as follow:

$$\begin{aligned} Z_{g_{11}} &= 7.1 pu \\ Z_{g_{13}} &= 8.4 pu \\ Z_{g_{23}} &= 14.9 pu \\ Z_{g_{25}} &= 16.2 pu \end{aligned} \tag{4.19}$$

Therefore using (4.14) and (4.19), the virtual impedance limits can be calculated, as given in the following.

$$\begin{aligned} Z_{eq_{11}} &\leq 1.98 pu \\ Z_{eq_{13}} &\leq 2.94 pu \\ Z_{eq_{23}} &\leq 2.38 pu \\ Z_{eq_{25}} &\leq 2.75 pu \end{aligned} \tag{4.20}$$

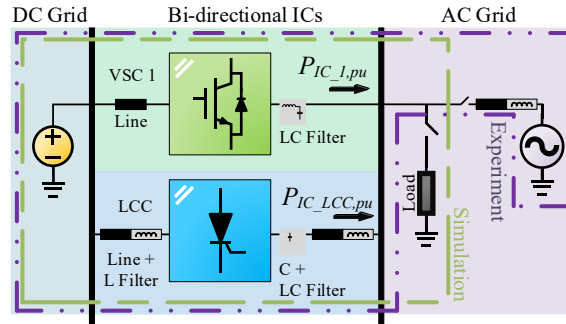
Taking the maximum permissible norm for virtual impedances the harmonic compensation current for 11th, 13th, 23rd, and 25th are $0.0579 pu$, $0.0490 pu$, $0.0277 pu$, and $0.0255 pu$. Similarly, the VS-IC's apparent power can be calculated as $0.76 pu$.

The harmonics and reactive power compensation can take a considerable amount of VS-IC's rated capacity. In this regard, the reactive power compensation takes the majority of the rated capacity compared to the harmonics compensation. Replacing all passive compensating units with the equivalent active-controlled VS-ICs seems to be an unviable option due to the cost concern. Therefore, harmonics compensation can be addressed by VS-ICs due to their lower power requirement, and reactive power compensation can be tackled with effective utilization of passive components along VS-ICs support to balance the cost with performance.

4.4 Simulation Results

In order to check for the effectiveness of the proposed control scheme, the simulation and experimental tests are conducted using the simplified structure of the proposed system, as depicted in Fig. 4.11. The simulation is conducted considering an AC-grid connected to parallel 12-pulse LC- and VS-ICs through an

impedance, representing the transmission line. In addition to the proposed high power quality exchanging feature of the proposed structure, its potential to provide a high-power quality for a sensitive load is evaluated using an experimental test. The ICs are intended to provide the required high-quality power for a load, directly connected to the ICs at the PCC.



The circuit components are selected as it is given in Table 4.1. The DC sub-grid's aggregated slack and power terminals are replaced with a DC source in both experimental and simulation tests.

Table 4.1: The tested grid's parameters.

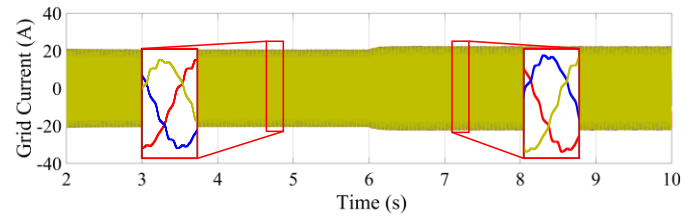
System	Parameter	Value	
DC Sub-grid	DC voltage	150V	
AC Sub-grid	Load (<i>Experiment</i>)	6 Ω and 5 Ω	
	Line Impedance (<i>Simulation</i>)	0.25 Ω + 0.5 mH	
	AC phase voltage (<i>Simulation</i>)	30 v	
	AC frequency (<i>Simulation</i>)	60 Hz and 59.9 Hz	
IC	VS-IC	Switching frequency	5kHz
		Filter (LC)	5mH/80 μ F
	LC-IC	Filter DC (L)	0.5mH
		Filter AC (C)	80 μ F
		Transformer (n1/n2)	1/1

Also controlling parameters can be found in Table 4.2.

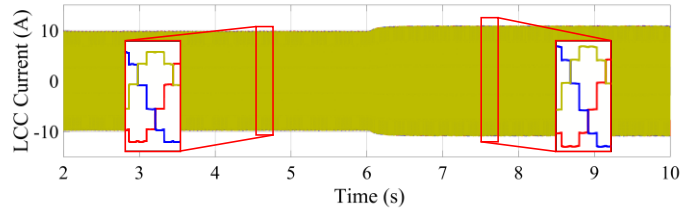
Table 4.2: Control system's controlling parameters for simulation and experiment.

Parameter	Value	Parameter	Value
k_P	12	a	0.1
k_I	300	k_c	0.3
ω_{cut}	8	k_{P_l}	0.5
ω_0	$2 \times 60\pi$	H_{p_l}	0.02
T_L	12580		

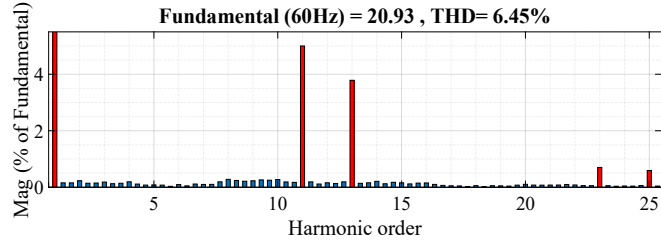
The test is conducted with and without compensation to illustrate the impact of the proposed scheme on power quality. Due to the fact that the proposed compensation technique is applied to the control system in the very inner loop, its impact on the outer unified control loop can be neglected. Therefore, the test does not try to cover the performance of the unified control scheme and solely focuses on LCC's harmonics compensation.



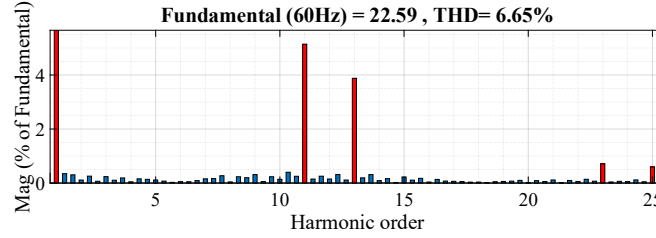
(a)



(b)



(c)



(d)

Fig. 4.12: Uncompensated simulation results. (a) Grid current. (b) LCC current. (c) Grid current THD in first interval. (d) Grid current THD in second interval.

Initially, a simulation is conducted taking the circuit structure as it is given in Fig. 4.11 and circuit components as provided in Table 4.1. In order to check for the impact of system properties changes on harmonics compensation performance, the AC frequency is dropped by 0.1 Hz at the second 3 of the simulation, dividing the simulation into two intervals. As it can be seen in the simulation results, shown in Fig. 4.12 and Fig. 4.13, the ICs injected active power is increased due to supportive features of the proposed unified control. The simulation results for the condition in which the harmonics compensation control is not applied are provided in Fig. 4.12. As shown in Fig. 4.12, in both first and second intervals, the grid's injected current THD exceeds the grid standard [84]. In addition to that, the harmonics orders 11th, 13th, 23rd, and 25th current ratio exceeds the standard limits with their value equal to 5%, 3.7%, 0.7%, and 0.6%. Therefore, based on the available simulation results, the harmonics orders 11th, 13th, 23rd, and 25th should be compensated.

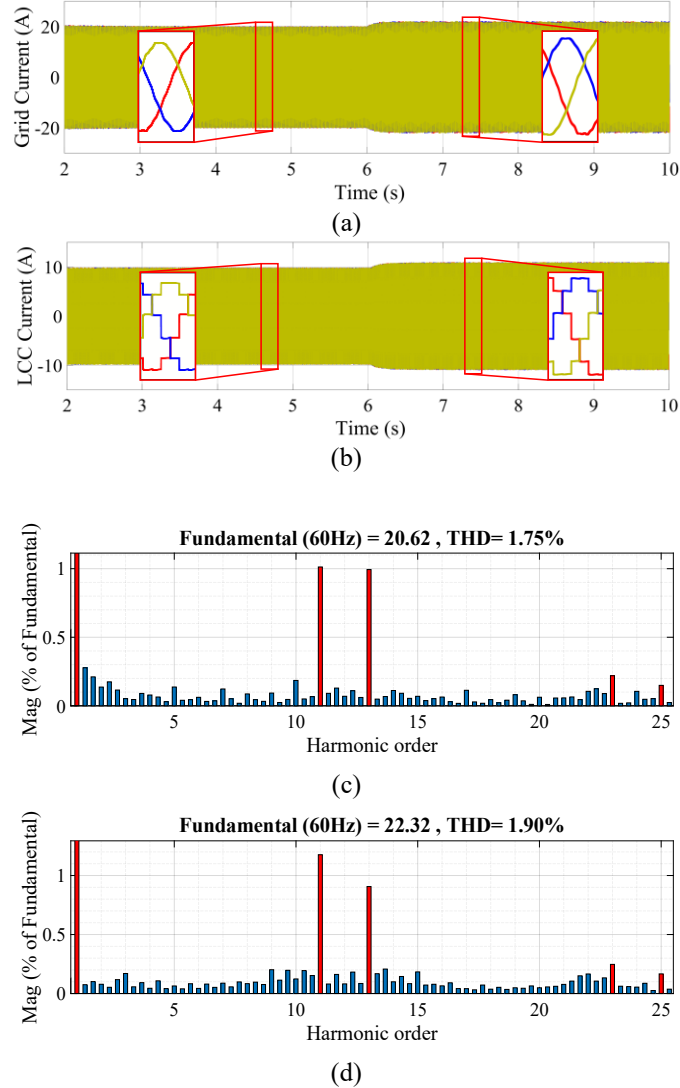


Fig. 4.13: Compensated simulation results. (a) Grid current. (b) LCC current. (c) Grid current THD in first interval. (d) Grid current THD in second interval.

The simulation results for the condition in which the harmonics compensation is implemented to the control system are provided in Fig. 4.13. Considering the transmission line impedance and based on the (4.14) the values for the virtual impedances should be considered lower than 0.58Ω , 0.86Ω , 0.69Ω , and 0.8Ω for 11th, 13th, 23rd, and 25th harmonics orders, respectively. In this condition, the value of the virtual impedance for each of the 11th, 13th, 23rd, and 25th harmonics orders are designed as 0.4Ω , 0.6Ω , 0.66Ω , and 0.61Ω , respectively, into VS-IC's control scheme considering system stability as depicted in Fig. 4.6. The frequency is dropped 0.1 Hz at the second 3 of the simulation to portrait the impact of the

harmonics compensation in case of a change in system element. As it can be seen in the first interval, the injected current by ICs to the grid has a THD of around 1.75%. The harmonics orders 11th, 13th, 23rd, and 25th current ratio is also dropped to 1%, 1%, 0.2%, and 0.15% below the grid requirements.

Similarly, as can be seen in Fig. 4.13, in the second interval, the grid current's THD is equal to 1.90%. Therefore, the individual harmonic orders 11th, 13th, 23rd, and 25th have their current ratio equal to 1.1%, 0.9%, 0.2%, and 0.16%. Therefore, it can be concluded that in both test conditions, the harmonics orders and current ratios are kept within the standard requirements. The required power for compensating for the LC-IC's harmonics order, S_N , is calculated to be equal to around 187 VA for the simulated system, which is comparably smaller compared to the injected power. Such a control scheme can be easily implemented into the VS-ICs in the proposed configuration without a need for outstanding capacity expansion.

In order to high the effectiveness of the proposed control scheme, the simulation results with and without compensation are provided in a single run as given in Fig. 4.14(a), (b). Fig. 4.14(a) shows the grid current when the AC frequency is set to 60 Hz, and Fig. 4.14(b) shows the results for the condition in which the grid frequency is dropped by 0.1 Hz. The compensating signal is removed in second 2 of the simulation to show the effectiveness of the proposed scheme. As it can be seen in both power exchange conditions the compensated signal has very low THDs, similar to the provided results before, equal to 1.74% and 1.91% in two loading conditions.

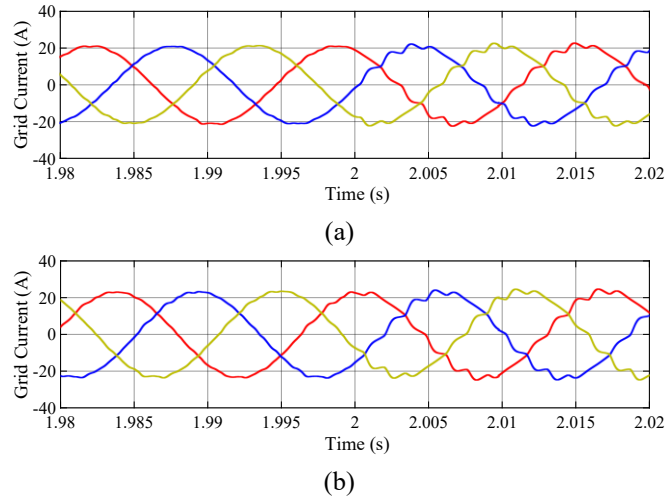


Fig. 4.14: Simulation results for grid current with and without compensation. (a) Grid frequency 60 Hz. (b) Grid frequency is dropped 0.1 Hz.

4.5 Experimental Results

The experimental test is conducted considering the circuit is given in Fig. 4.11 and the components as provided in Table 4.1. The interlinking converter is achieved by connecting a 2-level VSC and a 12-pulse LCC in parallel. The control method is conducted on the MicroLabBox 1202 controller. The analog to digital conversion (ADC) and PWM pulse emission is realized on the embedded programmable FPGA (Xilinx Kintex-7 XC7K325T). The performance of the 12-LCC is imitated using two fully controlled current source converters. The experimental setup and controller unit are shown in Fig. 4.15.

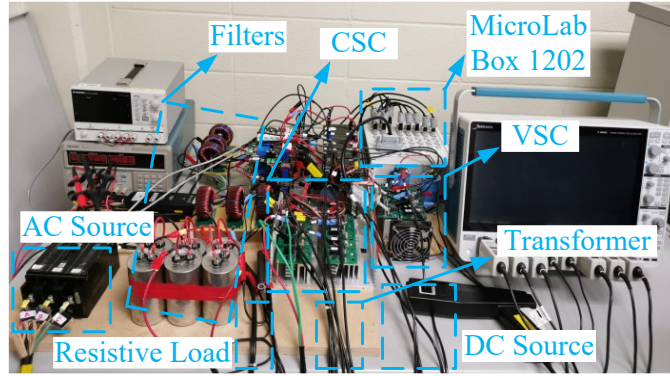


Fig. 4.15: The experimental setup.

Fig. 4.16 shows the experimental results for the condition in which the harmonics compensation is not applied. The results include load current, load voltage, and LC-IC current. In this test, the load is assumed to be sensitive to the voltage quality. Therefore, the control system will compensate for the load's voltage quality by analyzing it for harmonic orders and compensating for the out-of-the-range values. Similar to before, in this test, the load current represents the combination of the LC-IC, and VS-IC exchanged power. In the test process, AC load is changed from 6Ω to 5Ω , showing the compensating capability of the proposed technique.

As it is given in Fig. 4.16, in both loading conditions, the total harmonic distortion (THD) of the current is around 5.23% and 5.01% for the first and second loading conditions, respectively. Also, as it can be seen, the individual harmonic orders, 11th, 13th, and 23rd, are experiencing a high amount of distortion in load voltage and current as shown in Fig. 4.17 and Fig. 4.18, respectively.

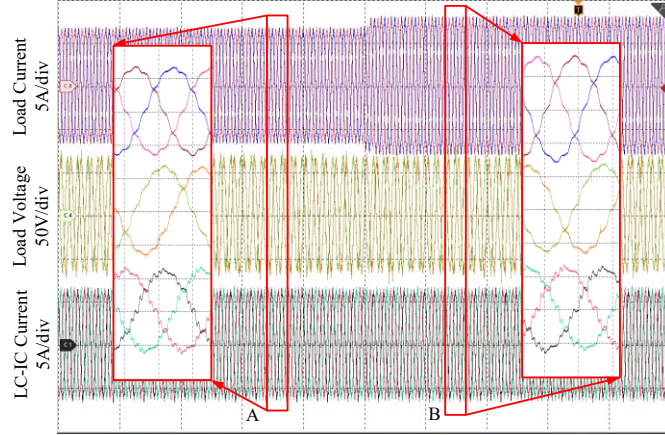
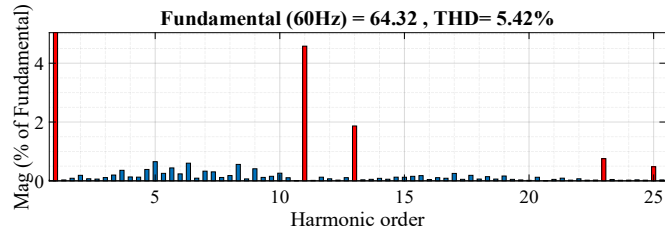
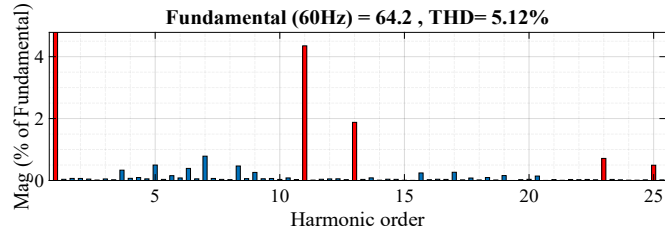


Fig. 4.16: Experimental results for the condition without compensation.

Therefore, compensating for such harmonics orders to improve the voltage quality to the desired range is anticipated as provided in available standards. In this regard, the harmonic compensation is applied to the LC-IC current's harmonics orders by VS-IC, improving the load current's overall quality and expected load voltage. Therefore, the harmonics compensation will target the 11th, 13th, and 23rd harmonic orders. The experimental results for the test condition with harmonic compensation control are shown in Fig. 4.19. A compensating signal, based on a virtual impedance of a $1.2\angle 150^\circ$, $2\angle 24^\circ$, and $1.7\angle -103^\circ$ for 11th, 13th, and 23rd harmonic orders, are applied to the VS-IC control system. According to the measurements, the 25th harmonic order is appeared to be low enough and harmonic compensation is not required. The THD of the injected current to the load and the value of the individual harmonic orders after harmonics compensation as well as THD of the load voltage and individual harmonic orders, can be found in Fig. 4.20 and Fig. 4.21, respectively. The available measurements show that the desired harmonics compensation and system stability are achieved using the proposed control scheme with THD less than 2.5% for both load voltage and current in first and second loading conditions.

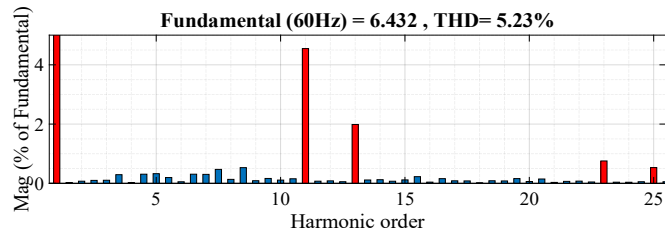


(a)

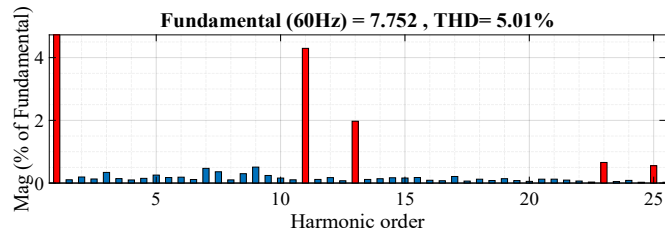


(b)

Fig. 4.17: Load voltage THD without harmonics compensation. (a) First loading condition. (b) Second loading condition.



(a)



(b)

Fig. 4.18: Load current THD without harmonics compensation. (a) First loading condition. (b) Second loading condition.

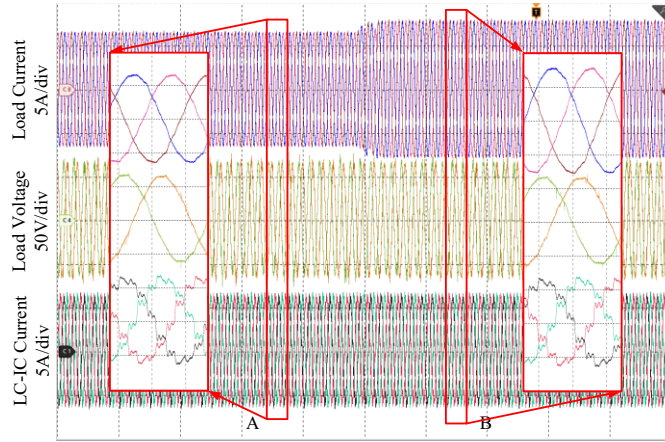
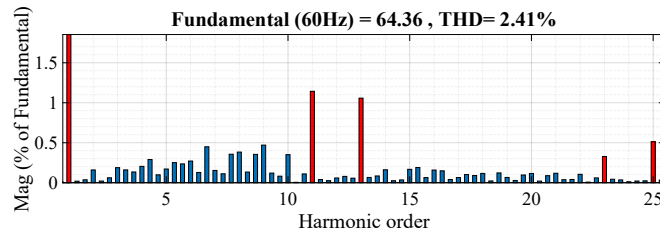
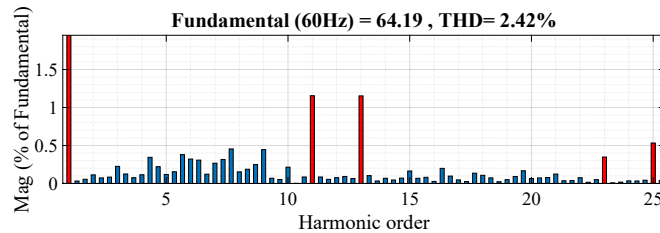


Fig. 4.19: Experimental results for the condition with harmonics compensation.

As it can be seen in Fig. 4.20, the load voltage's ratio of the 11th harmonic order with respect to the main harmonic order is dropped from 4.6% in the first loading condition and 4.3% in the second loading condition to around 1.1% for both first and second loading conditions. Similarly, the 13th harmonics order ratio drops from 1.8% in the first and second loading conditions to 1% and 1.1%, respectively. The 23rd harmonic order ratio compared to the main harmonic order drops from around 0.75% and 0.71% in first and second loading conditions, respectively, to around 0.3%. Similarly, the load current's THD and individual harmonics order's ratios, as shown in Fig. 4.21, is dropped considerable resulting in improved voltage quality.



(a)



(b)

Fig. 4.20: Load Voltage THD with harmonics compensation. (a) First loading condition. (b) Second loading condition.

As explained previously, the required power of the harmonics compensating signal can be calculated using (4.15). Taking LC-IC's exchanged power and circuit parameters as it is given in Table 1, the S_N is calculated to be equal to 4.8 VA and 7.2 VA in first and second loading conditions, respectively. Also, the provided reactive power by VS-IC for the parallel LC-IC is around 12 var, which is equal to the subtraction of the LC-IC's required reactive power from the amount provided by the passive filter. As it can be understood, the required harmonics compensating power is considerably smaller than the LC-IC's required reactive power. Therefore, both passive and active reactive power compensation and active harmonic compensation by parallel VS-ICs can be recommended as the most viable approach. In this regard, the power quality can be kept within the desired range while the expenses are saved.

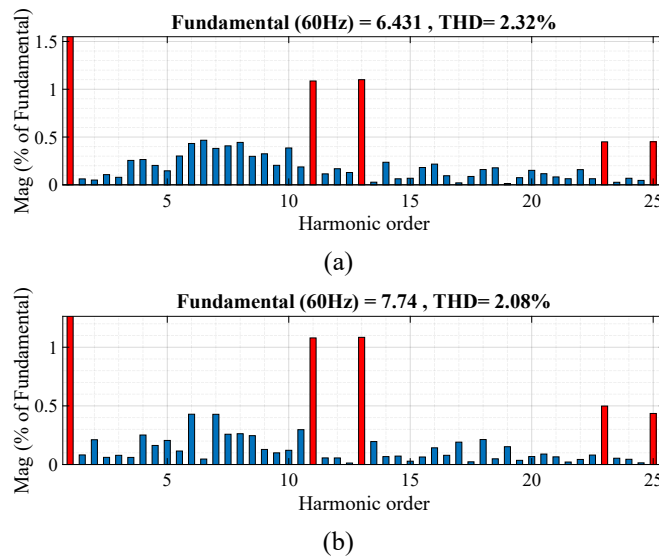


Fig. 4.21: Load current THD with harmonics compensation. (a) First loading condition. (b) Second loading condition.

So, in summary, the value of the selected virtual impedance in various harmonics orders and resulting compensation values are provided in Table 4.3. The provided results show the worst of the two loading conditions for better representation.

Table 4.3: Virtual impedance and compensation value of the simulation and experiment.

Harmonic	Virtual impedance		Harmonic percentage (Sim. – Exp.)	
	Simulation	Experiment	Before	After
11 th	0.4Ω	1.2Ω	5% - 4.3%	1% - 1.1%
13 th	0.6Ω	2Ω	3.7% - 1.8%	1% - 1%
23 rd	0.66Ω	1.7Ω	0.7% - 0.71%	0.2% - 0.3%
25 th	0.61Ω	-	0.6% - ...	0.15% - ...

4.6 Conclusion

A compensating technique for the proposed parallel LCC-VSC interlinking converter, rectifying the LCC unit's power quality issues is proposed in this chapter. In this method, the compensating signal is directly injected into the reference signal bypassing the main control system's limitations. The proposed technique's effect on system stability is studied by modelling the system considering the compensating feedforward. The parallel VSC's peak current capacity is calculated considering the system's harmonics and reactive power requirements. The provided experimental and simulation results prove the effectiveness of the harmonics' compensation in several operating scenarios. Also, it could be seen that reactive power compensation can be considerably larger than the required harmonic compensation if not managed properly. It is concluded that a combination of both active and passive reactive power compensation along with an active harmonic compensation can be taken as a proper method to achieve the desired power quality while saving expenses.

Chapter 5

Unbalanced PCC Voltage Compensation with Parallel LCC/VSC Interlinking Converters

According to LCC's limitations, several circumstances in a grid can lead to its commutation failure and system stability loss, namely a sudden AC voltage drop (more than 5%), excessive harmonics, a DC voltage drop, etc. Furthermore, as stated in [90], commutation failures are mostly due to AC system fault voltage disturbances, and it is known that such voltage disturbances cannot be completely avoided. In this regard, the magnitude of the fault, its corresponding voltage drop, and its phase shift can dictate the severity of the incident. Therefore, AC voltage unbalance can account for an LCC's commutation failure and system instability in the power system.

Voltage unbalance is a common phenomenon in power systems. Several works in the literature address voltage unbalance issues by proposing various compensating techniques. Mainly, the PCC's voltage is analyzed to extract the negative and positive sequences component [91]–[97]. Then, the PCC voltage's negative sequence component is used to calculate the required compensating signal as it is given in [96]. The strength of the designated conversion unit's compensating signal should be implemented considering the system's stability and power capacity.

Also, the CF mitigation methods for the LCCs have been studied for decades in several publications [90], [98], [99]–[108]. The mitigation methods attempt to address the issue using improved control [90], [98], [99]–[106] or by implementing some changes to the structure of the conversion unit [107], [108]. The control-based methods improve the system's performance by reducing the possibility of commutation failure. Recalculation of extinction angle based on the system's

condition [100]–[104] as well as improved switching cycles [99], [102], [105], [106] are two of the common approaches. . Furthermore, in addition to the modified control, changes to the circuit’s configuration can improve the performance of the LCC unit in this matter. For example, a common approach is implementing capacitor banks in series with LCC valves to improve the LCC’s commutation. However, such modifications in the LCC unit are costly, complicate the control, and add to the maintenance cost. However, as mentioned in [90], despite the implementation of mitigation techniques, commutation failure is unavoidable in most cases. This is because an improved extinction angle adds to the reactive power consumption of the conversion unit, resulting in a further AC voltage drop that can escalate the AC grid’s faulty situation.

Thus, this chapter conducted the unbalanced compensation of the PCC AC voltage in a hybrid AC/DC grid with LC- and VS-ICs. The control freedom provided by VSC can significantly improve the performance of the parallel LCC unit by mitigating the adverse effects of the PCC faults. Therefore, in this chapter, a voltage unbalance compensating scheme is implemented into the control system of the parallel LCC-VSC interfacing units to prevent continuous commutation failure in a hybrid AC/DC grid. The control system is modelled to compensate for the voltage unbalance and adequately improve system stability. Therefore, a stability analysis is also provided in the manuscript. Furthermore, the peak current capacity of the compensating unit is calculated to comply with the power transfer capacity of the unit while power quality is improved. In the end, the real-time simulation results are provided to verify the effectiveness of the proposed system.

5.1 LC-IC’s Control Scheme Under Unbalanced Condition

As explained in section I, several methods and algorithms are proposed in the literature to mitigate the commutation failure issue of the LCC in the power system. The commutation failure in the LCCs is mainly due to the voltage dip, voltage

phase-angle shift, and DC current increase. As it is shown in Fig. 5.1(a), the commutation voltage drop will affect the commutation. Since the overlap area should stay the same, the end of the commutation will be extended by the drop of the voltage, resulting in a short extinction angle. Furthermore, voltage backward phase shift can impact commutation, as it is depicted in Fig. 5.1(b). The increase in the DC current can also impact the commutation, as shown in Fig. 5.1(c), by increasing the overlap area and shrinking the extension angle.

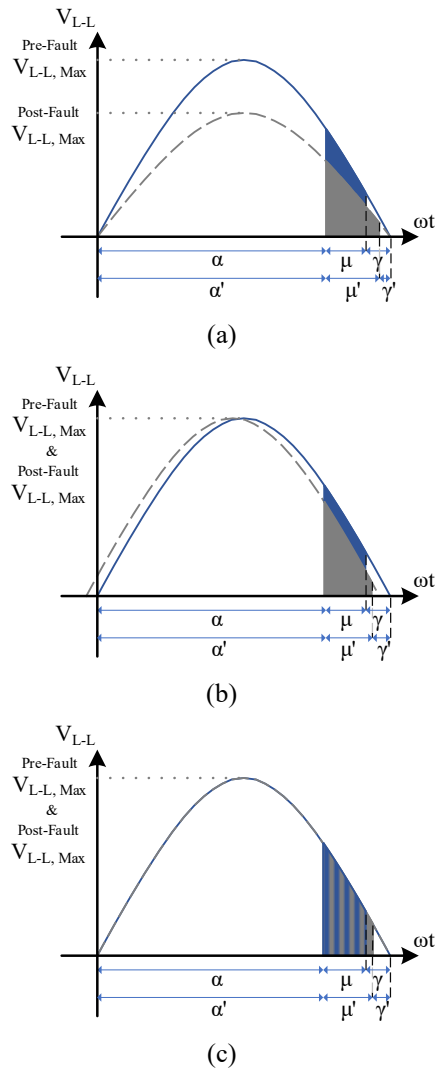


Fig. 5.1: Reduction of commutation region due to, (a) commutation voltage reduction, (b) commutation voltage backward phase shift, and (c) DC current increase.

Among the available publications, firing-angle-based controls are widely accepted to deal with CF effectively. Equidistance pulse control [99] is one of the

available techniques in the literature. In this technique, the pulse spacing is independent of AC line voltage and can be used to eliminate abnormalities. Pulse frequency control (PFC) and pulse phase control (PPC) are two of the methods following this phase-locked looped (PLL)-based technique. Furthermore, extinction angle control is one of the commonly used methods to deal with commutation failure due to voltage drop, see Fig. 1.3. [101] proposed an extinction angle control-based technique that embraces a power system equivalent Thevenin model as a base to calculate proper extinction angle to avoid CF. The power system equivalent model, as shown in Fig. 5.2, from the inverter bus point of view is depicted in Fig. 5.3. Z_F is taken as a fault impedance while the grid and conversion unit's voltage sources are set to zero. Z_u and Z_l are upper sides and line impedances, while x represents the fault location from inverter bus. Using the Thevenin system equivalent model and conducting the necessary calculations as given in [101], the required angle deduction for a safe commutation can be calculated as $\Delta\alpha$.

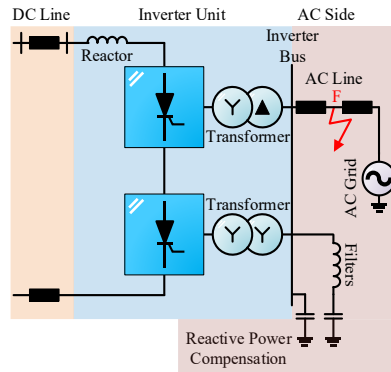


Fig. 5.2: LCC's inverter unit circuit layout.

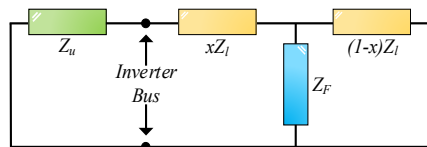


Fig. 5.3: Thevenin equivalent model of the LCC seen from inverter bus.

$$\Delta\alpha = \gamma_{\min} - \underbrace{\arccos\left(\sqrt{\frac{2\pi\omega L_u(E_t - V_b)\cos\phi_b}{3V_b Z_t} + \cos^2\alpha_i}\right)}_{\gamma_i} \quad (5.1)$$

where γ_{\min} , E_t , V_b , Z_t , ϕ_b , and α_i are the minimum extinction angle to avoid commutation failure, Thevenin equivalent voltage, voltage measurements, Thevenin equivalent impedance, phase angle, and valves firing angle. Based on (5.1), a decrease of Z_t will increase $\Delta\alpha$ resulting in a higher extinction angle and, as a result, higher reactive power consumption. In general, the reactive power consumption of the LCC's can take up to 50 to 60% of the supplied active power at the rated load. The value of the reactive power consumption can be approximated by (5.2). Based on (5.2), higher values for the extinction angle increase the reactive power consumption [109].

$$Q_{LCC} = P_{d_LCC} \sqrt{\left[\frac{1 + 0.5x_{com}P_{d_LCC}}{\cos\gamma}\right]^2} - 1 \quad (5.2)$$

where P_{d_LCC} , x_{com} , and $\cos\gamma$ are LCC's supplied power on the DC side, commutation reactance, and extinction angle. It can be concluded that despite the fact that extinction angle control can significantly improve the performance of the LCC's under fault conditions. However, reactive power consumption can be a greater concern for a grid under a fault, especially in a situation when the grid is weak. Therefore, in some cases, to prevent the system from becoming excessively unstable, disconnection of the LCC unit is recommended.

As pointed out, in most cases, despite with the implementation of improved mitigation techniques for LCCs operation, the CF is unavoidable. Therefore, employing an alternate method to compensate for the unbalanced voltage alongside LCC mitigating techniques should be considered to improve the system stability. The details regarding the control of the LCC unit in such a structure and different operation states can be found in [110].

5.2 VSC Control Under Unbalanced Condition

The control structure of the VS-ICs in the proposed system is depicted in Fig. 5.4. The block diagram of the VS-IC's positive sequence control system without unbalanced compensation is depicted in Fig. 5.4. The VS-IC will use double-loop control to track reference value. $G_{PR}(s)$ and $G_{delay}(s)$ represent the proportional resonance (PR) controller and switching and computation delay time in the form of a function. The PR controller and delay function details can be found in [111], [112]. Also, similar to the LC-IC unit, the VS-IC's droop-based control details can be found in [110].

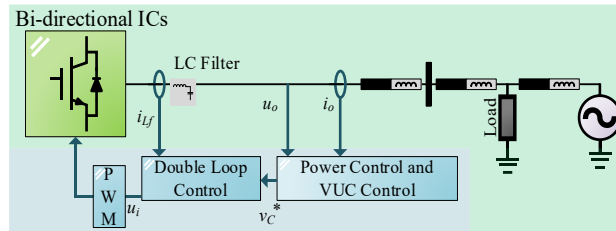


Fig. 5.4: VS-IC's control structure.

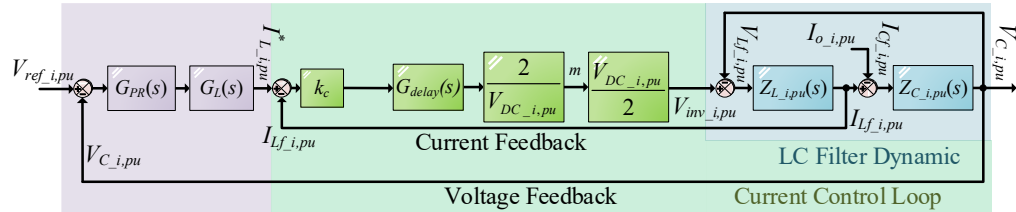


Fig. 5.5: The proposed VS-ICs double loop control.

Based on the proposed structure, the parallel voltage source interlinking converters (VS-ICs) can be used to compensate for PCC voltage oscillations to help LC-IC avoid commutation failure. The VUC control scheme is used as provided in [96] to rectify the PCC voltage unbalanced issue. The VUC control aims to normalize the negative-sequence components of the PCC voltage. The VUC method establishes a droop control to compensate for the voltage's negative-sequence using local voltage measurements and negative sequence reactive power, Q^- , as an index to evaluate the severity of the fault. The block diagram of the control scheme is depicted in Fig. 5.6.

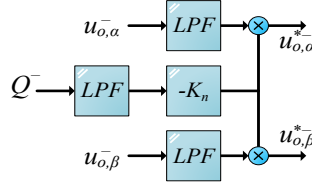


Fig. 5.6: Block diagram of a typical VUC controller.

The value of the Q^- is calculated using (4.1).

$$Q^- = u_{rms} \sqrt{(i_{o,\alpha}^-)^2 + (i_{o,\beta}^-)^2} \quad (5.3)$$

where u_{rms} , and $i_{o,\alpha}^-$ and $i_{o,\beta}^-$ are the rms value of the rated voltage, and negative sequence component of the output current. The low pass filters will be used to remove the unwanted oscillations from the measurements and prevent the sudden changes to the reference values. The negative-sequence reactive power Q^- , is multiplied by negative-sequence voltage droop gain K_n and then by output voltage's instantaneous negative-sequence to create a reference signal. Based on the provided control scheme, the negative-sequence voltage droop gain can be defined as it is given in (5.4).

$$K_n = \frac{\Delta VUC}{\max\{Q^- u_o^-\}} \quad (5.4)$$

Based on the available study's conclusion, the effectiveness of the compensating performance will increase with higher values for K_n [92]. In section III, it will be shown that the value of the K_n can change system stability. Therefore, proper design of the negative sequence compensating signal's droop gain is crucial.

5.3 System Modelling and Stability Analysis Under Unbalanced Condition

In order to check for the effectiveness of the control system in such an environment system modeling and stability analysis will be conducted. The stability analysis, in addition to checking for the feasibility of the proposed control system, determines negative-sequence voltage droop gain maximum impact range. The control scheme of the VS-IC without negative sequence compensation is depicted

in Fig. 4.1. Based on Fig. 4.1, the following equation can be found, as it is stated in [109]:

$$V_{C_i,pu} = G_{V_i}(s)V_{ref_i,pu} - Z_{V_i}I_{o_i,pu} \quad (5.5)$$

where $G_{V_i}(s)$ and $Z_{V_i}(s)$ are the control system closed-loop transfer function and output impedance, respectively. $G_{V_i}(s)$ and $Z_{V_i}(s)$ are defined as (5.6).

$$\begin{cases} G_{V_i}(s) = \frac{G_{PR_i}(s)G_L(s)G_{delay}(s)k_c}{G_{Den_i}(s)} \\ Z_{V_i} = \frac{k_c G_{delay}(s) + Z_{L_i,pu}}{G_{Den_i}(s)} \\ G_{Den_i}(s) = G_{PR_i}(s)G_L(s)G_{delay}(s)k_{c_i} + G_{delay}(s)Z_{C_i,pu}^{-1}k_{c_i} + Z_{L_i,pu}Z_{C_i,pu}^{-1} + 1 \end{cases} \quad (5.6)$$

As shown in Fig. 5.5, the $G_L(s)$ lead function is used as defined in (5.7) to improve system stability. The details regarding the design procedure for the lead function can be found in [110].

$$G_L(s) = \frac{1 + aT_Ls}{1 + T_Ls} \quad (5.7)$$

Based on the line and controlling parameters provided in Table 5.1, the positive- and negative-sequence Bode diagrams of the $G_{V_i}(s)$ and $Z_{V_i}(s)$ are depicted in Fig. 5.7 and Fig. 5.8.

Table 5.1: The VS-IC parameters and control.

System	Parameter	Value
VS-IC	K_c	0.9
	K_p	10
	K_i	250
	ω_{cut}	8
	t_{Delay}	0.1 μ s
	Filter (LC)	5mH/80 μ F
Load	Z_L	66 Ω /0.17H

As shown in Fig. 5.7, the magnitude of the $G_V(s)$ is the same for positive and negative sequences. Also, as expected, the phase angles of the positive and negative sequence are opposite. The magnitude and phase angle of the $Z_V(s)$ are also equal and in opposite direction, respectively, as expected, as shown in Fig. 5.8.

Considering, Fig. 5.4 and Fig. 5.6, the controlling block diagrams of the VS-ICs, the following equation can be defined [113].

$$VUC = -Q^- \cdot u_o^- \cdot K_n \quad (5.8)$$

where u_o^- represents the phasor of the output voltage. Taking the output impedance of the VS-IC into consideration, as shown in Fig. 5.8, Q^- can be calculated as it is given in (5.9) [94].

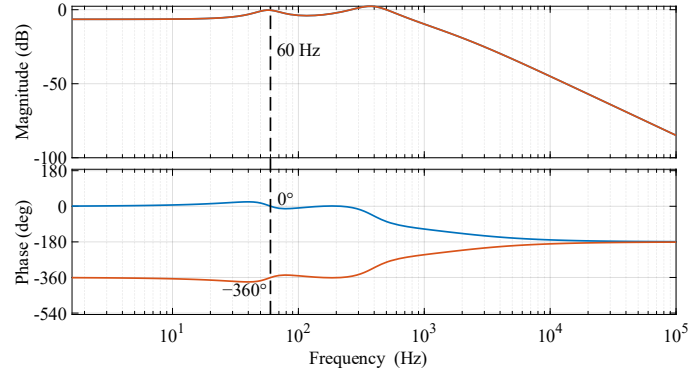


Fig. 5.7: Bode diagrams of positive-sequence and negative-sequence closed-loop transfer functions.

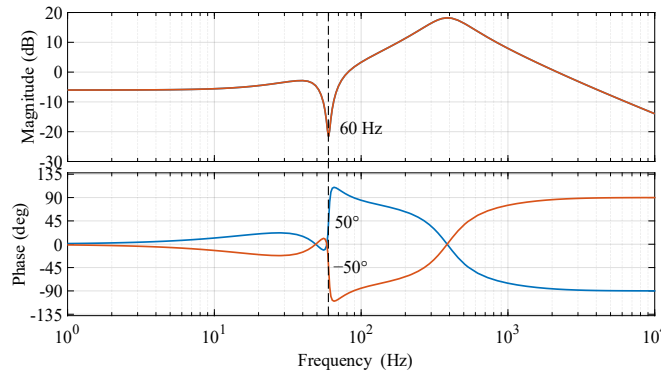


Fig. 5.8: Bode diagrams of positive-sequence and negative-sequence impedance.

$$Q^- = 3 \cdot X_v \cdot (I_o^-)^2 \cdot LPF(s) \quad (5.9)$$

By substituting (5.9) into (5.8) and linearizing the resulting equation, the small-signal representation can be calculated as it is given in (5.10).

$$VUC = -\left[3.\hat{u}_o^-.X_v.(I_o^-)^2 + 6.u_o^-.X_v.I_o^-. \hat{I}_o^-\right].K_n.LPF(s) \quad (5.10)$$

Using the symmetrical components theory, the system can be represented as it is given in Fig. 5.9 [94], [114]. As explained in [94], [114], a single-phase load is connected between two phases to calculate positive- and negative-sequence current in this model.

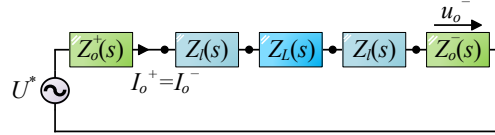


Fig. 5.9: The equivalent system circuit for calculation of I_o^- .

where $Z_L(s)$ and $Z_I(s)$ are the load and transmission line impedance, also, U^* is the rms value of the phase voltage.

Therefore, the voltage imbalance compensation implementation in the control system results in the following small-signal equation.

$$\hat{V}_o^- = G_{CL}(s).\hat{I}_o^- \quad (5.11)$$

where

$$G_{CL}(s) = \frac{6.G_V^-(s).Z_o^-(s).X_v.U^{*2}.K_n.LPF(s)}{Z_L^2(s) + 3.G_V^-(s).X_v.U^{*2}.K_n.LPF(s)} - \frac{Z_o^-(s).Z_L(s)}{Z_L^2(s) + 3.G_V^-(s).X_v.U^{*2}.K_n.LPF(s)} \quad (5.12)$$

By increasing the value of K_n , as it is stated in [113], the compensation effect will increase. However, K_n 's impact on control system stability should be taken into consideration. Therefore, the value of the K_n , as depicted in Fig. 5.10, is changed from 0.0000001 to 0.00001. As can be seen, the control system tends to become unstable increasing K_n beyond 0.000003.

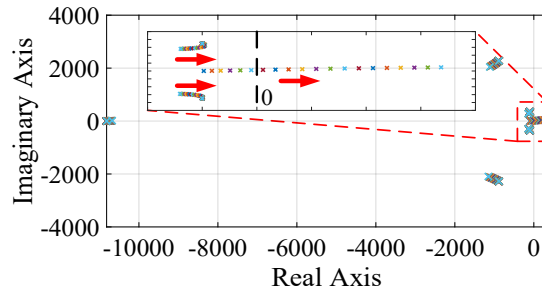


Fig. 5.10: Poles of G_{CL} for different K_n values.

According to [115], voltage unbalanced in the grid should be kept below 2% for normal operating conditions. Taking the maximum permitted voltage oscillation and K_n values as 2% and 0.0000022, the $\max\{Q^-.u_o^-\}$ can be calculated as it is given in (5.13).

$$\max\{Q^-.u_o^-\} = 9091u_o \quad (5.13)$$

5.4 Power Rating Studies

In addition to the control system stability, the power capacity of the VS-IC should be properly calculated. As expected, the power transfer capacity of the VS-IC should include both active and reactive powers' positive- and negative sequence components.

$$p_{VS-IC} = u_o \cdot i_o = (u_o^+ + u_o^-) \cdot (i_o^+ + i_o^-) = \begin{pmatrix} u_o^+ \cdot i_o^+ & u_o^- \cdot i_o^- \\ P_{VS-IC}^+ & P_{VS-IC}^- \end{pmatrix} + \begin{pmatrix} u_o^+ \cdot i_o^- + u_o^- \cdot i_o^+ \\ \tilde{p}_{VS-IC} \end{pmatrix} \quad (5.14)$$

$$q_{VS-IC} = u_{o\perp} \cdot i_o = (u_{o\perp}^+ + u_{o\perp}^-) \cdot (i_o^+ + i_o^-) = \begin{pmatrix} u_{o\perp}^+ \cdot i_o^+ + u_{o\perp}^- \cdot i_o^- \\ Q_{VS-IC}^+ & Q_{VS-IC}^- \end{pmatrix} + \begin{pmatrix} u_{o\perp}^+ \cdot i_o^- + u_{o\perp}^- \cdot i_o^+ \\ \tilde{q}_{VS-IC} \end{pmatrix} \quad (5.15)$$

where u_o^+ , u_o^- , i_o^+ , and i_o^- are positive and negative sequence components of the PCC voltage and VS-IC's output current. Similarly, P_{VS-IC}^+ , P_{VS-IC}^- , Q_{VS-IC}^+ , and Q_{VS-IC}^- are the positive and negative sequence of the VS-IC's average active and reactive power. Also, \tilde{p}_{VS-IC} and \tilde{q}_{VS-IC} are oscillatory terms of instantaneous active and reactive power.

In order to reach a proper design for the exchanged power capacity, the aforementioned components should be defined. As it has been mentioned in [117] and based on the upper explanations, positive sequence voltage and current, u_o^+ and i_o^+ , can be calculated using VS-IC's droop-based unified control schemes as it is depicted in Fig. 5.11.

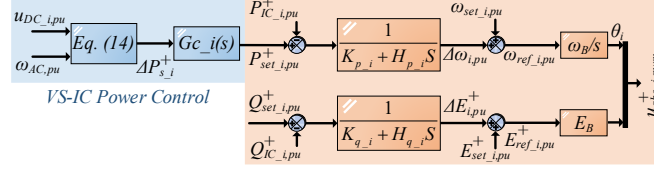


Fig. 5.11: VS-IC's droop-based unified control scheme.

where (5.16) is designed based on the AC and DC sub-grids droop equivalent control schemes. Additional information on the performance of **Error! Reference source not found.**'s control scheme can be found in [117].

$$\Delta P_{s,i}^+ = \left[P_{AC,pu}^+ + k_{AC} (\omega_{AC,pu}^* - \omega_{AC,pu}) \right] - K \times \left[P_{DC,pu}^+ + k_{DC} (U_{DC,pu}^* - u_{DC,i,pu}) \right] \quad (5.16)$$

Knowing the exact value of the load and by following the provided design procedure the required power capacity can be determined. The value of the v_c^- according to the VUC control scheme can be calculated using (5.8). In order to determine the value of the i_{DG}^- it is assumed that a three-phase unbalanced load (Z_{L1} , Z_{L2} , Z_{L3}) is connected to PCC in a star connection. As it is given in [115], the negative sequence current can be defined (Note that (5.17) is a generic representation of a three-phase load and can be extended to single-phase, etc. loads):

$$\bar{i}_{Load} = \frac{U(\alpha^2 Z_{L1} + \alpha Z_{L2} + Z_{L3})}{Z_{L1} Z_{L3} + Z_{L2} Z_{L3} + Z_{L1} Z_{L2} + Z^- Z_{L1} + Z^+ Z_{L1} + 3Z^+ Z^-} \quad (5.17)$$

where U is the voltage of the PCC under balanced conditions. Also, Z^+ and Z^- are positive and negative sequence impedances seen from the PCC, as it is depicted in Fig. 5.12.

$$Z^+ = Z_{Grid}^+ \parallel Z_{VS-IC}^+, \quad Z^- = Z_{Grid}^- \parallel Z_{VS-IC}^- \quad (5.18)$$

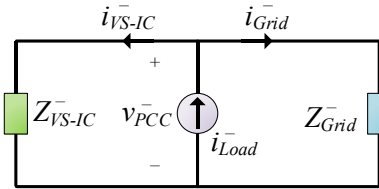


Fig. 5.12: Negative sequence model of the VS-IC.

Based on the presented control scheme on top, the negative sequence virtual impedance can be created to absorb the voltage oscillations and compensate for the PCC voltage. Therefore, the negative sequence active and reactive power

components based on the designed procedure can be calculated as provided in (5.19).

$$\begin{cases} P_{VS-IC}^- = u_o^- \cdot i_o^- = u_o^- \cdot i_{Load}^- \cdot \frac{Z_{Grid}^-}{Z_{VS-IC}^- + Z_{Grid}^-} \\ Q_{VS-IC}^- = u_{o\perp}^- \cdot i_o^- = u_{o\perp}^- \cdot i_{Load}^- \cdot \frac{Z_{Grid}^-}{Z_{VS-IC}^- + Z_{Grid}^-} \end{cases} \quad (5.19)$$

However, in the condition in which the exact value of the load is not available negative sequence droop function can be used to determine the required compensation power. Based on the fact that any sudden voltage drops greater than 5% can result in a commutation failure. Also, as pointed out, based on the available grid codes, the voltage unbalanced in the power system is required to be less than 2% in the normal operating condition of the system. Therefore, for example, to calculate the required compensation power, a 20% voltage unbalance is taken for the system. The value of the Q_{VS-IC}^- can be calculated using (5.13) considering the 2% voltage oscillation limit, K_n as 0.0000022, and 20% voltage drop, resulting in 0.0455 MVAR. Based on (5.14) and (5.15), the value of the P_{DG}^- can be calculated as 0.0455 MW. Taking the base value as 1 MVA, the required compensation power to reduce the PCC voltage oscillation from 20% to 2% in this example system will be approximated to 0.1 p.u. Similarly, by taking the line-to-line fault impedance equal to $331 \angle -84.5^\circ$ a 20% voltage drop can be expected. Therefore, using (5.17), (5.18), and (5.19) the required compensation power can be calculated as 1 MVA. It can be seen than in an equal loading and system conditions an equal compensating signal can be expected to reach a desired performance.

It is worth mentioning that, if a proper compensation is not achieved. The operation of the LC-IC should be limited due to the significant possibility of the continuous commutation failure, which can be a major damaging factor for the system stability and the exchanged power.

5.5 Real-time Simulation Results

In order to check for the effectiveness of the proposed control scheme in the proposed configuration, a real-time simulation test is conducted. The test is conducted using a simplified circuit configuration of the system as it is given in Fig. 2.1, with a single LC-IC and VS-IC working in parallel. The circuit components for the test are provided in Table 5.2.

Table 5.2: The tested grid's parameters.

System	Parameter	Value	
DC Sub-grid	DC voltage	14 kV	
AC Sub-grid	Line Impedance	$0.25 \Omega + 0.5 \text{ mH}$	
	AC phase voltage (<i>Simulation</i>)	4.7 kv	
	AC frequency (<i>Simulation</i>)	60 Hz	
IC	VS-IC	Switching frequency	5 kHz
		Filter (LC)	5 mH/80 μ F
	LC-IC	Filter DC (L)	50 mH
		Filter AC (C)	80 μ F
		Transformer (n1/n2)	1/1

The proposed control scheme is tested by applying a 12% voltage oscillation to the grid voltage at 30 to 40 s of the simulation as shown in Fig. 5.13(b). As expected, and as it is depicted in Fig. 5.13(a), the PCC voltage oscillations will result in the LC-IC's commutation failure. Such behavior can result in overall system instability as a result of propagated oscillations and disturbed power transfer.

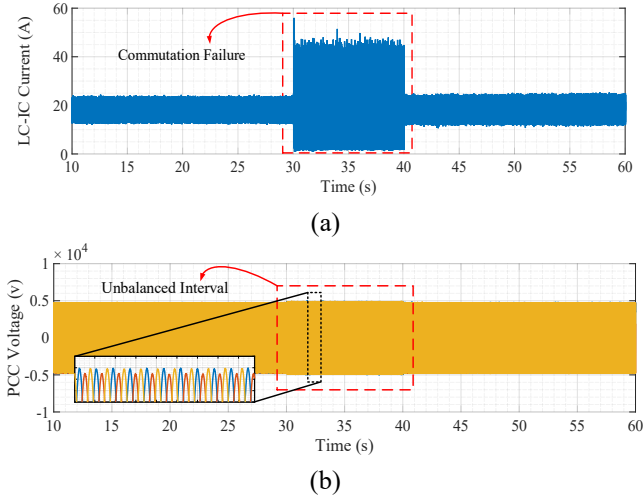


Fig. 5.13: Real-time simulation results without VUC control. (a) LCC current. (b) PCC Voltage.

In the next step a compensating signal is applied to PCC voltage taking K_n as 0.0000022. As depicted in Fig. 5.14(a), (b) the PCC voltage oscillations is removed and LC-IC commutation is facing no failure during this interval as a result. In order to show the compensation signal impact on the PCC voltage a zoomed in demonstration is provided in Fig. 5.15. In the applied unbalanced interval 30 to 40 s, the compensating signal is added to the control system at 35 s of the real-time simulation leaving the PCC voltage first interval (30 to 35 s) unbalanced and the second interval (35 to 40 s) with balanced PCC voltage. The zoomed in real-time simulation result shows that following the proposed system a successful voltage compensation is achieved by removing the voltage oscillations. As a result, successful smooth commutation is expected for the LC-IC unit.

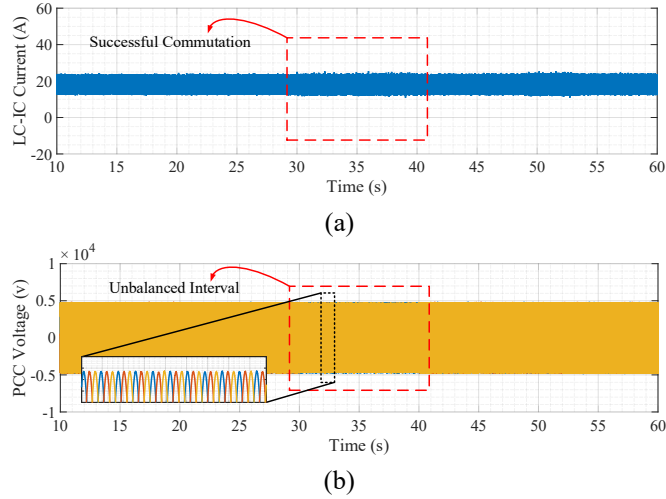


Fig. 5.14: Real-time simulation results with VUC control. (a) LCC current. (b) PCC Voltage.

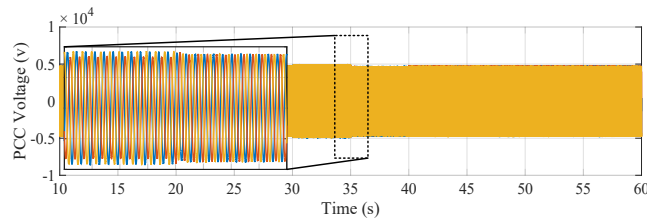


Fig. 5.15: Real-time simulation results for PCC voltage with and without compensation.

Furthermore, in order to check for the controlling signal effect on the stability of the system the value of the K_n is selected to a value out of the provided stable area. As can be seen in Fig. 5.16(a), (b), the unstable control system for VS-IC can result in an overall system instability and essentially commutation failure for the LC-IC.

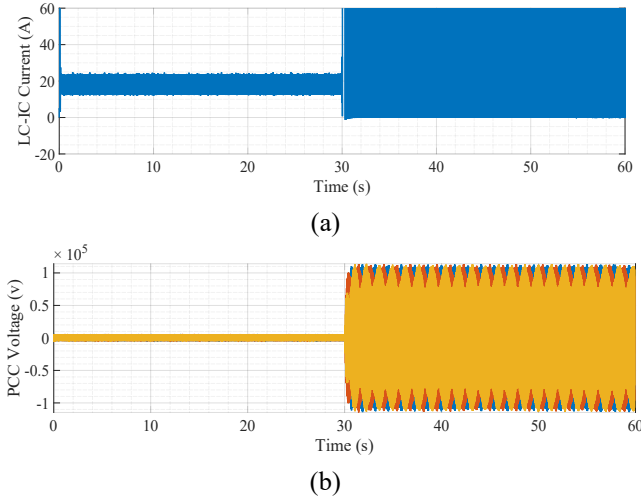


Fig. 5.16: Real-time simulation results for unstable controlling condition. (a) LC-IC current. (b) PCC voltage.

5.6 Conclusion

The proposed parallel LCC/VSCs and their limitations and advantages are briefly explained in this chapter. The VUC control scheme and its structure are extensively explained. As given, the negative sequence reactive power is used as a droop index to compensate for the voltage oscillations creating a proper droop equivalent control. The value of the aforementioned compensation coefficient can impact the voltage quality as well as control system stability. Therefore, a stability study is conducted to evaluate a proper compensating coefficient while maintaining system stability. The required calculations for estimating the power rating of the conversion unit are also provided. It is shown that the strength of the virtual impedance can estimate the strength of the compensation unit. Finally, the real-time simulation results are provided. As shown, the negative sequence components of the PCC voltage are significantly reduced. The proposed compensation algorithm successfully helps the LC-IC avoid continuous commutation failure, proving the proposed system's performance.

Chapter 6

Conclusion and Future plans

6.1 Thesis Conclusions and Contributions

The main objective of this thesis is to propose an alternative expansion approach to the interlinking converters in a hybrid AC/DC grid, integrating LCC and VSCs to take advantage of the benefits of both technologies. Accordingly, in order to accomplish this objective, respected control schemes are proposed supporting the system in every operational state. Thus, the conclusions and contributions of this research are as follows:

- To take advantage of both VS and LC conversion units, an integrated configuration is proposed for implementation in a hybrid AC/DC grid. The integrated unit's power transfer capacity is higher, the system is far more controllable, and the price is kept low. The proposed configuration is intended to be implemented in two scenarios. The first scenario is an expansion of the available LCC-based installations with parallel VS-ICs as discussed in Chapter 2. For the most part, in the first scenario the general structure of the LC-IC is maintained, including passive filtering and compensating elements. Therefore, it can be expected that the control system will retain its general form with some changes and improvements in applicable areas. The proposed configuration for ICs was able to control the hybrid AC/DC grid's properties in every operating condition for both implementation scenarios. The unique structure of the proposed parallel LCC-VSC interlinking units in the hybrid AC/DC grid enabled the LC-IC to adopt droop equivalent control by manipulating its conventional (V-I) graph control. In the expansion of the existing LCC-based installations, as provided in Chapter 2, the LCC's droop equivalent control supports the AC sub-grid frequency in normal and AC sub-grid support operating states. However, in the case of a significant sudden voltage drop on

the AC sub-grid, constant extinction angle control should be adapted by the LCC to prevent continuous commutation failure. In the case of a DC voltage fault on the DC sub-grid, the LC-IC unit should adopt VDCOL control to more easily assist the system to avert the fault.

- The second scenario, which takes an advantage of the proposed parallel configuration, is for new installations in which the bidirectional power delivery is not equal in both directions as that described in Chapter 3. The unified control scheme for the parallel LCC-VSC-based new installation, as is given in Chapter 3, argues that the LC-IC's droop equivalent control can be further improved to accommodate the AC sub-grid frequency as well as the DC voltage as its droop equivalent control's objective. Similarly, due to the physical limitations of the LCCs in operation and control, in the case of a sudden voltage drop in the AC side, it is necessary for the LC-IC to adopt extinction angle control as a precautionary plan. In this regard, a unified control scheme is proposed for the IC's control in both scenarios. The unified control scheme enables the conversion units to manage the various operating states of the hybrid AC/DC grid. Such a control scheme is proposed to put the hybrid AC/DC grid's system properties into an augmented control system. The proposed droop equivalent controls for LC- and VS-ICs include grid properties such as AC sub-grid frequency, and DC sub-grid voltage as their function's objectives, respectively. The LC-IC and VS-IC control systems are modeled and their respective control schemes in each operational state are provided. A stability analysis is conducted to select the best controlling parameters for both scenarios. Realtime and experimental evaluations are conducted. The results validate the performance of the proposed techniques.
- Harmonics has proved to be a critical problem for LCCs due to the low switching frequency nature of such a conversion unit. As discussed, in expanding the existing LCC-based installations, the conventional structure of the LCC units is in place. Accordingly, passive elements will be used to filter out harmonics. However, as discussed in Chapter 4, for the parallel LCC-VSC-

based new installation the parallel VS-IC units will be used to remove harmonics. In this regard, as provided in Chapter 4, the LCC's harmonic orders will be extracted, and a compensating signal will be used to attenuate the oscillations. In order to reach the desired performance, the implemented virtual impedance is modeled, and stability analysis is conducted. Based on the stability analysis, it is clear that both the norm and angle of the harmonics compensating signals can impact the stability of the system. Eventually, to properly calculate the power ratio of the parallel VS-IC, the required compensating signal is calculated.

- In the current power system, the distribution of load and generation can lead to an unbalanced voltage on the PCC. Also, a sudden change to the system, such as a fault, can lead to voltage balance loss on the PCC. The impact of such phenomena on the performance of the parallel LCC-VSC in a hybrid AC/DC grid is studied in Chapter 5 and precautionary methods are proposed. The LCCs conventionally use extinction angle control to prevent commutation failure in the case of an unbalanced voltage on the PCC. Based on the exceptional features of the proposed configuration, VS-ICs are used to compensate for the voltage oscillations, attenuating the unbalanced voltage's impact on the LC-IC's performance. In this regard, a VUC technique is implemented in the proposed system. The negative sequence voltage and negative sequence reactive power is used as an index to calculate the required compensating signal. In order to reach the desired performance a droop equivalent control is used to produce the required compensating signal based on the system's condition. Therefore, the VS-IC's control scheme is modeled in detail and a stability analysis is conducted. Based on the system's model and stability analysis and by properly selecting the droop coefficient the desired performance for the droop equivalent control is achieved. Essentially, real-time simulation results are provided to verify the effectiveness of the proposed technique.

6.2 Suggestions for Future Works

The suggestions for extending this research are as follows:

- Developing an expansion plan for the future hybrid AC/DC grid from the perspective of the VSC unit's structure, taking medium/high voltage and power as an objective. Different voltage source converters can react differently to the changes to the power system, such as DC voltage loss or AC voltage/frequency loss. Such a study requires a reevaluation of the system's unified control scheme concerning supporting the sub-grids during every operating condition. In addition to that, ancillary services can be affected due to the changes to the VS-IC's control and response.
- Study the LCC's low-frequency DC voltage oscillations' impact on the system's behaviour and attempts to compensate for it. The LCC terminal's DC voltage and the DC current contain oscillations as a result of low-frequency rectification. These oscillations can impact the exchanged power quality and even introduce additional harmonics orders to the system that need to be resolved separately.
- Study the impact of the meshed grid on the proposed configuration, considering control and various VSC configurations. Unlike the generic hybrid AC/DC network, the meshed configuration can face complications in terms of control and stability. Therefore, properly supporting the system during the AC or DC fault and providing the system with necessary support are the topics that need to be studied. Furthermore, system modelling and ancillary services for better performance and higher stabilities are the other terms that need to be considered.

References

- [1] Z. Zhuo et al., "Transmission Expansion Planning Test System for AC/DC Hybrid Grid With High Variable Renewable Energy Penetration," in *IEEE Transactions on Power Systems*, vol. 35, no. 4, pp. 2597-2608, July 2020.
- [2] A. Bagheri, C. Zhao, F. Qiu and J. Wang, "Resilient Transmission Hardening Planning in a High Renewable Penetration Era," in *IEEE Transactions on Power Systems*, vol. 34, no. 2, pp. 873-882, March 2019.
- [3] Q. Fu et al., "Microgrid Generation Capacity Design With Renewables and Energy Storage Addressing Power Quality and Surety," in *IEEE Transactions on Smart Grid*, vol. 3, no. 4, pp. 2019-2027, Dec. 2012.
- [4] F. Nejabatkhah, Y. W. Li and K. Sun, "Parallel Three-Phase Interfacing Converters Operation Under Unbalanced Voltage in Hybrid AC/DC Grid," in *IEEE Transactions on Smart Grid*, vol. 9, no. 2, pp. 1310-1322, March 2018.
- [5] J. D. Watson and I. Lestas, "Control of interlinking converters in hybrid AC/DC grids: network stability and scalability," in *IEEE Transactions on Power Systems*.
- [6] X. Liu, Y. Liu, J. Liu, Y. Xiang and X. Yuan, "Optimal planning of AC-DC hybrid transmission and distributed energy resource system: Review and prospects," in *CSEE Journal of Power and Energy Systems*, vol. 5, no. 3, pp. 409-422, Sept. 2019.
- [7] Canada Energy Regulator, "Canada's Energy Transition: Historical and Future Changes to Energy Systems – Update – An Energy Market Assessment," Canada Energy Regulator, NE2-23E-PDF, 2019. Available: www.cer-rec.gc.ca
- [8] X. Li, Z. Li, L. Guo, J. Zhu, Y. Wang and C. Wang, "Enhanced Dynamic Stability Control for Low-Inertia Hybrid AC/DC Microgrid With Distributed Energy Storage Systems," in *IEEE Access*, vol. 7, pp. 91234-91242, 2019.

- [9] B. Papari, C. S. Edrington, I. Bhattacharya and G. Radman, "Effective Energy Management of Hybrid AC–DC Microgrids With Storage Devices," in *IEEE Transactions on Smart Grid*, vol. 10, no. 1, pp. 193-203, Jan. 2019.
- [10] X. Liu, P. Wang and P. C. Loh, "A Hybrid AC/DC Grid and Its Coordination Control," in *IEEE Transactions on Smart Grid*, vol. 2, no. 2, pp. 278-286, June 2011.
- [11] Q. Xu, X. Hu, P. Wang, J. Xiao, P. Tu, C. Wen, and M. Y. Lee, "A decentralized dynamic power sharing strategy for hybrid energy storage system in autonomous DC microgrid," *IEEE Trans. Ind. Electron.*, vol. 64, no. 7, pp. 5930–5941, Jul. 2017.
- [12] Q. Xu, J. Xiao, X. Hu, P. Wang, and M. Y. Lee, "A decentralized power management strategy for hybrid energy storage system with autonomous bus voltage restoration and state-of-charge recovery," *IEEE Trans. Ind. Electron.*, vol. 64, no. 9, pp. 7098–7108, Sep. 2017.
- [13] Z. Jin, L. Meng, J. M. Guerrero, and R. Han, "Hierarchical control design for a shipboard power system with DC distribution and energy storage aboard future more-electric ships," *IEEE Trans. Ind. Informat.*, vol. 14, no. 2, pp. 703–714, Feb. 2018.
- [14] F. Nejabatkhah, Y. W. Li and H. Tian, "Power Quality Control of Smart Hybrid AC/DC Microgrids: An Overview," in *IEEE Access*, vol. 7, pp. 52295-52318, 2019, doi: 10.1109/ACCESS.2019.2912376.
- [15] R. Peña-Alzola, M. A. Bianchi and M. Ordonez, "Control Design of a PFC With Harmonic Mitigation Function for Small Hybrid AC/DC Buildings," in *IEEE Transactions on Power Electronics*, vol. 31, no. 9, pp. 6607-6620, Sept. 2016.
- [16] D. Jovcic and K. Ahmed, *High Voltage Direct Current Transmission: Converters, System and DC Grid*. New York, NY, USA: Wiley, 2015.
- [17] H. Rao et al., "Key technologies of ultra-high voltage hybrid LCC-VSC MTDC systems," in *CSEE Journal of Power and Energy Systems*, vol. 5, no. 3, pp. 365-373, Sept. 2019.

- [18] G. Li et al., "Feasibility and Reliability Analysis of LCC DC Grids and LCC/VSC Hybrid DC Grids," in *IEEE Access*, vol. 7, pp. 22445-22456, 2019.
- [19] A. Zheng, C. Guo, P. Cui, W. Jiang and C. Zhao, "Comparative Study on Small-Signal Stability of LCC-HVDC System With Different Control Strategies at the Inverter Station," in *IEEE Access*, vol. 7, pp. 34946-34953, 2019.
- [20] J. Wang, Y. Gong, C. Fu, Z. Wen and Q. Wu, "A novel phase-locked loop for mitigating the subsequent commutation failures of LCC-HVDC systems," in *IEEE Transactions on Power Delivery*.
- [21] D. Kwon, Y. Kim and S. Moon, "Modeling and Analysis of an LCC HVDC System Using DC Voltage Control to Improve Transient Response and Short-Term Power Transfer Capability," in *IEEE Transactions on Power Delivery*, vol. 33, no. 4, pp. 1922-1933, Aug. 2018.
- [22] G. P. Adam et al., "Improved Two-Level Voltage Source Converter for High-Voltage Direct Current Transmission Systems," in *IEEE Journal of Emerging and Selected Topics in Power Electronics*, vol. 5, no. 4, pp. 1670-1686, Dec. 2017.
- [23] I. González-Torres, H. Miranda-Vidales, J. Espinoza, C.-F. Méndez-Barrios, and M. González, "State feedback control assisted by a gain scheduling scheme for three-level NPC VSC-HVDC transmission systems," *Electr. Power Syst. Res.*, vol. 157, pp. 227–237, Apr. 2018.
- [24] S. Liu, X. Wang, Y. Meng, P. Sun, H. Luo, and B. Wang, "A decoupled control strategy of modular multilevel matrix converter for fractional frequency transmission system," *IEEE Trans. Power Del.*, vol. 32, no. 4, pp. 2111–2121, Aug. 2017.
- [25] H. Mahmoudi, M. Aleenejad, and R. Ahmadi, "Modulated model predictive control of modular multilevel converters in VSC-HVDC systems," *IEEE Trans. Power Del.*, vol. 33, no. 5, pp. 2115–2124, Oct. 2018.
- [26] B. Zhao et al., "Practical Analytical Model and Comprehensive Comparison of Power Loss Performance for Various MMCs Based on IGCT in HVDC

- Application," in *IEEE Journal of Emerging and Selected Topics in Power Electronics*, vol. 7, no. 2, pp. 1071-1083, June 2019.
- [27] D. Van Hertem et al., "Substations for Future HVdc Grids: Equipment and Configurations for Connection of HVdc Network Elements," in *IEEE Power and Energy Magazine*, vol. 17, no. 4, pp. 56-66, July-Aug. 2019.
- [28] R. Feldman et al., "A hybrid modular multilevel voltage source converter for HVDC power transmission," *IEEE Trans. Ind. Appl.*, vol. 49, no. 4, pp. 1577-1588, Jul. 2013.
- [29] Cheng-hao Li, Peng Zhan, J. Wen, Mei-qi Yao, N. Li and W. Lee, "Offshore wind farms integration and frequency support control utilizing hybrid multi-terminal HVDC transmission," 2013 IEEE Industry Applications Society Annual Meeting, Lake Buena Vista, FL, 2013, pp. 1-9.
- [30] X. Chen et al., "Integrating Wind Farm to the Grid Using Hybrid Multiterminal HVDC Technology," in *IEEE Transactions on Industry Applications*, vol. 47, no. 2, pp. 965-972, March-April 2011.
- [31] P. Zhan, C. Li, J. Wen, Y. Hua, M. Yao and N. Li, "Research on hybrid multi-terminal high-voltage DC technology for offshore wind farm integration," in *Journal of Modern Power Systems and Clean Energy*, vol. 1, no. 1, pp. 34-41, June 2013.
- [32] M. Eremia and C.-C. Liu, *Advanced Solution in Power Systems: HVDC FACT and Artificial Intelligence.*, New York, NY, USA:Wiley, 2016.
- [33] B. Gemmell and M. Korytowski, "Refurbishments in Australasia: Upgrades of HVdc in New Zealand and FACTS in Australia," in *IEEE Power and Energy Magazine*, vol. 14, no. 2, pp. 72-79, March-April 2016.
- [34] T. H. Nguyen, D. Lee and C. Kim, "A Series-Connected Topology of a Diode Rectifier and a Voltage-Source Converter for an HVDC Transmission System," in *IEEE Transactions on Power Electronics*, vol. 29, no. 4, pp. 1579-1584, April 2014.
- [35] E. N. Abildgaard, M. Molinas, "Modelling and control of the modular multilevel converter (MMC)", *Proc. Energy Procedia 2nd Renewable Energy Res. Conf.*, vol. 20, pp. 227-236, 2012.

- [36] T. Shu et al., "Probabilistic Power Flow Analysis for Hybrid HVAC and LCC-VSC HVDC System," in *IEEE Access*, vol. 7, pp. 142038-142052, 2019.
- [37] S. Dong, Y. Chi and Y. Li, "Active Voltage Feedback Control for Hybrid Multiterminal HVDC System Adopting Improved Synchronverters," in *IEEE Transactions on Power Delivery*, vol. 31, no. 2, pp. 445-455, April 2016.
- [38] Eremia Mircea, Chen-Ching Liu, Abdel-Aty Edris, *Advanced Solutions in Power Systems: HVDC FACTS and Artificial Intelligence*, John Wiley & Sons, 2016.
- [39] N. Iqtiyaniilham, M. Hasanuzzaman, and M. Hosenuzzaman, "European smart grid prospects, policies, and challenges," *Renewable and Sustainable Energy Reviews*, vol. 67, pp. 776–790, 2017.
- [40] R. Itiki, M. Manjrekar, S. G. D. Santo, and L. F. M. Machado, "Technical feasibility of Japan-Taiwan-Philippines HVdc interconnector to the Asia Pacific Super Grid," *Renewable and Sustainable Energy Reviews*, vol. 133, p. 110161, 2020.
- [41] E. Pierri, O. Binder, N. G. Hemdan, and M. Kurrat, "Challenges and opportunities for a European HVDC grid," *Renewable and Sustainable Energy Reviews*, vol. 70, pp. 427–456, 2017.
- [42] A. Aghahosseini, D. Bogdanov, L. S. Barbosa, and C. Breyer, "Analysing the feasibility of powering the Americas with renewable energy and inter-regional grid interconnections by 2030," *Renewable and Sustainable Energy Reviews*, vol. 105, pp. 187–205, 2019.
- [43] S. Peyghami, H. Mokhtari and F. Blaabjerg, "Autonomous Operation of a Hybrid AC/DC Microgrid with Multiple Interlinking Converters," in *IEEE Transactions on Smart Grid*, vol. 9, no. 6, pp. 6480-6488, Nov. 2018.
- [44] Y. Xia, Y. Peng, P. Yang, M. Yu and W. Wei, "Distributed Coordination Control for Multiple Bidirectional Power Converters in a Hybrid AC/DC Microgrid," in *IEEE Transactions on Power Electronics*, vol. 32, no. 6, pp. 4949-4959, June 2017.
- [45] J. Wang, C. Jin and P. Wang, "A Uniform Control Strategy for the Interlinking Converter in Hierarchical Controlled Hybrid AC/DC Microgrids,"

- in IEEE Transactions on Industrial Electronics, vol. 65, no. 8, pp. 6188-6197, Aug. 2018.
- [46] E. Aprilia, K. Meng, M. Al Hosani, H. H. Zeineldin and Z. Y. Dong, "Unified Power Flow Algorithm for Standalone AC/DC Hybrid Microgrids," in IEEE Transactions on Smart Grid, vol. 10, no. 1, pp. 639-649, Jan. 2019.
- [47] B. Liu et al., "An AC–DC Hybrid Multi-Port Energy Router With Coordinated Control and Energy Management Strategies," in IEEE Access, vol. 7, pp. 109069-109082, 2019.
- [48] X. Liu, P. Wang and P. C. Loh, "A Hybrid AC/DC Microgrid and Its Coordination Control," in IEEE Transactions on Smart Grid, vol. 2, no. 2, pp. 278-286, June 2011.
- [49] R. Majumder, "A Hybrid Microgrid With DC Connection at Back to Back Converters," in IEEE Transactions on Smart Grid, vol. 5, no. 1, pp. 251-259, Jan. 2014.
- [50] P. C. Loh, D. Li, Y. K. Chai and F. Blaabjerg, "Hybrid AC–DC Microgrids with Energy Storages and Progressive Energy Flow Tuning," in IEEE Transactions on Power Electronics, vol. 28, no. 4, pp. 1533-1543, April 2013.
- [51] P. C. Loh, D. Li, Y. K. Chai and F. Blaabjerg, "Autonomous Operation of Hybrid Microgrid With AC and DC Subgrids," in IEEE Transactions on Power Electronics, vol. 28, no. 5, pp. 2214-2223, May 2013.
- [52] P. C. Loh, D. Li, Y. K. Chai and F. Blaabjerg, "Autonomous Control of Interlinking Converter with Energy Storage in Hybrid AC–DC Microgrid," in IEEE Transactions on Industry Applications, vol. 49, no. 3, pp. 1374-1382, May-June 2013.
- [53] N. Eghtedarpour and E. Farjah, "Power Control and Management in a Hybrid AC/DC Microgrid," in IEEE Transactions on Smart Grid, vol. 5, no. 3, pp. 1494-1505, May 2014.
- [54] X. Li, L. Guo, C. Hong, Y. Zhang, Y. W. Li and C. Wang, "Hierarchical Control of Multiterminal DC Grids for Large-Scale Renewable Energy Integration," in IEEE Transactions on Sustainable Energy, vol. 9, no. 3, pp. 1448-1457, July 2018.

- [55] K. Rouzbehi, A. Miranian, J. I. Candela, A. Luna and P. Rodriguez, "A Generalized Voltage Droop Strategy for Control of Multiterminal DC Grids," in *IEEE Transactions on Industry Applications*, vol. 51, no. 1, pp. 607-618, Jan.-Feb. 2015.
- [56] K. Rouzbehi, A. Miranian, A. Luna and P. Rodriguez, "DC Voltage Control and Power Sharing in Multiterminal DC Grids Based on Optimal DC Power Flow and Voltage-Droop Strategy," in *IEEE Journal of Emerging and Selected Topics in Power Electronics*, vol. 2, no. 4, pp. 1171-1180, Dec. 2014.
- [57] H. Xiao, A. Luo, Z. Shuai, G. Jin and Y. Huang, "An Improved Control Method for Multiple Bidirectional Power Converters in Hybrid AC/DC Microgrid," in *IEEE Transactions on Smart Grid*, vol. 7, no. 1, pp. 340-347, Jan. 2016.
- [58] X. Lu, J. M. Guerrero, K. Sun, J. C. Vasquez, R. Teodorescu and L. Huang, "Hierarchical Control of Parallel AC-DC Converter Interfaces for Hybrid Microgrids," in *IEEE Transactions on Smart Grid*, vol. 5, no. 2, pp. 683-692, March 2014.
- [59] X. Li et al., "A Unified Control for the DC-AC Interlinking Converters in Hybrid AC/DC Microgrids," in *IEEE Transactions on Smart Grid*, vol. 9, no. 6, pp. 6540-6553, Nov. 2018.
- [60] J. He, Y. W. Li, J. M. Guerrero, F. Blaabjerg and J. C. Vasquez, "An Islanding Microgrid Power Sharing Approach Using Enhanced Virtual Impedance Control Scheme," in *IEEE Transactions on Power Electronics*, vol. 28, no. 11, pp. 5272-5282, Nov. 2013.
- [61] Y. Han, H. Li, P. Shen, E. A. A. Coelho and J. M. Guerrero, "Review of Active and Reactive Power Sharing Strategies in Hierarchical Controlled Microgrids," in *IEEE Transactions on Power Electronics*, vol. 32, no. 3, pp. 2427-2451, March 2017.
- [62] H. Tian, Y. W. Li and P. Wang, "Hybrid AC/DC System Harmonics Control Through Grid Interfacing Converters with Low Switching Frequency," in *IEEE Transactions on Industrial Electronics*, vol. 65, no. 3, pp. 2256-2267, March 2018.

- [63] Q. Zhong and G. Weiss, "Synchronverters: Inverters That Mimic Synchronous Generators," in *IEEE Transactions on Industrial Electronics*, vol. 58, no. 4, pp. 1259-1267, April 2011.
- [64] H. Wu et al., "Small-Signal Modeling and Parameters Design for Virtual Synchronous Generators," in *IEEE Transactions on Industrial Electronics*, vol. 63, no. 7, pp. 4292-4303, July 2016.
- [65] Y. Cao et al., "A Virtual Synchronous Generator Control Strategy for VSC-MTDC Systems," in *IEEE Transactions on Energy Conversion*, vol. 33, no. 2, pp. 750-761, June 2018.
- [66] Y. W. Li, "Control and Resonance Damping of Voltage-Source and Current-Source Converters With LC Filters," in *IEEE Transactions on Industrial Electronics*, vol. 56, no. 5, pp. 1511-1521, May 2009.
- [67] F. Fang, Y. Wei Li and X. Li, "High Performance Unified Control for Interlinking Converter in Hybrid AC/DC Microgrid," 2018 IEEE Energy Conversion Congress and Exposition (ECCE), Portland, OR, 2018, pp. 3784-3791.
- [68] Z. Song et al., "Small signal modeling and parameter design of virtual synchronous generator to weak grid," 2018 13th IEEE Conference on Industrial Electronics and Applications (ICIEA), Wuhan, 2018, pp. 2618-2624.
- [69] D. Jovcic, K. Ahmed, *High-Voltage Direct Current Transmission Converters Systems and DC Grids*, USA, NJ, HobokenWiley, 2015.
- [70] A. Ekstrom and G. Liss, "A Refined HVDC Control System," in *IEEE Transactions on Power Apparatus and Systems*, vol. PAS-89, no. 5, pp. 723-732, May 1970.
- [71] T. Funaki and K. Matsuura, "Predictive firing angle calculation for constant effective margin angle control of CCC-HVDC," in *IEEE Transactions on Power Delivery*, vol. 15, no. 3, pp. 1087-1093, July 2000.
- [72] J. D. Ainsworth, "The Phase-Locked Oscillator - A New Control System for Controlled Static Convertors," in *IEEE Transactions on Power Apparatus and Systems*, vol. PAS-87, no. 3, pp. 859-865, March 1968.

- [73] F. Karlecik-Maier, "A new closed loop control method for HVDC transmission," in *IEEE Transactions on Power Delivery*, vol. 11, no. 4, pp. 1955-1960, Oct. 1996.
- [74] Chapter 12 - Control and Protection of UHVDC Transmission Systems, *UHV Transmission Technology*, Academic Press, 2018, 469 - 497
- [75] IEEE Guide for Planning DC Links Terminating at AC Locations Having Low Short-Circuit Capacities, *IEEE Std. 1204–1997*, Dec. 31, 1997.
- [76] S. Filizadeh, A. M. Gole, D. A. Woodford and G. D. Irwin, "An Optimization-Enabled Electromagnetic Transient Simulation-Based Methodology for HVDC Controller Design," in *IEEE Transactions on Power Delivery*, vol. 22, no. 4, pp. 2559-2566, Oct. 2007.
- [77] F. Nejabatkhah and Y. W. Li, "Overview of Power Management Strategies of Hybrid AC/DC Microgrid," *IEEE Transactions on Power Electronics*, vol. 30, no. 12, pp. 7072-7089, Dec. 2015.
- [78] J. He, Y. W. Li and M. S. Munir, "A Flexible Harmonic Control Approach Through Voltage-Controlled DG–Grid Interfacing Converters," in *IEEE Transactions on Industrial Electronics*, vol. 59, no. 1, pp. 444-455, Jan. 2012.
- [79] H. M. A. Ahmed, A. B. Eltantawy and M. M. A. Salama, "A Generalized Approach to the Load Flow Analysis of AC–DC Hybrid Distribution Systems," in *IEEE Transactions on Power Systems*, vol. 33, no. 2, pp. 2117-2127, March 2018.
- [80] F. Nejabatkhah, Y. W. Li and H. Tian, "Power Quality Control of Smart Hybrid AC/DC Microgrids: An Overview," in *IEEE Access*, vol. 7, pp. 52295-52318, 2019.
- [81] J. He, B. Liang, Y. W. Li and C. Wang, "Simultaneous Microgrid Voltage and Current Harmonics Compensation Using Coordinated Control of Dual-Interfacing Converters," in *IEEE Transactions on Power Electronics*, vol. 32, no. 4, pp. 2647-2660, April 2017.
- [82] J. He and Y. W. Li, "Analysis, Design, and Implementation of Virtual Impedance for Power Electronics Interfaced Distributed Generation," in *IEEE*

- Transactions on Industry Applications*, vol. 47, no. 6, pp. 2525-2538, Nov.-Dec. 2011.
- [83] X. Wen, Y. W. Li and J. He, "A distribution system harmonic compensation approach using DG-grid interfacing converters at low switching frequency," 2014 IEEE Applied Power Electronics Conference and Exposition - APEC 2014, Fort Worth, TX, 2014, pp. 995-1001.
- [84] IEEE Recommended Practice and Requirements for Harmonic Control in Electric Power Systems, IEEE Std. 519-2014, Jun. 2014.
- [85] C. Kim, V. Sood, G. Jang, S. Lim and S. Lee, HVDC Transmission: Power Conversion Applications in Power Systems, NJ, Hoboken:Wiley, 2009.
- [86] V. K. Sood, HVDC and FACTS Controllers: Applications of Static Converters in Power Systems, Boston, MA, USA:Kluwer, 2004.
- [87] R. Zeng, L. Xu, L. Yao, S. J. Finney and Y. Wang, "Hybrid HVDC for Integrating Wind Farms With Special Consideration on Commutation Failure," in IEEE Transactions on Power Delivery, vol. 31, no. 2, pp. 789-797, April 2016.
- [88] S. Cui and S. Sul, "A Comprehensive DC Short-Circuit Fault Ride Through Strategy of Hybrid Modular Multilevel Converters (MMCs) for Overhead Line Transmission," in IEEE Transactions on Power Electronics, vol. 31, no. 11, pp. 7780-7796, Nov. 2016.
- [89] "IEEE Standard Definitions for the Measurement of Electric Power Quantities Under Sinusoidal, Nonsinusoidal, Balanced, or Unbalanced Conditions," in IEEE Std 1459-2010 (Revision of IEEE Std 1459-2000), pp.1-50, 19 March 2010.
- [90] C. V. Thio, J. B. Davies, and K. L. Kent, "Commutation failures in HVDC transmission systems," *IEEE Trans. Power Deliv.*, vol. 11, no. 2, pp. 946-957, Apr. 1996, doi: 10.1109/61.489356.
- [91] B. Liu, Z. Liu, J. Liu, R. An, H. Zheng, and Y. Shi, "An Adaptive Virtual Impedance Control Scheme Based on Small-AC-Signal Injection for Unbalanced and Harmonic Power Sharing in Islanded Microgrids," *IEEE*

- Trans. Power Electron.*, vol. 34, no. 12, pp. 12333–12355, Dec. 2019, doi: 10.1109/TPEL.2019.2905588.
- [92] Y. Han, P. Shen, X. Zhao, and J. M. Guerrero, “An Enhanced Power Sharing Scheme for Voltage Unbalance and Harmonics Compensation in an Islanded AC Microgrid,” *IEEE Trans. Energy Convers.*, vol. 31, no. 3, pp. 1037–1050, Sep. 2016, doi: 10.1109/TEC.2016.2552497.
- [93] H. Liu, J. Zhou, P. Li, and W. Wei, “An improved droop control strategy of three-phase inverter for grid voltage unbalance compensation,” in *2017 IEEE 3rd International Future Energy Electronics Conference and ECCE Asia (IFEEC 2017 - ECCE Asia)*, Jun. 2017, pp. 110–115. doi: 10.1109/IFEEC.2017.7992427.
- [94] M. Savaghebi, A. Jalilian, J. C. Vasquez, and J. M. Guerrero, “Autonomous Voltage Unbalance Compensation in an Islanded Droop-Controlled Microgrid,” *IEEE Trans. Ind. Electron.*, vol. 60, no. 4, pp. 1390–1402, Apr. 2013, doi: 10.1109/TIE.2012.2185914.
- [95] N. R. Merritt, C. Chakraborty, and P. Bajpai, “New Voltage Control Strategies for VSC-Based DG Units in an Unbalanced Microgrid,” *IEEE Trans. Sustain. Energy*, vol. 8, no. 3, pp. 1127–1139, Jul. 2017, doi: 10.1109/TSTE.2017.2657660.
- [96] Y. Peng, Z. Shuai, J. M. Guerrero, Y. Li, A. Luo, and Z. J. Shen, “Performance Improvement of the Unbalanced Voltage Compensation in Islanded Microgrid Based on Small-Signal Analysis,” *IEEE Trans. Ind. Electron.*, vol. 67, no. 7, pp. 5531–5542, Jul. 2020, doi: 10.1109/TIE.2019.2934021.
- [97] M. Savaghebi, A. Jalilian, J. C. Vasquez, and J. M. Guerrero, “Secondary Control Scheme for Voltage Unbalance Compensation in an Islanded Droop-Controlled Microgrid,” *IEEE Trans. Smart Grid*, vol. 3, no. 2, pp. 797–807, Jun. 2012, doi: 10.1109/TSG.2011.2181432.
- [98] F. Cheng *et al.*, “A new AC fault ride-through strategy for HVDC link with serial connected LCC-VSC hybrid inverter,” *CSEE J. Power Energy Syst.*, pp. 1–12, 2021, doi: 10.17775/CSEEJPES.2020.03510.

- [99] P. C. Sen, M. L. MacDonald, and D. J. Clarke, "A novel equidistant pulse control scheme for thyristor converters," *Can. Electr. Eng. J.*, vol. 3, no. 3, pp. 10–14, Jul. 1978, doi: 10.1109/CEEJ.1978.6591410.
- [100] L. Zhang and L. Dofnas, "A novel method to mitigate commutation failures in HVDC systems," in *Proceedings. International Conference on Power System Technology*, Oct. 2002, vol. 1, pp. 51–56 vol.1. doi: 10.1109/ICPST.2002.1053503.
- [101] S. Mirsaeidi, X. Dong, D. Tzelepis, D. M. Said, A. Dyśko, and C. Booth, "A Predictive Control Strategy for Mitigation of Commutation Failure in LCC-Based HVDC Systems," *IEEE Trans. Power Electron.*, vol. 34, no. 1, pp. 160–172, Jan. 2019, doi: 10.1109/TPEL.2018.2820152.
- [102] H.-I. Son and H.-M. Kim, "An Algorithm for Effective Mitigation of Commutation Failure in High-Voltage Direct-Current Systems," *IEEE Trans. Power Deliv.*, vol. 31, no. 4, pp. 1437–1446, Aug. 2016, doi: 10.1109/TPWRD.2016.2520928.
- [103] Z. Wei, Y. Yuan, X. Lei, H. Wang, G. Sun, and Y. Sun, "Direct-Current Predictive Control Strategy for Inhibiting Commutation Failure in HVDC Converter," *IEEE Trans. Power Syst.*, vol. 29, no. 5, pp. 2409–2417, Sep. 2014, doi: 10.1109/TPWRS.2014.2302010.
- [104] S. Tamai, H. Naitoh, F. Ishiguro, M. Sato, K. Yamaji, and N. Honjo, "Fast and predictive HVDC extinction angle control," *IEEE Trans. Power Syst.*, vol. 12, no. 3, pp. 1268–1275, Aug. 1997, doi: 10.1109/59.630470.
- [105] J. Wang *et al.*, "Improved predictive calculation-based extinction angle control for HVDC," *Int. J. Electr. Power Energy Syst.*, vol. 128, p. 106633, Jun. 2021, doi: 10.1016/j.ijepes.2020.106633.
- [106] C. Guo, Y. Liu, C. Zhao, X. Wei, and W. Xu, "Power Component Fault Detection Method and Improved Current Order Limiter Control for Commutation Failure Mitigation in HVDC," *IEEE Trans. Power Deliv.*, vol. 30, no. 3, pp. 1585–1593, Jun. 2015, doi: 10.1109/TPWRD.2015.2411997.
- [107] Y. Xue, X.-P. Zhang, and C. Yang, "Commutation Failure Elimination of LCC HVDC Systems Using Thyristor-Based Controllable Capacitors," *IEEE*

- Trans. Power Deliv.*, vol. 33, no. 3, pp. 1448–1458, Jun. 2018, doi: 10.1109/TPWRD.2017.2776867.
- [108] Y. Xue, X.-P. Zhang, and C. Yang, “Series Capacitor Compensated AC Filterless Flexible LCC HVDC With Enhanced Power Transfer Under Unbalanced Faults,” *IEEE Trans. Power Syst.*, vol. 34, no. 4, pp. 3069–3080, Jul. 2019, doi: 10.1109/TPWRS.2019.2899065.
- [109] R. R. Ahrabi and Y. Li, “Harmonics compensation of the LCC in a parallel LCC-VSCs configuration for a hybrid AC/DC network,” in *2021 IEEE Energy Conversion Congress and Exposition (ECCE)*, Oct. 2021, pp. 77–83. doi: 10.1109/ECCE47101.2021.9595921.
- [110] R. R. Ahrabi, Y. W. Li, and F. Nejabatkhah, “Unified Control of the Parallel LCC-VSCs Interlinking Converters in a Hybrid AC/DC Network,” *IEEE Trans. Smart Grid*, pp. 1–1, 2021, doi: 10.1109/TSG.2021.3137300.
- [111] Y. W. Li, “Control and Resonance Damping of Voltage-Source and Current-Source Converters With LCL Filters,” *IEEE Trans. Ind. Electron.*, vol. 56, no. 5, pp. 1511–1521, May 2009, doi: 10.1109/TIE.2008.2009562.
- [112] H. Tian, Y. W. Li, and P. Wang, “Hybrid AC/DC System Harmonics Control Through Grid Interfacing Converters With Low Switching Frequency,” *IEEE Trans. Ind. Electron.*, vol. 65, no. 3, pp. 2256–2267, Mar. 2018, doi: 10.1109/TIE.2017.2740822.
- [113] J. He, Y. W. Li, and F. Blaabjerg, “An Enhanced Islanding Microgrid Reactive Power, Imbalance Power, and Harmonic Power Sharing Scheme,” *IEEE Trans. Power Electron.*, vol. 30, no. 6, pp. 3389–3401, Jun. 2015, doi: 10.1109/TPEL.2014.2332998.
- [114] J. D. Glover and M. Sarma, *Power System Analysis and Design*, 2nd ed. Boston, MA: PWS Publ. Comp., 1993.
- [115] F. Ghassemi and M. Perry, “Review of Voltage Unbalance Limit in The GB Grid Code CC.6.1.5 (b),” p. 35.
- [116] F. Nejabatkhah, Y. W. Li, and B. Wu, “Control Strategies of Three-Phase Distributed Generation Inverters for Grid Unbalanced Voltage Compensation,”

- IEEE Trans. Power Electron.*, vol. 31, no. 7, pp. 5228–5241, Jul. 2016, doi: 10.1109/TPEL.2015.2479601.
- [117] R. R. Ahrabi, Y. W. Li, and L. Ding, “Modelling and Design of Parallel LCC-VSC Interlinking Converters Unified Controller in AC/DC Network,” *IEEE J. Emerg. Sel. Top. Power Electron.*, pp. 1–1, 2021, doi: 10.1109/JESTPE.2021.3110711.
- [118] P. Kundur, N. Balu and M. Lauby, "2" in *Power System Stability and Control*, USA, NY, New York:McGraw-Hill, vol. 19, pp. 22-41, 1994.

Appendix

The design procedure for the LCC-based installations expansion control scheme is provided in this section. The operation states are studied in detail, and proper controlling parameters are acquired accordingly. The parallel LCC-VSC-based new installation's control scheme's parameters design will follow a similar procedure as the LCC-based expansion installations control scheme; however, to avoid repetitive practice, its details are not provided.

6.3 Parameters Design Based on a Power-sharing

Operation State

Initially, for better clarification, the operation of a single LC-IC in such a hybrid AC/DC grid is studied. Taking $G_{LCC}(s)$ as $G_{KLCC}(s)G_{LCC_D}(s)$, the exchanged power by LC-IC operating individually is calculated as:

$$\Delta P_{LCC,pu} = \frac{\Delta P_{set_LCC,pu} G_{LCC_D}(s)}{1 + \frac{G_{LCC}(s)}{k_{AC}}} - \frac{\frac{G_{LCC}(s)}{k_{AC}} [\Delta P_{AC,pu}^* + \Delta P_{AC_P,pu}]}{1 + \frac{G_{LCC}(s)}{k_{AC}}} \quad (0.1)$$

For simplification purposes (0.1) is rewritten as follow:

$$\Delta P_{LCC,pu} = G_{1,LCC}(s) \Delta P_{set_LCC,pu} + G_{2,LCC}(s) (\Delta P_{AC,pu}^* + \Delta P_{AC_P,pu}) \quad (0.2)$$

To check for the control system's stability while only an LC-IC is operating as an IC, the pole placements are provided in the form of Fig. 0.1 and Fig. 0.2. The results show the pole-placement of the $G_{1,LCC}$ and $G_{2,LCC}$.

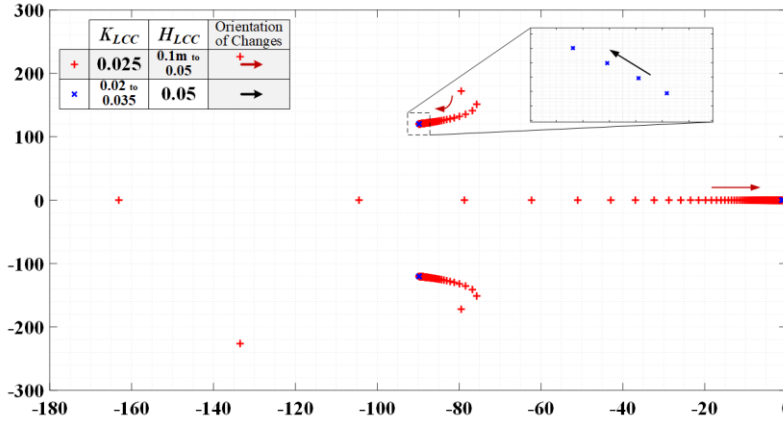


Fig. 0.1: Stability study of LC-IC's $G_{1,LCC}$ function, changing K_{LCC} 's and H_{LCC} 's values and their impact on poles placement.

As shown in Fig. 33, keeping $H_{LCC} = 0.05$ and changing K_{LCC} from 0.02 to 0.035, the $G_{1,LCC}$ pole-placements does not change considerably. Accordingly, the impact on the dynamic of the system also will be limited. By keeping $K_{LCC} = 0.025$ and changing the value of the H_{LCC} from 0.00001 to 0.05, the pole on the real axis moves toward the imaginary axis, and a pair of conjugate poles moves farther from the imaginary axis and less noticeably closer to the real axis. It can be seen that the inertia coefficient affects the pole-placements more than K_{LCC} , which will accordingly impact the settling time and the overshoot value show in Fig. 0.1.

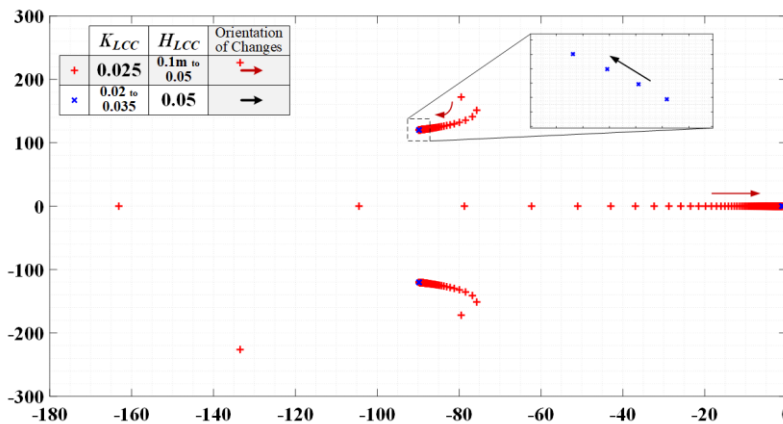


Fig. 0.2: Stability study of LC-IC's $G_{2,LCC}$ function, changing K_{LCC} 's and H_{LCC} 's values and their impact on poles placement.

Similar studies are applied to the $G_{2,LCC}$ to check for its stability. Observing pole-placements of $G_{2,LCC}$, shown in Fig. 0.2, it can be seen that poles behave almost similar to the changes like $G_{1,LCC}$'s. It can be learnt from pole-placements of $G_{1,LCC}$

and $G_{2,LCC}$ that H_{LCC} has a higher impact on LC-IC's dynamic and stability compared to the K_{LCC} . It is essential to consider the sheer importance of the droop equivalent control and power-sharing, designing the K_{LCC} .

For the combined LC-IC and VS-ICs performance, the control system's stability in this operation mode is tested using the IC's linearized exchanged power transfer function (0.3).

$$\Delta P_{IC,pu} = \frac{\Delta P_{set_LCC,pu} G_{LCC_D}(s) - \Delta P_{AC,pu}^* \frac{G_{ILCC}(s)}{k_{AC}}}{1 + (1+K) \sum_{i=1}^N G_{IC_i}(s) + \frac{G_{ILCC}(s)}{k_{AC}}} - \left(\frac{G_{ILCC}(s)}{k_{AC}} + \sum_{i=1}^N G_{IC_i}(s) \right) \frac{\Delta P_{AC_P,pu}}{1 + (1+K) \sum_{i=1}^N G_{IC_i}(s) + \frac{G_{ILCC}(s)}{k_{AC}}} + \frac{K \sum_{i=1}^N G_{IC_i}(s) \Delta P_{DC_P,pu}}{1 + (1+K) \sum_{i=1}^N G_{IC_i}(s) + \frac{G_{ILCC}(s)}{k_{AC}}} \quad (0.3)$$

(0.3) is simplified into (0.4):

$$\Delta P_{IC,pu} = G_{1,IC1}(s) \Delta P_{set_LCC,pu} + G_{2,IC1}(s) \Delta P_{AC,pu}^* + G_{3,IC1}(s) \Delta P_{AC_P,pu} + G_{4,IC1}(s) \Delta P_{DC_P,pu} \quad (0.4)$$

(0.3) imply the impact of LC-IC and VS-ICs function on the dynamic and stability of the control system. The system's stability will be studied by changing the $G_{c_i}(s)$'s proportional gain η_i and its' lead and delay times, τ_{l_i} and τ_{d_i} , respectively. The impact of LC-IC's inertia H_{LCC} on the pole-placements, along with additional variables, are shown in Fig. 0.3. The damping value and setting time of the VS-IC's exchanged-power function are chosen as $\zeta_i = 0.74$ and $t_{s_i} = 0.0175s$, respectively.

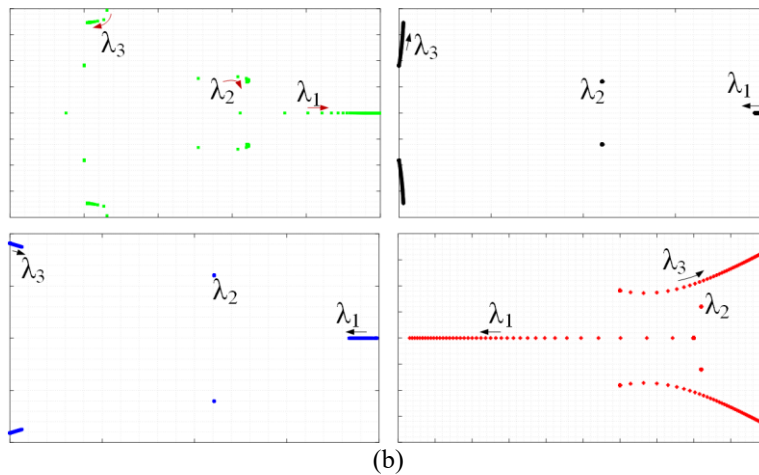
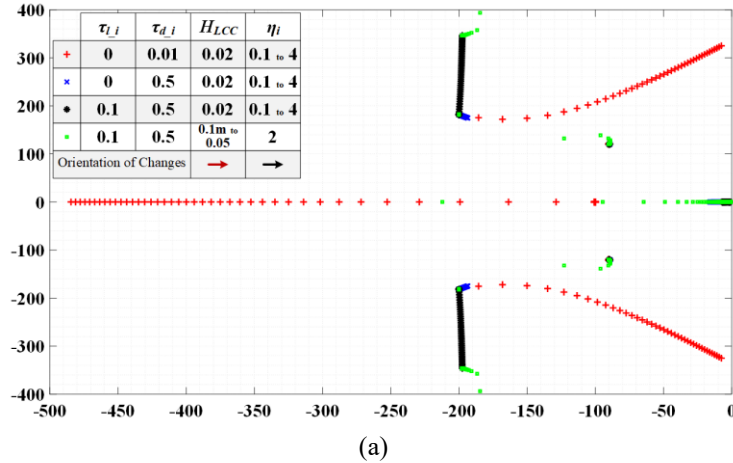


Fig. 0.3: Impact of $G_{c_i}(s)$ on $P_{IC}(s)$ poles-placement of the function $G_{3,IC1}(s)$. a) Overall poles placement. b) Impact of individual changes.

The pole-placements of the $G_{3,IC1}(s)$ is shown in Fig. 0.3. The test gives a reasonable view of the controlling parameter's impact on the system. It can be learned from Fig. 0.3, when τ_{l_i} and τ_{d_i} are equal to 0 and 0.01, respectively, pole-placements have the highest shift by changing the variables compared to other options. Also, it is expected that the system shows a faster but oscillatory response by increasing the value of η_i from 0.1 to 4. This is an expected circumstance that is based on the presence of a pair of conjugate poles getting closer to the imaginary axis and the pole on the real axis distancing from the imaginary axis, as shown in Fig. 0.3. Comparing the two other testing conditions, $\tau_{l_i} = 0, \tau_{d_i} = 0.5$ and $\tau_{l_i} = 0.1, \tau_{d_i} = 0.5$, the particular choice with higher τ_{l_i} shows better performance. This is due to the pair of conjugate poles, λ_3 , away from the imaginary axis, compared

to the other options. Adopting the variables as $\tau_{l_i} = 0.1$, $\tau_{d_i} = 0.5$ and increasing the value of H_{LCC} from 0.0001 to 0.05, the system shows better performance for the lower values of the H_{LCC} . This is due to a pole's position on the real axis farther from the imaginary axis and a pair of conjugate poles, λ_2 , limited relocation from the imaginary axis. Following the results, it is expected that the $\tau_{l_i} = 0.1$ and $\tau_{d_i} = 0.5$ with sufficient value for H_{LCC} to perform better for this state of operation (i.e., better settling time, lower overshoot, and oscillations). The system response to the practiced variables of the H_{LCC} and the entire dynamic of the $G_{3,IC1}(s)$ show that lower values for H_{LCC} has a faster response.

Similar studies are also feasible for the $G_{1,IC1}(s)$, $G_{2,IC1}(s)$, and $G_{4,IC1}(s)$. However, due to the lack of space, it is not provided here.

Observing the system's overall behavior in this state shows that the higher values for η_i result in a better response. However, the value of the η_i cannot be considered exceedingly high without proper compensation. Also, the system response is significantly better for the smaller values of the H_{LCC} .

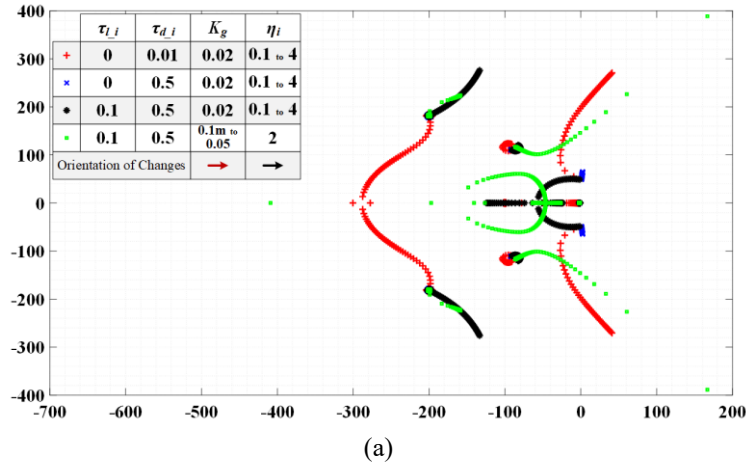
It can be learned from the studies that controlling parameters have a serious projection on the dynamic and stability of the system.

6.4 Parameters Design Based on DC Sub-grid Support Operation State

The steady-state representation of DC voltage can be calculated using (2.40) and (2.41) as shown in the following:

$$\left\{ \begin{array}{l} \Delta U_{DC,pu} = \Delta P_{DC,P,pu} G_{D0}(s) - \Delta P_{set_LCC,pu} G_{D1}(s) + \Delta P_{AC,P,pu} G_{D2}(s) + \\ \quad \Delta P_{DC,pu}^* K G_{D2}(s) + \Delta U_{DC,pu}^* G_{D3}(s) \\ G_{D0}(s) = \frac{1 + \sum_{i=1}^N G_{IC_i}(s)}{G_{D_Denom}(s)}, \quad G_{D1}(s) = \frac{G_{LLCC}(s)}{G_{D_Denom}(s)}, \\ G_{D2}(s) = \frac{\sum_{i=1}^N G_{IC_i}(s)}{G_{D_Denom}(s)}, \quad G_{D3}(s) = \frac{G_{LLCC}(s) + Kk_{DC} \sum_{i=1}^N G_{IC_i}(s)}{G_{D_Denom}(s)} \\ G_{D_Denom}(s) = s \frac{CU_{dcB}^2}{S_B} \left(1 + \sum_{i=1}^N G_{IC_i}(s) \right) + G_{LLCC}(s) + Kk_{DC} \sum_{i=1}^N G_{IC_i}(s) \end{array} \right. \quad (0.5)$$

The stability of the control system in this mode of operation is subject to the stability of the $G_{D0}(s)$, $G_{D1}(s)$, $G_{D2}(s)$, and $G_{D3}(s)$. However, to save space and base on the fact that these transfer functions share several similarities in their formulation, only the stability of the $G_{D3}(s)$ will be shown here. $G_{D3}(s)$ include controlling parameters for both LC-IC and VS-IC. Fig. 0.4 shows pole-placements of the $G_{D3}(s)$.



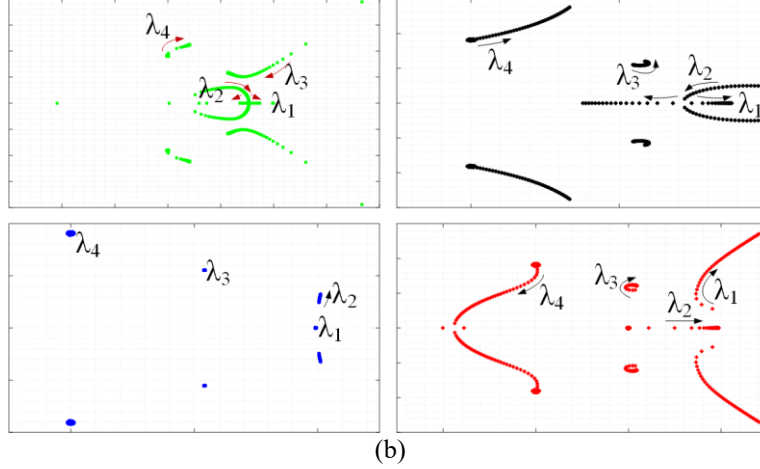


Fig. 0.4: Impact of $G_c(s)$ and $G_{DLCC}(s)$ on the poles placement of the $G_{D3}(s)$. a) Overall poles placement. b) Impact of individual changes.

Similar to the power-sharing operation condition, the damping and setting time for VS-IC assumed to be $\zeta_i = 0.74$ and $t_{s_i} = 0.0175s$. Also, LC-IC uses a similar control function as in a power-sharing operation known as $G_{LCC_D}(s)$ (2.15). To test the effect of $G_c(s)$ and $G_{DLCC}(s)$ on the performance of the control system in this mode of operation, the values of τ_{l_i} , τ_{d_i} , and K_g is changed as it is given in Fig. 0.4(a) while the K_d is kept on 0.002. In three of the tests, the value of the K_g is assumed to be equal to 0.02, while τ_{l_i} , τ_{d_i} , and η_i are changed. Similarly, in the next try, the values of τ_{l_i} , τ_{d_i} , and η_i are kept constant on 0.1, 0.5, and 2, respectively, while K_g changed from 0.0001 to 0.05. Selecting $\tau_{l_i} = 0$, $\tau_{d_i} = 0.01$, and $K_g = 0.02$ for $G_{D3}(s)$ and increasing the value of the η_i as it can be seen in Fig. 0.4(a), (b), the system becomes unstable. In addition to that, even in the stable region, a pair of conjugate poles get closer to the imaginary axis by increasing the value of η_i resulting in an oscillatory performance for the system. For the state when $\tau_{l_i} = 0$, $\tau_{d_i} = 0.5$, and $K_g = 0.02$ the control system is unstable for almost all the η_i values. The condition with $\tau_{l_i} = 0.1$, $\tau_{d_i} = 0.5$, and $K_g = 0.02$ is another operation point that the control system is tested in. In this condition, the poles are in stable areas regardless of η_i 's value. For the smaller value of η_i , a pair of conjugate poles, λ_2 , are closer to the imaginary axis that will result in limited oscillatory performance. By increasing the value of η_i , a pair of conjugate poles, λ_2 , moves away from the imaginary axis, which will improve the response of the control system. To better understand the effect of control system parameters on system stability, the variables

are selected as $\tau_{l_i} = 0.1$, $\tau_{d_i} = 0.5$, $\eta_i = 2$ and K_g is changed from 0.0001 to 0.05. The closed-loop control system's pole-placements, as can be seen in Fig. 0.4(a), (b), shows unstable performance for low inertia values. Increasing the LC-IC's inertia coefficient K_g , a pair of conjugate poles moves from the right-hand plane to the stable region.

As it has been mentioned, by increasing the LC-IC's inertia coefficient, K_g , the stability of the control system will increase. Furthermore, a reasonable decrease in the VS-IC's delay time τ_{d_i} , improves the dynamic considerably.

6.5 Finalizing the Control Parameters

Reviewing the stability design regarding power-sharing operation, it can be seen that $\tau_{l_i} = 0.1$, $\tau_{d_i} = 0.2$, and $\eta_i = 2$ for the VS-IC control loop and taking $H_{LCC} = 0.001$ result in reliable dynamic and stable performance. Clearly, based on the provided pole-placements in Fig. 0.3, the system shows stable performance in a wide range of control parameters. However, as it is shown, the aforementioned controlling parameters contribute to the improved dynamic. The stability of the system in DC sub-grid support is tested for several sets of control parameters, as shown in Fig. 0.4. It can be learnt that taking $\tau_{l_i} = 0.1$, $\tau_{d_i} = 0.2$, and $\eta_i = 2$ puts the system in the widest safe stable spectrum. However, as can be seen, the value of the K_g has a significant impact on the stability of the system in this region. Based on the positioning of the poles, it can be learned that system is more stable for higher values of the K_g . Therefore, taking $K_g = 0.02$, the system operates in a stable region while showing adequate dynamic as given in Fig. 0.4. The system's expected dynamic response in Fig. 0.4 shows that lowering the value of the τ_{d_i} to 0.2 improved system performance.

It can be concluded that the AC sub-grid support does not need different controlling parameters compared to power-sharing operation. Moreover, the power-sharing and DC sub-grid support modes share similar control parameters for VS-ICs. On the other hand, LC-IC's physical limit enforces the system to switch between power-sharing and DC sub-grid support states. Incorporating the

controlling parameters for VS-ICs in power-sharing and DC sub-grid support states, it can be concluded that $\tau_{l_i} = 0.1$, $\tau_{d_i} = 0.2$, and $\eta_i = 2$ is a fitting choice for all the states. Whereas LC-IC uses a separate controlling function for power-sharing and DC sub-grid support states (but with the same inner loop controller) that leads to independent controlling parameters as provided previously.

6.6 Exchanged Power Capacity Design

So, in summary the IC's exchanged power system level control can be depicted as it is given in Fig. 0.5.

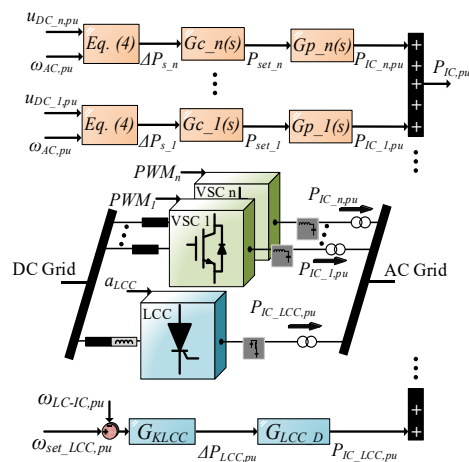


Fig. 0.5: ICs overall system level power exchange control.

In order to achieve superior performance for the proposed system, a correct estimation of the IC's power ratio can be effective. As stated previously, the VS-ICs are added to the already existing LCC-based installation in order to expand the power exchange capacity, add reverse power flow capability, and potentially reduce the reactive power and harmonics compensation filter sizes of LCC. Based on different considerations, the power capacity of the VSC can be calculated and also the power ratio between LC-IC and VS-IC can also be achieved. The required capacity for expansion of the system's exchange power and reverse power flow requirement is system-level requirements and very application dependent. These values can be obtained based on specific project requirements. As it is given in [85],

the LCCs consumed reactive power is around 50 to 60% of the supplied active power at the rated load. Based on [118], around 30% of the consumed reactive power can be mitigated by harmonics filters. Capacitor banks can compensate for the remaining reactive power. In an expansion and retrofit project with the existing LCC system, since the equipment regarding the reactive power compensation is already installed, using the VS-IC for all of the required reactive power compensation may not be economically practical. Therefore, providing support for reactive power compensation during the transients to limit its negative impact on the system seems to be a reasonable task. Such purpose typically requires a certain percentage of LCC active power from the VSC, which is project-dependent due to the impracticability of random step changes. As an example, the filter step change for the Cheju-Haenam transmission line project (HVDC) is around 10% assuming a voltage step switching limited to 5%. Also, the power capacity required for the harmonic compensation is less than 10% of the LC-IC's overall exchanged power. Furthermore, the required power to compensate for LC-IC's harmonics is around 10% of the exchanged active power by LC-IC. Similar to the reactive power compensation, the harmonics compensation can be provided by passive filters, which are already available as part of the existing LCC configuration. However, the deviation of the passive component from their actual value due to the degradation can impact passive filters compensation quality. This issue can be easily mitigated using parallel units with proper harmonics compensation control.

Based on the aforementioned discussions, a combination of passive and active techniques for reactive power compensation is suitable for the proposed system. The combined capacity requirement of reactive power and harmonic compensation (assuming a full harmonics compensation by parallel VS-IC) can be in the range of 20% of the LCC's active power. Note that evaluating the exact ratio requires an in-depth cost study that is out of the scope of this work. Further combined with the exchange power requirements of the IC discussed earlier, the VS-IC capacity can be properly determined.